Simulation Based Optimal Design of Exoskeletons to Reduce Metabolic Cost and Improve Energy Efficiency

by

Ali KhalilianMotamed Bonab

Submitted to
the Graduate School of Engineering and Natural Sciences
in partial fulfillment of
the requirements for the degree of
Master of Science

SABANCI UNIVERSITY

April, 2021

Simulation Based Optimal Design of Exoskeletons to Reduce Metabolic Cost and Improve Energy Efficiency

Ali KhalilianMotamed Bonab

APPROVED BY

DATE OF APPROVAL: .....

Simulation-Based Optimal Design of Exoskeletons
to Reduce Metabolic Cost and Improve Energy Efficiency

Ali KhalilianMotamed Bonab

Mechatronics Engineering M.Sc. Thesis, April 2021

Thesis Supervisor: Prof. Volkan Patoğlu

Keywords: Physical human-robot interaction, exoskeleton design, multi-criteria design optimization, musculoskeletal simulations, simulation-based assistive device design.

Wearable robotic assistive devices have the potential to improve the metabolic efficiency of human locomotion. Developing exoskeletons that can reduce the metabolic cost of human locomotion is challenging, since there is no systematic mechatronic design approach for the design of such exoskeletons. A systematic design approach necessitates a means for a rigorous and fair comparison of effects of different exoskeleton designs and assistance torque profiles on the human metabolic cost of locomotion. Conducting such investigations through human subject experiments with physical devices is generally infeasible, while design studies relying on musculoskeletal models hold high promise in providing effective design guidelines, as the effect of devices and various assistance torques on muscle recruitment and metabolic cost can be studied systematically.

In this thesis, a simulation-based design approach is introduced to systematically design exoskeletons that reduce the metabolic cost of locomotion. Along these lines, a Pareto optimization approach is proposed to enable rigorous and fair comparisons of effects of different exoskeletons designs and assistance torques on the metabolic cost of locomotion, under some realistic physical limits on actuator torques. The proposed systematic mechatronics system design approach is demonstrated by introducing a bi-articular exoskeleton design and comparing its efficiency with commonly used mono-articular exoskeletons. In particular, the power consumption of and metabolic rate reduction due to assistance provided by bi-articular and mono-articular hip-knee exoskeletons are optimized simultaneously during unloaded and loaded walking conditions, and rigorous comparison among such devices is presented. Furthermore, the effect of regeneration on the

power consumption of exoskeletons and the detrimental effects of inertial properties of exoskeletons on the metabolic cost of locomotion are studied by superposing these effects on the Pareto-front curves.

Our results explain the effect of heavy loads on the optimal assistance profiles and provide guidelines on choosing the optimal device configurations under actuator torque limitation, device inertia, and regeneration effects. The multi-criteria comparison of devices indicates that on the one hand, similar assistance levels can be achieved by both exoskeletons; on the other hand, mono-articular exoskeletons demonstrate better performance on reducing the peak reaction forces, while the power consumptions of bi-articular exoskeletons are less affected by the loading of subjects. Furthermore, the inclusion of device inertia results in significantly less detrimental effects on the metabolic cost of subjects and does not affect the Pareto-optimality of solutions for bi-articular exoskeletons, while non-dominated configurations are significantly affected by the device inertia for mono-articular exoskeletons.

Dış İskeletlerin Metabolik Desteğinin ve Enerji Sarfiyatının Benzetim Tabanlı Optimizasyonu

Ali KhalilianMotamed Bonab

Mekatronik Mühendisliği Yüksek Lisans Tez, Nisan 2021

Tez Danışmanı: Prof. Dr. Volkan Patoğlu

Anahtar Kelimeler: Fiziksel insan-robot etkileşimi, dış iskelet tasarımı, çok kriterli tasarım optimizasyonu, kas-iskelet simülasyonları, simülasyon tabanlı yardımcı cihaz tasarımı

Giyilebilir robotik yardımcı cihazlar, insan hareketinin metabolik verimliliğini artırma potansiyeline sahiptir. Sistematik bir mekatronik dizayn yaklaşımı olmadığından dolayı, insanın harcadığı metabolik enerjiyi azaltabilecek dış iskeletler geliştirmek zordur. Sistematik bir tasarım yaklaşımı, farklı dış iskelet tasarımları ve yardımcı tork profillerinin insanın yürürken harcadığı enerjiyi adil ve titiz bir şekilde karşılaştırmasını zorunlu kılar. Bu tür araştırmaların fiziksel cihazlarla insan denek deneyleri yoluyla yürütülmesi genellikle mümkün değildir, ancak kas-iskelet modellerine dayanan tasarım çalışmaları, cihazların ve çeşitli yardımcı torkların kas alımı ve metabolik maliyet üzerindeki etkisi sistematik olarak çalışılabildiğinden, etkili tasarım kılavuzları sağlamada büyük umut vaat etmektedir.

Bu tezde, hareketin metabolik maliyetini azaltan dış iskeletlerin sistematik olarak tasarlanması için simülasyon tabanlı bir tasarım yaklaşımı ele alınmıştır . Bu doğrultuda, farklı dış iskelet tasarımlarının ve yardımcı torkların hareketininsanın harcadığı enerji üzerindeki etkilerinin, aktüatör torkları üzerindeki bazı gerçekçi fiziksel sınırlar altında titiz ve adil bir şekilde karşılaştırılmasını sağlamak için bir Pareto optimizasyon yaklaşımı önerilmektedir. Önerilen sistematik mekatronik sistem tasarım yaklaşımı, aktuatörleri eklemlerde olmayan bir dış iskelet tasarımı sunarak ve etkinliğini yaygın olarak kullanılan aktuatörleri eklemlerde olan dış iskeletlerle karşılaştırarak gösterilmiştir. Özellikle„ aktuatörleri eklemlerde olmayan ve olan dış iskeletlerde, kalça-diz dış iskeletlerinin sağladığı yardım sayesinde güç tüketimi ve metabolizma hızının azalması, yüksüz ve yüklü yürüme koşullarında eşzamanlı olarak optimize edilir ve bu tür cihazlar arasında detaylı bir karşılaştırma sunuldu. Dahası, rejenerasyonun dış iskeletlerin güç tüketimi üzerindeki etkisi ve dış iskeletlerin eylemsizlik özelliklerinin hareketin metabolik

maliyeti üzerindeki zararlı etkileri, bu etkiler Pareto-ön eğrilere üst üste getirilerek incelenmiştir.

Sonuçlarımız, ağır yüklerin optimum destek profilleri üzerindeki etkisini açıklamakta ve aktüatör tork sınırlaması, cihaz ataleti ve rejenerasyon etkileri altında optimum cihaz konfigürasyonlarını seçme konusunda kılavuzlar sağlamaktadır. Cihazların çok kriterli karşılaştırması, bir yandan, her iki dış iskelet tarafından da benzer destek seviyelerinin elde edilebileceğini göstermektedir; Öte yandan, aktuatörleri eklemlerde olan dış iskeletler, tepe tepkime kuvvetlerini azaltmada daha iyi performans gösterirken, aktuatörleri eklemlerde olmayan dış iskeletlerin güç tüketimleri deneklerin yüklenmesinden daha az etkilenir. Ayrıca, cihaz ataletinin dahil edilmesi, deneklerin metabolik enerji üzerinde önemli ölçüde daha az zararlı etkilere neden olur ve aktuatörleri eklemlerde olmayan dış iskeletler için çözümlerin Pareto-optimalliğini etkilemezken, baskın olmayan konfigürasyonlar ise aktuatörleri eklemlerde olan dış iskeletler için cihaz ataletinden önemli ölçüde etkilenir.

Acknowledgements

During these three years, I learned that work is less about the work and more about the people. Therefore, I would like to acknowledge those who have been by my side throughout my master's study and have played an important role in making this thesis possible.

First of all, I owe my deepest gratitude to my supervisor, Prof. Volkan Patoğlu, who has supported me throughout my research. I am blessed and honored to have Prof. Volkan Patoğlu as the advisor of my research. His encouragement, patience, kindness, and support, beside his immense knowledge and work ethics, have aspired me to become an enthusiastic and diligent researcher. I can see his positive impressions in every aspect of my personal and academic life, and I will try to live up to his standards and expectations throughout my professional journey.

I would like to thank committee members of this thesis: Assist. Prof. Melih Türkseven and Assist. Prof. Hande Argunşah, for their time, interest, and insightful questions, and helpful comments to fulfill the potential of this work.

Being a member of the Human-Machine Interaction laboratory at Sabanci University has endowed me the chance to make great friends during my master's study in Turkey. I want to express my thanks to all members of HMI, Cogntive Robotic laboratories and other labmates for all their unconditional support, guidance, and help during these years. As an international student at Sabanci University, the warm and friendly environment of our laboratory made me feel at home.

I would like to thank my roommate and warm-hearted friend, dear Fatih Emre Tosun. Fatih, Dr. Vahid Tavakol, and I spent most of our amazing times together in Istanbul, Izmir, and Bodrum.

I want to thanks dear Umut Çalişkan who was my labmate and is my great friend and dear Zeynep Özge Orhan for their unconditional support and heartfelt friendship. I will never forget how our long conversations together helped us feel relieved when we were under pressure from our research.

I also want to thanks my oldest and best friends dear Dr. Hesam Farzaneh and dear Behrad Taherniya, who were always by my side during hard and happy times in these years. I have always known that Hesam and Behrad are there to help me during hard times, and we always have fantastic fun times and adventures when we are together.

I wish to express my thanks to my dear friend and labmate Ali Yaşar for all his sincere supports, generous friendship, and fantastic fun times we have had together. Fatih and Ali gave me the necessary distractions from my research and made my stay in Istanbul memorable.

It is a pleasure to thank my friends Çağatay Irmak, Uğur Mengilli, Ayhan Aktaş, Mehmet Emin Mumcuoğlu and Naida Fetic for the wonderful times we shared and their genuine friendship. I would like to express my sincere gratitude to Dr. Gökay Çoruhlu and Dr. Mustafa Yalçın for their unconditional help throughout my research. I also want to express my gratitude to Dr. Hamed Rezanejad, Dr. Milad Shakeri, and Dr. Rahman Khorramfar for all their guidance and consultation before and during my master's study.

Last but indeed foremost, I want to thank my parent and my family from the bottom of my heart for their unwavering love, unconditional support, and understanding. I cannot thank my parents, Mehry Zare and Morteza KhalilianMotamed Bonab, enough for their consistent support in my time of need. I would not have any of my achievements without their sacrifices and love. I want to thank my brother Amir KhalilianMotamed Bonab. I am glad to have such a generous and supportive brother, and I wish him the bests in the world as a future architect.

I will never be able to thank enough my mom, Mehry, for what she has done for me and her unconditional love. When I am talking to my grandma and my mom, I cannot feel anything but their heart-touching love. Nothing in the world ever can make me feel more alive and happy than seeing my mom's and my grandma's smile.

To my beloved family...

Contents

List of Figures

List of Tables

List of Algorithms

Chapter 1

Introduction

1.1 Motivation

The versatility and bipedalism of human locomotion are both unique and one of the most important characteristics of humans among the mammalian mobility types [1]. While bipedal locomotion has a low energy cost of transport [1], the human musculoskeletal system is not optimal for performing all locomotion tasks [2]. For instance, it has been proven that running is considerably less efficient than walking for humans [3, 4].

Bipedal locomotion can lose its efficiency through aging, disease and injury, which can profoundly affect the quality of life due to a loss of independence and mobility [5]. Even though training can improve the efficiency of locomotion [6], by increasing the stiffness of the tendons [7], and rehabilitation can help patients to achieve near-normal locomotion in the long term [8], the muscle and tendon tissues fundamentally constrain the dynamic properties of the muscles. Musculoskeletal system compromises between enhancing the efficiency of the desired task and its adaptability [2], and persistence of the neuromotor deficits even after the rehabilitation constrains the patients from completely resolving the gait issues and reaching complete independence [8].

By taking advantage of assistive devices that are not bounded by any fundamental biological limitations, a musculotendon system can be customized to increase the efficiency of performing locomotion tasks. Assistive devices can be used for patients to improve their quality of life by recovering to their normal gait pattern and decreasing their dependency; assistive devices can also be employed to reduce the risk of injuries due repetitive tasks, such as walking with heavy loads [9–11].

Despite the progress that has been made on designing exoskeletons assisting healthy individuals, elderly and disabled subjects suffering impaired gait cycles, there is no systematic mechatronic design approach for exoskeletons to improve metabolic cost of human locomotion. A systematic design approach necessitates a means for rigorous and fair comparison of effects of different exoskeleton designs and assistance torque profiles on human metabolic cost of locomotion. However, studies based on comprehensive human subject experiments are not feasible. Such human-in-the-loop studies are challenging as multiple device prototypes need to be implemented, appropriate volunteers need to be recruited, safety of trials need to be established and sufficient number of experiments need to be conducted to achieve statistically reliable results. Furthermore, inability to collect certain information without introducing sensors inside the body [2], difficulty or impossibility of some measurements [12], and effects of training and fatigue on performance of subjects [13, 14] pose as some other important limitations of human-in-the-loop studies.

Simulation-based studies to design assistive devices can complement the experimental design approach to overcome many of these challenges. Studying assistive devices through musculoskeletal simulations facilitates the research by reducing the need for physical prototyping and enables researchers to carry out fast, automated, and repeatable studies in a controlled environment, where different analyses can be conducted on human musculoskeletal models without the risk of injuries.

1.2 Contributions

The contributions of this thesis are as follows:

- We introduce a simulation-based design approach to systematically design exoskeletons that reduce metabolic cost of locomotion. Along these lines, we propose a Pareto optimization approach that enables rigorous and fair comparison of effects of different exoskeletons designs and assistance torques on metabolic cost of locomotion.

- We demonstrate the proposed systematic mechatronics system design approach by introducing a bi-articular exoskeleton design and comparing its efficiency with commonly used mono-articular exoskeletons

Our multi-criteria optimization results subsume single objective optima. In particular, our results include the solution to a commonly addressed single objective optimization problem that aims to maximize metabolic rate reduction of exoskeletons without considering their power consumption or torque capabilities, commonly referred to as ideal exoskeleton optimization [2, 15].

- Our ideal exoskeleton optimization results verify that, without any limits on actuator torques and power consumption, both ideal mono-articular and bi-articular devices can reach the same level of metabolic rate reduction under the same total power consumption.

- We show that the assistance torques not only improve the metabolic rate, but can also decrease the peak reaction forces and moments at the knee, patellofemoral, and hip joints considerably.

- We verify that assistance provided by the exoskeletons not only has a direct effect of ideal exoskeletons on the muscular activities of the hip and knee joints in the sagittal plane but also indirectly affect the activity of muscles at the ankle joint and the muscles related to the hip abduction.

- We show that loading subjects with a heavy backpack results in a predictable change in assistance profiles, by causing a proportional increase in the magnitude and the time shift.

While ideal exoskeleton optimizations can provide several useful insights, different exoskeleton designs cannot be meaningfully compared without introducing some

realistic physical limits on actuator torques and considering the power consumption of these devices. Along these lines, we introduce different levels of peak torque constraints on actuators of both mono-articular and bi-articular exoskeletons and compare their performance by considering the metabolic cost reduction and the power consumption metrics, simultaneously.

- We show that introducing sufficiently large torque limits to the actuators of both devices does not have a large impact on the metabolic cost reduction, while such limits can cause a considerable reduction in the power consumption of the exoskeletons.
- We also show that both devices can reach similar performance levels for different assignments of peak torques to hip and knee joints, while larger peak torque limits are required for mono-articular exoskeletons compared to bi-articular devices.
- Despite the similar assistance levels provided by both exoskeletons, mono-articular exoskeletons demonstrate better performance on reducing the peak reaction moments and forces, while the power consumption of bi-articular exoskeletons is less affected by the loading of subjects.
- We demonstrate the effect of regeneration on the power consumption of exoskeletons by superposing this effect on the Pareto-front curves.
- We show that regeneration can have a significant impact on power efficiency of exoskeletons, as it can improve the power consumption of these devices from 6.54% $\pm$ 2.60% to 25.76% $\pm$ 4.34%, depending on the efficiency of regeneration system, the kinematics of the exoskeleton, and the torque/power limitations of the actuators.
- Our results indicate that the knee actuators of mono-articular devices have more regeneration potential, while all actuators of the bi-articular devices have large regeneration potential.

We also demonstrate the detrimental effects of inertial properties of exoskeletons on metabolic cost of locomotion, by superposing this effect on the Pareto-front

curves. In particular, we estimate the effect of additional mass and inertia on metabolic rate of subjects for mono-articular and bi-articular exoskeletons based on [16] and quantify these effects through a modified version of the augmentation factor proposed in [17].

- Our results indicate that the added device inertia causes optimal mono-articular and bi-articular devices lose their efficiency by 42.51% ± 0.17%–55.51% ± 0.11%, and 35.12% ± 0.21%–49.67% ± 0.21%, respectively.
- For bi-articular exoskeletons, inertial effects simply shift the Pareto-front curve, without significantly affecting the Pareto-optimal configurations, while non-dominated configurations are significantly affected by the device inertia for the mono-articular exoskeletons.

1.3 Outline

The rest of the thesis is organized as follows:

Chapter 2 provides the related work on assistive devices, biarticular actuation, and simulation-based design and analysis.

Chapter 3 presents the design and analysis of studied exoskeletons, including kinematic modeling, exoskeletons characterization, and actuator selection for the exoskeletons.

Chapter 4 is dedicated to musculoskeletal simulations in which the musculoskeletal model, assistive devices modeling, and the procedures used for performing and verifying the simulations and analyses were explained. The **section 4.7** and **section 4.9** present and discuss the results of simulations performed for untethered and tethered exoskeletons under ideal conditions, without constraints on their performance.

Chapter 5 presents the simulation-based multi-criteria optimization explaining the workflow of the Pareto optimization approach on the Opensim framework and detailing the objective functions considered. The **5.2**, **5.3**, and **5.4** sections present the electrical regeneration effect on optimal trade-off curves and the metabolic model that captures the effect of adding mass and inertia and the introduced modified augmentation factor, respectively. The rest of this chapter presents the results for the performed multi-criteria optimizations simulations and analyses.

In **Chapter 6**, selected cases from the optimal trade-off curves were studied in detail, and four different types of comparisons between the devices and the loading conditions were conducted.

This thesis is concluded by Conclusions and future work presented in **Chapter 7** in which the summary of contributions and a discussion of future directions are presented.

Chapter 2

Related Work

2.1 Lower Limb Exoskeletons

The first efforts to develop mobile powered exoskeletons were initiated in 1890 [18]. Despite efforts and progress in accomplishing untethered exoskeleton over a century [19], in 2000 Defense Advanced Research Projects Agency (DARPA) initiated the Exoskeletons for Human Performance Augmentation (EHPA) Program [20], and the first mobile and functional exoskeleton, named Berkeley Lower Extremity Exoskeleton (BLEEX) was developed to augment soldiers' capability of carrying heavy loads over long distances [21]. Sarcos and MIT exoskeletons were introduced [19] after BLEEX as untethered exoskeletons. The same technology with the purpose of assisting impaired populations also was already initiated [22], and ReWalk is one of the well-known exoskeletons [23] which has recently been approved by FDA [24]. The Hybrid Assistive Limbs (HAL) project [25] is another notable project assisting SCI, stroke, and other patients suffering from impaired bipedal walking. Reviews on exoskeletons, prostheses ,and orthoses are available in the literature [19, 24–27].

The main objective of many assistive devices is to reduce the metabolic cost of locomotion and, in particular, to decrease the metabolic energy required for running and/or walking. Although efforts on designing exoskeletons to reach this goal were initiated decades ago, the researchers have only recently succeeded in

accomplishing this goal. In 2013, Malcolm *et al.* [28] reported that a 6% ± 2% metabolic cost reduction was achieved by a tethered ankle exoskeleton. Later, Mooney *et al.* [17] and Collins *et al.* [29] also reported that their untethered ankle exoskeletons reduced metabolic energy consumption during walking by 8% and 7.2%, respectively. The metabolic cost reduction for running was achieved by Lee *et al.* [30] using a tethered hip exoskeleton in which they were able to improve the metabolic cost by 5.4% using simulation-optimized assistance torque profiles.

Several assistive devices have improved metabolic cost of locomotion since these initial studies [31]. Most of these devices assist the hip [30, 32–43] or the ankle [17, 28, 29, 44–47] joints, with the exception of untethered active knee exoskeleton in [48] which has been reported to reduce the metabolic burden of incline walking by 4.2% while carrying loads. Among these devices, the tethered exoskeletons have been reported to improve metabolic burden by 5.4%–17.4%, while untethered devices reduced the metabolic cost by 3.3%–19.8%. The hip exoskeletons showed superior performance compared to the ankle devices: metabolic cost improvements of tethered and untethered hip devices were reported as 17.4% and 19.8%, respectively, while tethered and untethered ankle exoskeleton improved walking efficiency by 12% and 11%. All devices that have been reported to improve the metabolic cost of human running were developed for the hip joint: passive hip devices [35, 37] reduced the metabolic burden by 6.4%–8%, while active hip devices [33, 34] reduced metabolic cost by 3.9%–5.4%, respectively. In addition to assisting healthy subjects, some assistive devices have been successfully employed in improving the walking economy of elderly [39, 42, 49] and patients with gait abnormality [50]. For instance, in [50], a 32% ± 9% metabolic cost reduction is reported for post-stroke patients during walking using a tethered exosuit. Readers are referred to comprehensive survey paper for details of these studies [19, 24–27, 31].

2.2 Bi-articular Actuation

Despite the developments in recent years, a number of challenges need to be surmounted to achieve high metabolic cost reduction to assist people more economically. One of the remarkable challenges on designing an efficient exoskeleton is mass minimization [16, 17, 51] and more importantly, minimizing distal masses [16] has a significant effect on exoskeleton efficiency since adding any mass to the distal extremity will increase the metabolic cost of the locomotion [16] and walking pattern [51]. To address this challenge, using passive exoskeletons without any actuation and power supply module has been proposed; although the metabolic cost reduction is low, they are lightweight assistive devices [29, 35]. An alternative solution is using tethered exoskeletons in which any heavy component is grounded, and actuation is off-board [28, 52]. However, these tethered exoskeletons restrict the mobility of the exoskeleton, and experimental results have been limited to lab-based scenarios.

It has been proven that human bipedal movement is an economical locomotion [1, 53] for various terrains [1, 54] and long distances [55]. It thus inspiration for designing efficient mobile exoskeletons not only to solve the distal mass and inertia problem but also to provide some additional advantages on the exoskeleton design such as lower power consumption. One of the main reasons for human bipedal locomotion efficiency is the presence of specific muscles, bi-articular muscles [56, 56, 57], which have several unique and notable roles on human locomotion.

A human lower limb has more muscles than is needed to actuate each degree of freedom(DOF) [57] which means that human lower extremity is redundantly actuated, consisting of mono-articular muscles, which is a type of muscles spanning a joint, and another type span two joints known as bi-articular muscles. Although the bi-articular muscles, i.e. muscles span two joints, are not necessary for performing movements, they have not been eliminated from the human muscular system during human musculoskeletal system evolution, indicating their advantage for human locomotion [57]. Moreover, the motor control system selects certain muscles to accomplish specific tasks [58], and the metabolic power consumption is one

of the main factors to select muscles to need to be activated among the muscles of desired degrees of freedom [57]. The significance of the bi-articular muscles in the energy economy of locomotion has been proven by several computational analyses [59, 60] studying bi-articular muscle activation during movement.

The effect of bi-articular muscles on locomotion and their benefits have been discussed in multiple studies [56, 57, 61, 62]. One of the key benefits of bi-articular muscles is transporting energy from proximal to distal joints produced by mono-articular muscles [56, 58, 63–66]; studies on jumping, which is a high power demanding task, revealed that power produced by mono-articular muscles at each joint is not sufficient to produce a high jump [63], and power transportation is necessary to meet the power requirement [63]. Moreover, this proximal to distal power flow allows for the distribution of the muscles weight, resulting in lower leg inertia [58] which inherently requires less energy to be actuated, leading to more economical locomotion [57, 58]. Elftman [67] also claimed, by studying the running task, that presence of bi-articular muscles can regenerate the negative work in phases of running in which adjacent joints have opposite power signs resulting in more economical movement [68] which was confirmed by [69] for walking and jumping as well.

Another central role of bi-articular muscles is facilitating the coupling of joint movement [57, 61]; thereby allowing control of the distal joint. For instance, if two joints are coupled with a stiff bi-articular muscle, displacement of a joint will cause the movement of another joint as well due to bi-articular muscle origin movement [61]. This phenomenon is called ligamentous action [70] which permits the location of most of the mono-articular muscles away from the distal joint and indirectly control them [61]; similar to the energy transportation feature of bi-articular muscles, this characteristic of bi-articular muscle leads to lower inertia leg [61, 70] which can decrease the metabolic cost of locomotion.

The third remarkable benefit of bi-articular muscles is controlling output force direction, which enables to get optimal output power. It has been shown that while most of the work is generated by mono-articular muscles, their output force

direction is not optimal [57]. Biarticular muscles are responsible for controlling output force direction [57], which must align with velocity to reach maximum output power [57]. It has also been proven that bi-articular muscles have lower contraction velocity than mono-articular muscles [61], resulting in the muscles having concurrent movements [71], and therefore higher muscle force compared to uniarticular muscles [57].

Biarticular muscle effect on limb stiffness has been studied by several researchers [72, 73]; one of the key findings is that loss of stiffness produced by bi-articular muscles cannot be compensated by mono-articular muscle stiffness [72, 73]. These studies revealed that the presence of multi-joint muscles would dramatically increase the central nervous system ability to modulate endpoint stiffness [73, 74]. Additionally, bi-articular muscle provides necessary coupling to regulate inter-limb interaction [75], and the absence of them would lead to elongated stiffness ellipse, reduce maximum achievable stiffness, and finally limit orientation range [72]. The stability effect of bi-articular muscles is another role that has been studied [76–78]. J. McIntyre *et al.* [76] proved that the presence of bi-articular muscles is necessary to provide a coupling enabling passive control of neuro-musculoskeletal system stability.

Considering all these advantages and roles of bi-articular muscles in human locomotion, it has inspired the robotics field researchers to adapt their designs to take advantage of bi-articular biological features [57]. Several actuators [79, 80], bipedal robots [77, 78, 81] ,and assistive devices have been designed based on multi-articular muscles configuration.

The bi-articular component has been used in designing several prostheses trying to mimic gastrocnemius muscle to reduce the actuators power consumption [82–86] where results represent a promising improvement on the efficiency of prostheses [86]. Several exoskeletons and exosuits are developed also to assist two joints simultaneously [32, 50, 52, 54, 87, 88]. Asbeck *et al.* [52] developed a soft exosuit assisting hip and ankle joints using the multi-articular concept on their design

and reported 21% to 19% nominal metabolic cost reduction. Another noteworthy soft bi-articular exosuit that has been designed for after stroke rehabilitation shows 32% metabolic cost reduction [50]. Quinlivan *et al.* [87] developed tethered multi-articular soft exosuit, which demonstrated 23% of metabolic burden reduction relative to powered of condition on healthy subject walking. Recently, Xiong *et al.* [89] proposed a multi-articular passive exoskeleton assisting hip and knee inspired by power transportation feature of bi-articular muscles where it stores negative mechanical work of knee joint and uses to assist hip extension, they succeeded to reduce the metabolic energy consumption by 7.6% without using any actuation module.

2.3 Simulation Based Analysis of Assistive Devices

Despite the progress that has been made on designing exoskeletons assisting healthy individuals, elderly and disabled subjects suffering impaired gait cycles, there is no systematic mechatronic design approach for exoskeletons to improve metabolic cost of human locomotion. A systematic design approach necessitates a means for rigorous and fair comparison of effects of different exoskeleton designs and assistance torque profiles on human metabolic cost of locomotion. However, studies based on comprehensive human subject experiments are not feasible. Such human-in-the-loop studies are challenging as multiple device prototypes need to be implemented, appropriate volunteers need to be recruited, safety of trials need to be established and sufficient number of experiments need to be conducted to achieve statistically reliable results. Furthermore, inability to collect certain information without introducing sensors inside the body [2], difficulty or impossibility of some measurements [12], and effects of training and fatigue on performance of subjects [13, 14] pose as some other important limitations of human-in-the-loop studies.

Simulation-based studies to design assistive devices can complement the experimental design approach to overcome many of these challenges. Studying assistive

devices through musculoskeletal simulations facilitates the research by reducing the need for physical prototyping and enables researchers to carry out fast, automated, and repeatable studies in a controlled environment, where different analyses can be conducted on human musculoskeletal models without the risk of injuries.

Simulation-based approaches have been used to design, optimize, and study different types of assistive devices [90]. Through these investigations, researchers suggested assistance profiles different than scaled biomimetic joint moments [2, 15]. Simulation-based studies also helped researchers to explain experimentally observed behaviors [91–93]. For instance, simulations showed that exoskeletons can have a negative effect on muscle fiber mechanics [93, 94]. Simulations have been used to suggest assistance strategies for subjects with impaired gait cycles [95, 96]. Grabke *et al.* [90] provides a comprehensive review of simulation-based studies on lower limb assistive devices.

OpenSim is an open-source software that has been extensively utilized in movement science related fields [12, 97]. Despite the limitations on musculoskeletal modeling and simulation [98], OpenSim enables researchers to investigate the human and animals movements by providing them with biomechanical models and simulation tools [12, 15]. OpenSim has been used to design and study assistive devices [2, 15, 99, 100]. For instance, Uchida *et al.* [2] simulated several combinations of ideal assistive devices on subjects running at 2 m/s and 5 m/s and reported that muscle activations can be decreased even in the muscles that do not cross the assisted joints, while they can be increased in some other muscles based on the configuration of the assistive device. Their simulation results confirmed and offered clarification on some of the similar phenomena observed in experimental studies. Effects of several ideal assistive devices on the metabolic cost of subjects carrying heavy loads have been studied by Dembia *et al.* [15]. This study suggests the effective joint configurations for ideal assistance and provides a perspective on how an assistive device can change muscular activities of subjects while carrying loads.

Recently, predictive simulations or simulation-based dynamic optimization approaches are emerging to study assistive devices. These approaches can capture the effect of assistive devices on the musculoskeletal kinematics and kinetics [101–103]. For instance, Nguyen *et al.* [104] have studied the effect of an ankle exoskeleton on subjects walking at normal speeds through predictive simulations, which enabled them not only to study the effect of the exoskeleton on the metabolic cost, but also to investigate how the exoskeleton affects subject's kinematics and ground reaction forces. Similarly, an active ankle powered prosthesis has been studied via predictive simulation framework by LaPre *et al.* [105]. Predictive simulations have also been employed to simulate knee [106] and ankle prostheses to investigate effects of various control approaches on them [107, 108]. Moreover, passive ankle prosthesis and ankle-foot orthosis stiffness has been optimized using this strategy [109, 110]. Finally, dynamic optimization approach has been used by Handford and Srinivasan [107, 108] to conduct a Pareto optimization of a robotic lower limb prosthesis, by simultaneously optimizing the metabolic and prosthesis cost rates.

2.4 Thesis Contribution to the Current State of Knowledge

This thesis presents a simulation-based mechatronic design approach to systematically design exoskeletons that can reduce the metabolic cost of locomotion. This approach can bridge the mechatronic design approach gap existing in the designing and controlling assistive wearable robotic. Furthermore, this thesis builds an engineering connection between the simulation-based and experimental-based studies aiming to develop optimal designs and optimal assistance profiles by introducing this design approach that can provide general guidelines for prototyping exoskeletons and designing experimental-based studies.

Along these lines, we propose a Pareto optimization approach that enables rigorous and fair comparison of effects of different exoskeletons designs and assistance torques on metabolic cost of locomotion. We demonstrate the proposed systematic

mechatronics system design approach by introducing a bi-articular exoskeleton design and comparing its efficiency with commonly used mono-articular exoskeletons. In particular, we simultaneously optimize power consumption of and metabolic rate reduction due to assistance provided by bi-articular and mono-articular hip-knee exoskeletons during unloaded and loaded walking conditions, and present a rigourous comparison among such devices.

The proposed bi-articular exoskeleton design is motivated by human anatomy, where bi-articulation is known to improve efficiency of human bipedal locomotion [56, 57, 111]. While a mono-articular hip-knee exoskeleton assists each joint directly by actuators mounted at these joints, the bi-articular hip-knee exoskeleton has all actuators mounted at the hip, mimicking bi-articular muscles in the human musculoskeletal system that improve locomotion performance, by enabling power transformation from proximal to distal joint [56, 63–65, 111, 112] and promoting power regeneration between adjacent joints [68, 69], facilitating the coupling of joint movements [57, 61], and improving distribution of muscle weight and leg inertia [57, 61, 112].

Our multi-criteria optimization results subsume single objective optima. In particular, our results include the solution to a commonly addressed single objective optimization problem that aims to maximize metabolic rate reduction of exoskeletons without considering their power consumption or torque capabilities, commonly referred to as ideal exoskeleton optimization [2, 15]. Our ideal exoskeleton optimization results verify that, without any limits on actuator torques and power consumption, both ideal mono-articular and bi-articular devices can reach the same level of metabolic rate reduction under the same total power consumption. Moreover, we show that the assistance torques not only improve the metabolic rate, but can also decrease the peak reaction forces and moments at the knee, patellofemoral, and hip joints considerably.

Furthermore, in addition to the direct effect of ideal exoskeletons on the muscular activities of the hip and knee joints in the sagittal plane, we verify that assistance provided by the exoskeletons can also indirectly affect the activity of muscles at

the ankle joint and the muscles related to the hip abduction. In addition, we show that loading subjects with a heavy backpack results in a predictable change in assistance profiles, by causing a proportional increase in the magnitude and the time shift.

As the main contribution of this thesis, we introduce different levels of peak torque constraints on actuators of both mono-articular and bi-articular exoskeletons and conduct a multi-criteria comparison of their performance by considering the metabolic cost reduction and the power consumption metrics, simultaneously.

We show that introducing sufficiently large torque limits to the actuators of both devices does not have a large impact on the metabolic cost reduction, while such limits can cause a considerable reduction in the power consumption of the exoskeletons. We also show that both devices can reach similar performance levels for different assignments of peak torques to hip and knee joints, while larger peak torque limits are required for mono-articular exoskeletons compared to bi-articular devices. Despite the similar assistance levels provided by both exoskeletons, mono-articular exoskeletons demonstrate better performance on reducing the peak reaction moments and forces, while the power consumption of bi-articular exoskeletons is less affected by the loading of subjects.

We demonstrate the effect of regeneration on the power consumption of exoskeletons by superposing this effect on the Pareto-front curves. We show that regeneration can have a significant impact on power efficiency of exoskeletons depending on the efficiency of regeneration system, the kinematics of the exoskeleton, and the torque/power limitations of the actuators. Our results indicate that the knee actuators of mono-articular devices have more regeneration potential, while all actuators of the bi-articular devices have large regeneration potential.

We also demonstrate the detrimental effects of inertial properties of exoskeletons on metabolic cost of locomotion, by superposing this effect on the Pareto-front curves. In particular, we estimate the effect of additional mass and inertia on metabolic rate of subjects for mono-articular and bi-articular exoskeletons based

on [16] and quantify these effects through a modified version of the augmentation factor proposed in [17].

Our results indicate that the added device inertia causes optimal mono-articular and bi-articular devices lose their efficiency by 42.51% ± 0.17%–55.51% ± 0.11%, and 35.12% ± 0.21%–49.67% ± 0.21%, respectively. For bi-articular exoskeletons, inertial effects simply shift the Pareto-front curve, without significantly affecting the Pareto-optimal configurations, while non-dominated configurations are significantly affected by the device inertia for the mono-articular exoskeletons.

Chapter 3

Exoskeletons Design and Analysis

3.1 Kinematic Modeling

The bi-articular exoskeleton is designed to assist the hip and knee joints. The exoskeleton is inspired by the bi-articular muscles and their functionality and the aim of the design was to keep the large portion of the device weight around the proximal joint (Hip) while delivering the required power to the distal joint (Knee). A parallelogram mechanism is purposed in the exoskeleton to accomplish this goal and take advantage of the biological features of bi-articular muscles in which the hip joint will be assisted by applying directly the torque on the joint and second actuator torque will be applied to knee joint through the parallelogram mechanism.. The purposed assistive device is shown in Figure 3.1 in which q_A to q_D represents the angles of joints, and $Torso$ to D and L_A to L_E stand for the bodies and link lengths, respectively, in the mechanisms, and the configuration level and motion level forward kinematics of the bi-articular exoskeleton can be written as Eq (3.1) and (3.3).

$$x_{Bi} = l_A \cos(q_A) + (l_E + l_D) \cos(q_B) \tag{3.1}$$

$$y_{Bi} = l_A \sin(q_A) + (l_E + l_D) \sin(q_B) \tag{3.2}$$

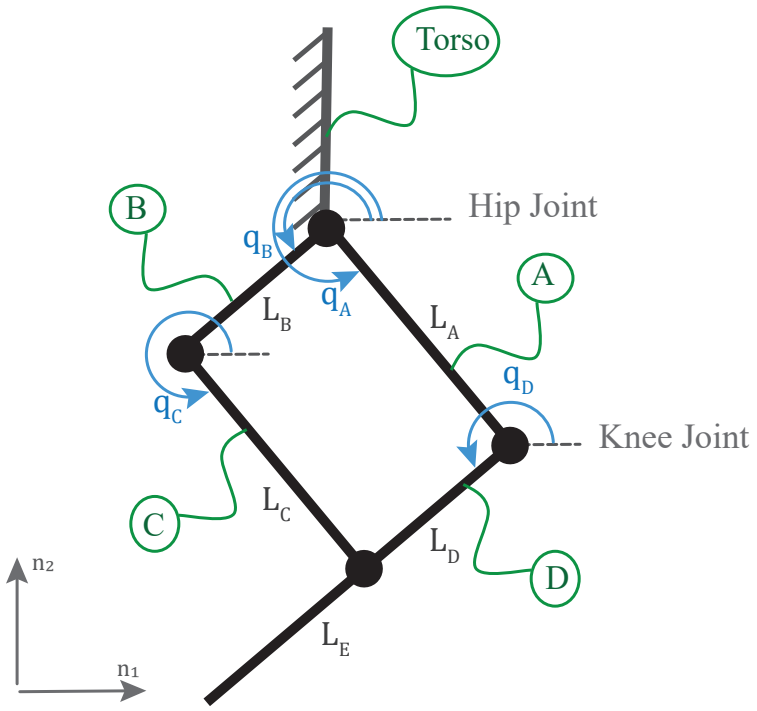

FIGURE 3.1: Bi-articular hip and knee robotics assistive device kinematic model.

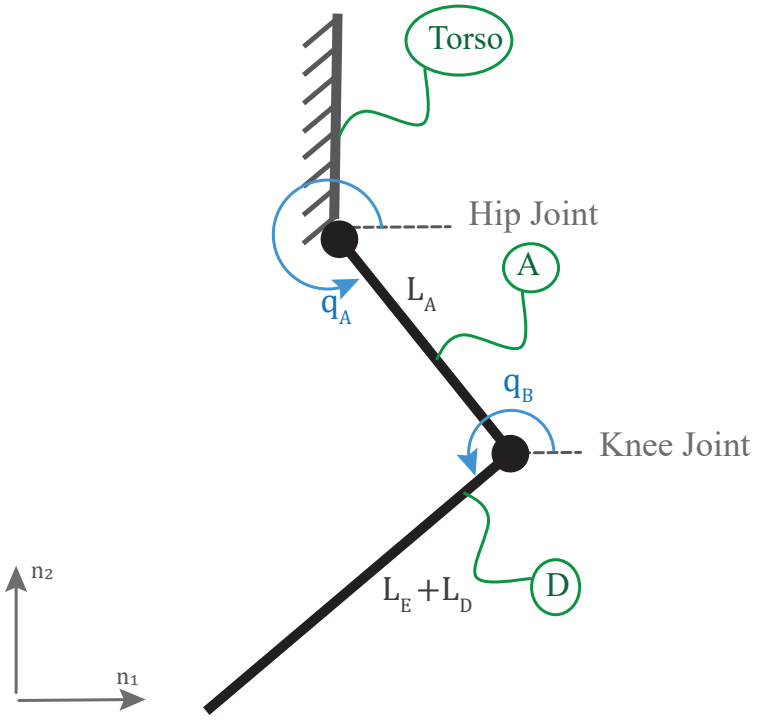

FIGURE 3.2: Mono-articular hip and knee robotics assistive device kinematic model.

$$J_{Bi} = \begin{bmatrix} -l_A \sin q_A & -(l_E + l_D)\sin(q_B) \\ l_A \cos(q_A) & (l_E + l_D)\cos(q_B) \end{bmatrix} \tag{3.3}$$

A mono-articular exoskeleton can be modeled as a two-link serial manipulator as shown in Figure 3.2 in which each joint was assisted by the joint actuator directly. The kinematics modeling of the mono-articular exoskeleton at the configuration and motion levels are represented in Eq (3.4) and (3.6), respectively.

$$x_{mono} = l_A \cos(q_A) + (l_E + l_D)\cos(q_A - q_B) \tag{3.4}$$

$$y_{mono} = l_A \sin(q_A) + (l_E + l_D)\sin(q_A - q_B) \tag{3.5}$$

$$J_{Mono} = \begin{bmatrix} -l_A \sin q_A - (l_E + l_D)\sin(q_A - q_B) \\ l_A \cos q_A + (l_E + l_D)\cos(q_A - q_B) \\ (l_E + l_D)\sin(q_A - q_B) \\ -(l_E + l_D)\cos(q_A - q_B) \end{bmatrix} \tag{3.6}$$

As can be interpreted from the kinematics of the exoskeletons , a linear mapping between mono-articular and bi-articular exoskeletons can be established to relate these two devices through a Jacobian as is represented in Eq (3.7).

$$\begin{gathered} \omega_{\text{monoarticular}} = J\omega_{\text{biarticular}} \\ \begin{bmatrix} {}^{\text{torso}}\omega_{\text{mono}}{}^{\text{femur}} \\ {}^{\text{femur}}\omega_{\text{mono}}{}^{\text{tibia}} \end{bmatrix} = \begin{bmatrix} 1 & 0 \\ -1 & 1 \end{bmatrix} \begin{bmatrix} {}^{\text{torso}}\omega_{\text{bi}}{}^{\text{femur}} \\ {}^{\text{torso}}\omega_{\text{bi}}{}^{\text{tibia}} \end{bmatrix} \end{gathered} \tag{3.7}$$

Where ${}^{\text{torso}}\omega_{\text{mono}}{}^{\text{femur}}$ and ${}^{\text{femur}}\omega_{\text{mono}}{}^{\text{tibia}}$ represent the angular velocities of the hip and knee actuators of the mono-articular exoskeletons, respectively, while ${}^{\text{torso}}\omega_{\text{bi}}{}^{\text{femur}}$ and ${}^{\text{torso}}\omega_{\text{bi}}{}^{\text{tibia}}$ stand for the angular velocities of the bi-articular hip and knee actuators, respectively. Using Eq (3.7) which is a mapping between the angular velocities of the exoskeletons, we can derive the mapping between the

torque provided by exoskeletons as shown in Eq (3.8).

$$\begin{gathered}\tau_{\text{biarticular}} = J^T \tau_{\text{monoarticular}} \\ \begin{bmatrix} \tau^{\text{torso/femur}}{}_{\text{bi}} \\ \tau^{\text{torso/tibia}}{}_{\text{bi}} \end{bmatrix} = \begin{bmatrix} 1 & 0 \\ -1 & 1 \end{bmatrix}^T \begin{bmatrix} \tau^{\text{torso/femur}}{}_{\text{mono}} \\ \tau^{\text{femur/tibia}}{}_{\text{mono}} \end{bmatrix}\end{gathered} \tag{3.8}$$

Where $\tau^{\text{torso/femur}}{}_{\text{bi}}$ and $\tau^{\text{torso/tibia}}{}_{\text{bi}}$ stand for torques of the bi-articular hip and knee actuators, respectively, and $\tau^{\text{torso/femur}}{}_{\text{mono}}$ and $\tau^{\text{femur/tibia}}{}_{\text{mono}}$ represent the torques of the mono-articular hip and knee actuators, respectively. This mapping between the bi-articular and mono-articular exoskeletons is valid under the assumption that the hip and knee actuators have no saturation. Hence, when the torques and velocities of the joints are available, both exoskeletons can provide the same level of assistance.

3.2 Actuator Selection

The exoskeletons are considered to be direct drive and in the direct drive exoskeleton, motors are chosen to maximize continues and peak torque [113] and acceleration capability. To select the suitable actuator, several motors which matching with our mechanical design criteria were collected and characterized. Peak specific torque can be characterize using Eq (3.9) proposed by [114].

$$K_t := \frac{K_t i_p}{m} \qquad \left[\frac{Nm}{kg}\right] \tag{3.9}$$

Where K_t is actuator's torque constant Nm/A, motor's peak current is i_p and m is motor's mass. To analyze continues torque of the actuators, Kenneally *et al.* [113] proposed a new metric named "Thermal Specific Torque" defined as Eq (3.10) representing the actuators' ability on torque generation in contrast with Joule heating wasting energy [113].

$$K_{ts} := \frac{K_t}{m}\sqrt{\frac{1}{R_{th}R}} \qquad \left[\frac{Nm}{kg\sqrt{^\circ C}}\right] \tag{3.10}$$

Where R and R_{th} are motor's electrical (Ω) and thermal resistance ($^{\circ}C/W$) respectively. Finally to analyze the acceleration capability, Wensing *et al.* [115] defined following equation:

$$AccelerationCapability = \frac{\tau}{J_{rotor}} \tag{3.11}$$

Where τ is nominal torque and J_{rotor} represents the rotor inertia. Using these metrics, several actuators were analyzed and based on the metrics results and availability, the actuator was selected.

3.3 Exoskeletons Characterization

To study the bi-articular design of exoskeleton, some features of exoskeletons was computed and compared with mono-articular configuration of exoskeleton.

3.3.1 Endpoint Stiffness

One of the bi-articular muscles feature is changing endpoint stiffness, to study this on exoskeletons the joint stiffness and endpoint stiffness can be analytically analyzed. The joint stiffness can be defined as $S = \partial T/\partial Q \in \mathbb{R}^{n\times n}$ where T and Q are joint torque and deflections and n is number of joints [80]. In the exoskeletons considered here, joint stiffness is equal to the actuators stiffness. The joint stiffness can be mapped to endpoint Cartesian stiffness through the exoskeletons Jacobian as in Eq (3.12).

$$K = J(q)^{-T} S J(q)^{-1} \tag{3.12}$$

Hogan [73] introduced a method to visualize the endpoint stiffness K. To represent the stiffness at the end-effector of mono-articular and bi-articular exoskeletons, the K matrix eigenvalues were derived and ellipsoid was shaped by minimum and maximum eigenvalues as a minor and major axes of the ellipsoid. Then the ellipsoids were transformed to the endpoint and oriented. To define the orientation of the ellipsoids, Euclidean space dot product definition was used [80]:

$$\theta = \arccos\left(\begin{bmatrix}1\\0\end{bmatrix}.\nu\right) \tag{3.13}$$

Where ν is denoted to normalized eigenvector corresponding to maximum eigenvalue and θ represents angle between the eigenvector ν and the $x-$axis. Since the exoskeletons are represented and analyzed in sagittal plane, using θ the rotation matrix can be easily computed :

$$R(\theta) = \begin{bmatrix} \cos(\theta) & -\sin(\theta) & 0 \\ \sin(\theta) & \cos(\theta) & 0 \\ 0 & 0 & 1 \end{bmatrix} \tag{3.14}$$

To translate the ellipsoids to the end-effector position, the kinematics of each configuration was used. It is worth mentioning that the transformation of the ellipsoid is a qualitative measurement while the size of ellipsoids is a quantitative analysis of exoskeletons as discussed in [80].

3.3.2 Velocity Manipulability

To measure the velocity that can be generated in operational space by the set of given joint space velocities and positions velocity manipulability can be used where it maps the surface of the sphere in joint velocity space into the surface of the ellipsoid in the end-effector velocity space [116]. This mapping can be written as Eq (3.15) to assess each configuration of the exoskeleton in terms of velocity manipulability:

$$v_e^T (J(q) J^T(q))^{-1} v_e = 1 \tag{3.15}$$

To orient and transform of the ellipsoids, Eq (3.13) and (3.14) was used. Maximum eigenvalue which corresponds to the major axis of the ellipsoid represents the largest velocity that can be achieved on the given configuration and minor axis represents the least possible velocity of the end-effector; additionally, achieving to unit eccentricity can lead to more isotropic motion of the endpoint along with all directions in operational space [116].

3.3.3 Force Manipulability

Based on the duality between motion level kinematics and statics, manipulability of a robot as well as the exoskeletons can be analyzed with reference to forces where the force manipulability can be defined as Eq (3.16) [116].

$$f_e^T(J(q)J^T(q))f_e = 1 \tag{3.16}$$

It can be noticed that the main difference between force and velocity manipulability is in the JJ^T resulting in the coincidence of principal axes and duality of their dimensions. As a result, achieving a large velocity will lead to low renderable force in operational space and vice versa [116]. It can be easily understood from the duality of velocity and force ellipsoid that isotropic force rendering in all direction requires the force ellipsoid to be closer to the sphere at operational space.

3.3.4 Reflected Inertia

One of the central features for bi-articular muscles is distal mass minimization and bi-articular configuration of the exoskeleton is also designed to keep the main portion of mass near to the human center of mass. To study this feature in the exoskeletons, reflected inertia of each configuration can be analytically studied as in Eq (3.17).

$$M_x = J^{-T}M_qJ^{-1} \tag{3.17}$$

Where the J represents the Jacobian where it needs to be full ranked [116], inertia matrix in joint and operational space are represented by M_q and M_x respectively.

3.4 Results

3.4.1 Actuator Specification

To select the actuator for exoskeletons, we select RE and EC-Flat series of actuators from MaxonMotor and HT, QB, and Megaflux series from Emoteq. Based on

the defined criteria actuators were characterized with respect to their outer diameter due to mechanical design considerations. Based on human kinematics during running and walking [117], high acceleration capability is required to track the kinematics of each joint where MaxonMotor EC series and Emoteq Megaflux have adequate capability on acceleration while it compatible with mechanical specifications.

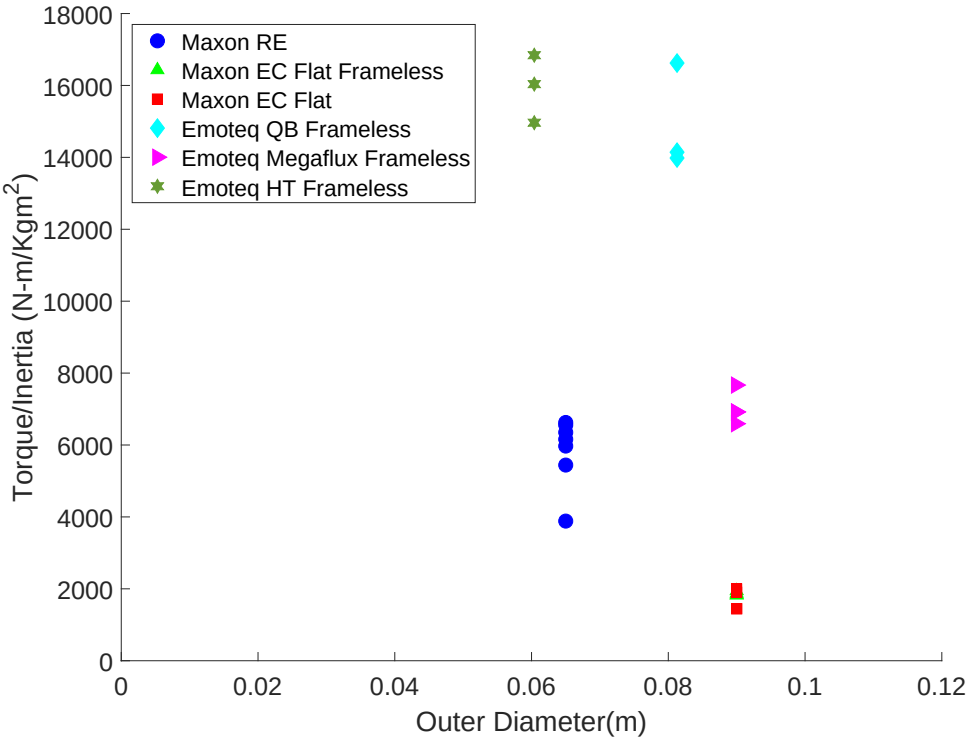

FIGURE 3.3: Actuators acceleration capability.

Exoskeleton actuation were considered as a direct drive actuation and based on kinetics of human joints, actuator needs to have a high peak torque as well as high continues torque to be able to assist human target joints, we characterized these two specifications based on metrics defined in Eq (3.9) and (3.10).

As shown in Figure 3.4 and 3.5, Emoteq megaflux and MaxonMotor EC Flat series has better performance in supplying peak and continues torques among the available actuators.

Based on these three criteria and the actuators availability for our group, we selected MaxonMotor EC 90 flat 260 W for both knee and hip actuation module

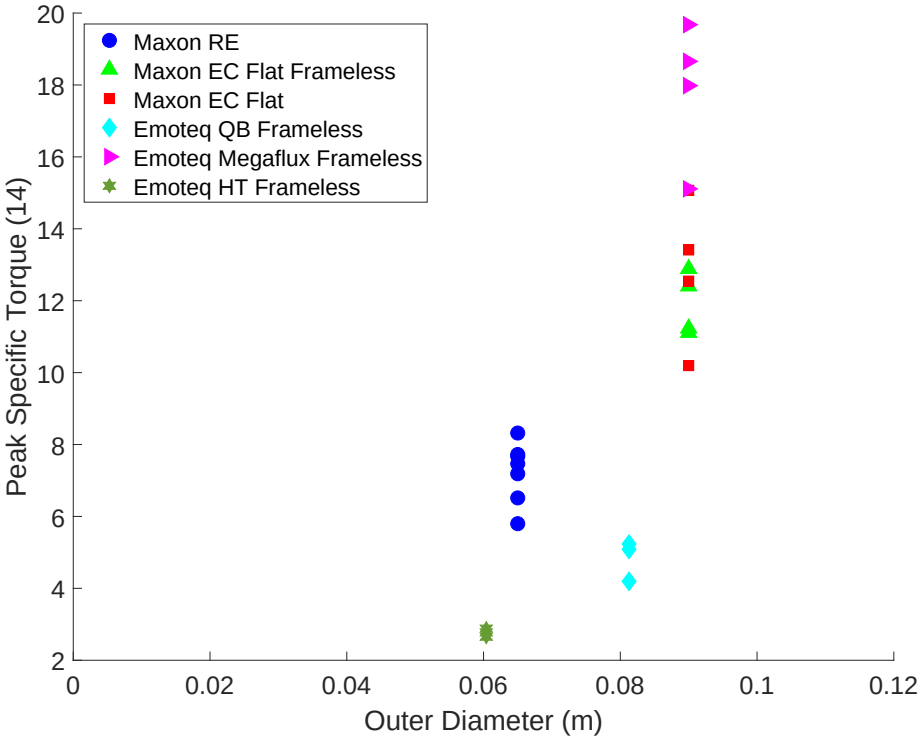

FIGURE 3.4: Peak specific torque.

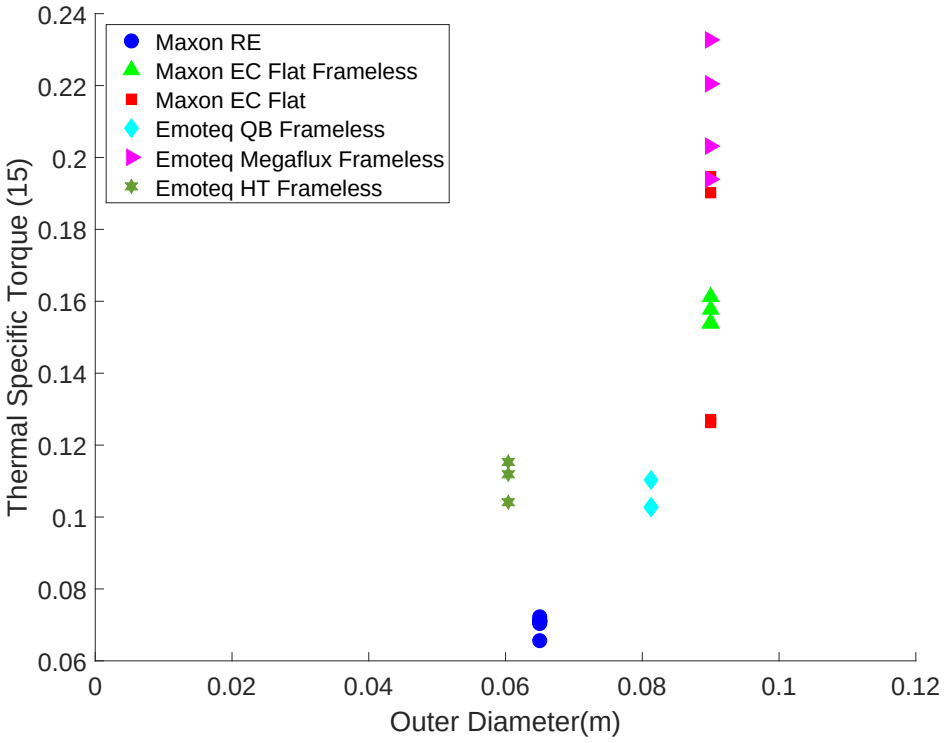

FIGURE 3.5: Thermal specific torque.

and from mechanical specs of exoskeletons, inertia and link length were extracted to characterize them.

3.4.2 Exoskeletons Characterization

The exoskeletons mechanism with dimensional and inertial specification extracted from the mechanical design were characterized to study their endpoint stiffness, manipulability ,and reflected inertia.

Figure 3.6 represents the exoskeletons endpoint stiffness in some of the knee and hip joint configurations during a walking gait cycle where bi-articular exoskeleton has better performance than uniarticular one. More quantitatively, in 65% of a walking gait cycle, bi-articular configuration of exoskeleton shows higher stiffness range than mono-articular exoskeleton enabling to adjust the endpoint stiffness according to human tasks required stiffness.

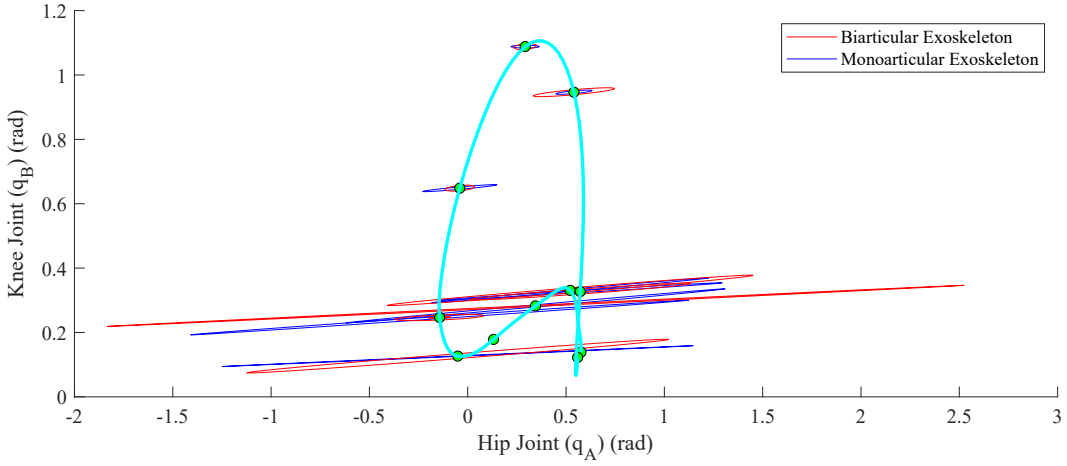

FIGURE 3.6: Exoskeletons endpoint stiffness range during a walking gait cycle.

Based on the bi-articular exoskeleton design, knee actuator was considered to apply and transform the torque form proximal to distal joint similar to bi-articular muscles, therefore, actuation module of knee were removed from knee joint by distal assist of the joint which was expected to reduce reflected inertia of exoskeleton needs to be actuated, out analysis on reflected inertia of each configuration of the exoskeleton confirmed this hypothesis and revealed that in 55% of a gait cycle, mono-articular exoskeleton has more reflected inertia than bi-articular one; this less reflected inertia reveals that bi-articular exoskeleton inherently requires less

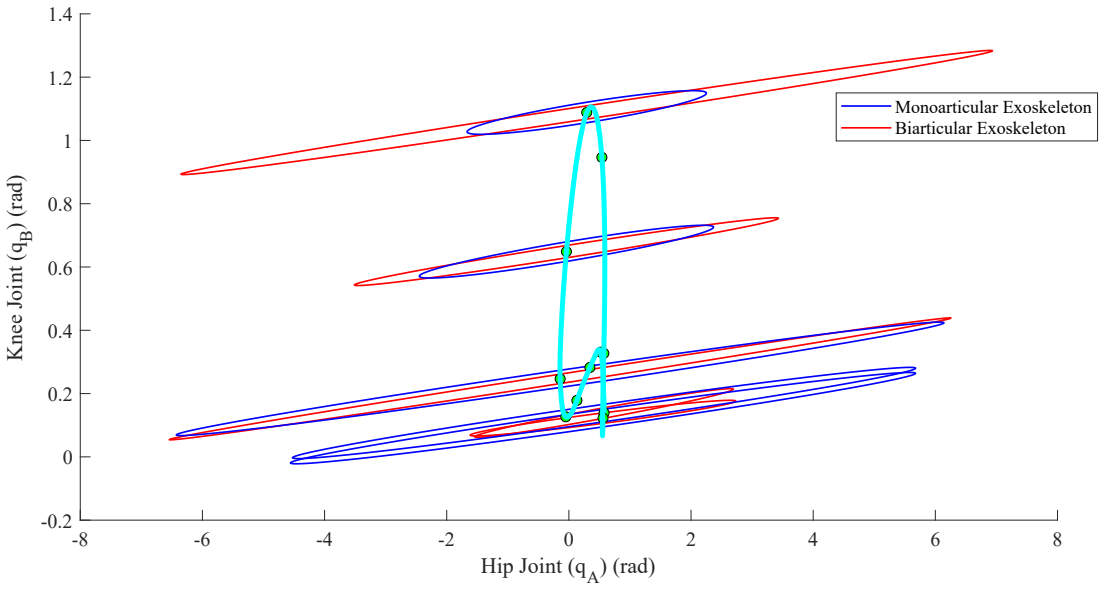

FIGURE 3.7: Exoskeletons endpoint stiffness range during a walking gait cycle.

actuation power. Manipulability analysis also disclosed bi-articular exoskeleton's larger and more isotropic force and velocity ellipsoids.

Chapter 4

Musculoskeletal Simulations

4.1 Musculoskeletal Model

The exoskeletons were studied through musculoskeletal simulations by conducting the simulations of seven subjects walking with no load and while carrying a 38 kg load on the torso at their chosen speed. The data used in this study was experimentally collected and processed by Dembia *et al.* [15] and has been made publicly available.

The musculoskeletal model used in the simulations, which was the same as the model used by [15], was a three-dimensional model developed by Rajagopal *et al.* [118] with 39 degrees of freedom in which the lower limbs were actuated using 80 massless musculotendon actuators, and the upper limb was actuated by 17 torque actuators [118]. This three-dimensional musculoskeletal model was adapted by locking some unnecessary degrees of freedom for both normal walking and walking with a heavy load scenarios and modeling the extra load on the torso of the musculoskeletal model for the walking with heavy load condition [15].

Since this research was built upon the study performed by [15], we followed similar terminologies in most of the cases to avoid any confusion. Therefore, the *loaded* condition refers to subjects walking while carrying a 38 kg load on their torso while

the *noload* condition references subjects walking without any extra load at their chosen speed.

4.2 Simulation Procedure

The first step of conducting the simulations for each subject is scaling the generic dynamic model to acquire a musculoskeletal model matching the anthropometry of each subject, which was performed using OpenSim Scale Tool, and the maximum isometric forces of the muscles were scaled according to the mass and height of each subject [15]. After obtaining the scaled model for each subject, the inverse kinematics for each subject was computed using OpenSim Inverse Kinematics Tool and the motion capture data collected experimentally to obtain the angle trajectories of joints.

At the next stage of the simulation workflow, the scaled model, inverse kinematics, and ground reaction forces were employed to run the RRA algorithm [97]. The RRA algorithm reduces the incompatibility of experimental data, including ground reaction forces and trace data, and the musculoskeletal model by slightly adjusting inertial properties and kinematics of the simulated subject. The adjusted model and kinematics generated by RRA were then employed to perform muscle driven simulations using a computed muscle control algorithm in OpenSim [119].

The computed muscle control (CMC) algorithm simulates the muscle recruitment of the subject by resolving the muscle redundancy problem using static optimization to find the required muscle excitations to track the adjusted kinematics. The CMC simulation output was then used to run the Analysis Tool of OpenSim to compute the metabolic power consumption, muscle moments, and joint reaction forces of the subject.

The OpenSim computed muscles control algorithm solves the muscle redundancy problem to track experimentally measured motion using effort-based objective, as represented in Eq (4.1). This objective function was optimized to obtain a set of

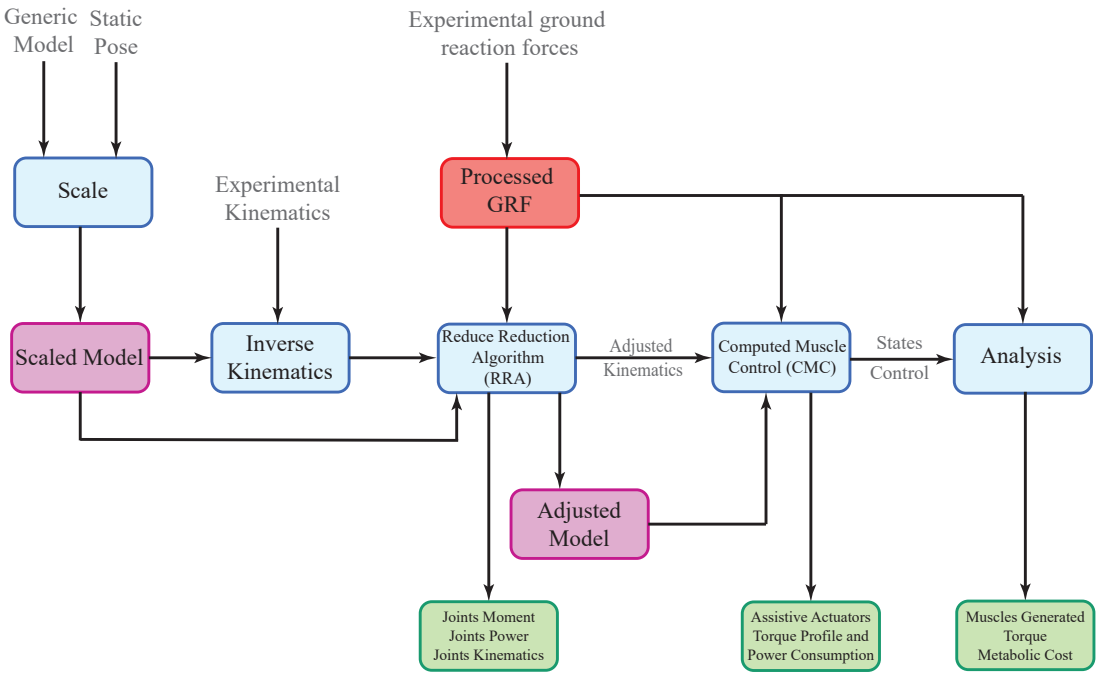

FIGURE 4.1: Opensim simulation procedure block diagram.

muscle excitations to track measured motions and forces within a specified tolerance at each time step during the motion of interest using a static optimization method [98]. Therefore, the kinematics and dynamics of the subject remain consistent during the simulations, and any additional mass and inertia on the subject that has not been captured by experiments cause a systematic error in the results.

$$J = \sum_{i \in nMuscles} a_i^2 + \sum_{i \in nReserves} \left(\frac{\tau_{r,i}}{w_{r,i}}\right)^2 \tag{4.1}$$

With the knowledge of the OpenSim neural control algorithm, we used the adjusted model and kinematics provided by [15] instead of reproducing all data from the beginning of the simulation procedure, which also helped ease the verification of the simulations procedure thanks to [15] for verified simulations data.

Metabolic model. To calculate the estimated instantaneous metabolic power of subjects, Umberger's muscle energetic model [120] which was modified by Uchida *et*

al. [121], was employed in which average power consumption of a muscle during a gait cycle was calculated using Eq (4.2) [121].

$$P_{avg} = \frac{m}{t_1 - t_0} \int_{t_0}^{t_1} \dot{E}(t)dt \tag{4.2}$$

Where m is muscle mass, and $\dot{E(t)}$ is the normalized metabolic power consumed. This model generates metabolic power of all muscles; the whole body metabolic power is then calculated by summing the metabolic power of all muscles [121]. To compute the gross metabolic power consumption of each subject, we integrated the metabolic power over the gait cycle and then normalized it to the mass of each subject.

As is mentioned in [15], due to experimental data insufficiency, the simulations of some subjects and trials were not a complete gait cycle; therefore, the metabolic power was calculated for a half of a gait cycle for these subjects and trials, which is a verified method for computing the power according to [15].

4.2.1 Joint reaction forces and moments analysis.

Since the equations of motion of the musculoskeletal model were formulated in terms of the generalized coordinates and generalized forces, the internal forces and moments were not solved while performing the computed muscles control or residual reduction algorithm simulations. Consequently, we employed a joint reaction analysis provided by OpenSim to compute the resultant forces and moments between two consecutive bodies in the kinematic chain connected via a joint. The contact forces and moments of joints were obtained by formulating them through the Newton-Euler equation of motion and solving them recursively from the distal to proximal joints.

The free body diagram of ith body and joint is provided in Figure 4.2, which was used for computing the reaction forces and moments of the of ith joint. The G, S_i, and J frames represent the ground or Newtonian frame, body frame, and joint frame (i.e. offset frame according to the OpenSim terminology). The $\sum \mathbf{F}_{muscles}$

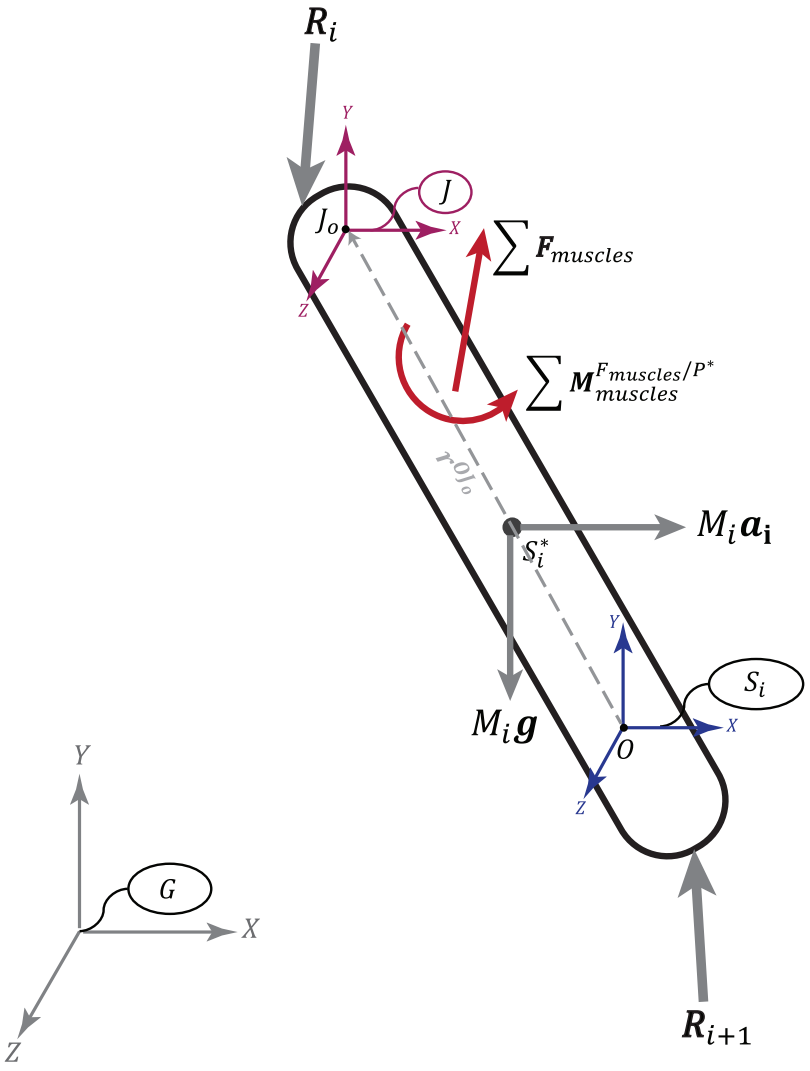

FIGURE 4.2: Free body diagram of a body.

and $\sum \mathbf{M}^{F_{muscles}/P^*}_{muscles}$ are resultant force and moment of the forces and moments of musculotendon actuators. The points O, S_i^*, and J_o are the origin of the body, center of mass of body, and center of joint. This free body diagram adopted from the figure represented in the Supplementary Material of [122]. The Newton-Euler formulation for ith body can be represented as Eq (4.3) as adapted from [122] which was solved to obtain the contact forces and moments acting on the body.

$$\begin{bmatrix} \mathbf{F_o} \\ \tau_\mathbf{o} \end{bmatrix} = M_i(q)\,\mathbf{a}_i + \mathbf{F}_{\text{constaints}} - \left(\sum \mathbf{F}_{\text{muscle}} + \mathbf{F}_{\text{external}} + \mathbf{F}_{\text{gravity}} + \mathbf{R}_{i+1} \right) \quad (4.3)$$

Where $M_i(q)$ and $\mathbf{a}_i$, respectively, represent the mass matrix of the body i and

vector of the linear and angular acceleration of body i expressed at ground frame, and $F_{constaint}$ accounts for the forces applied by constraints, if applicable. Through this equation F_{muscle}, $F_{external}$, and $F_{gravity}$ represent the force and moment applied by a muscle, forces applied externally (e.g. ground reaction forces and moments), and gravitational forces applied to the body respectively. Lastly, R_{i+1} accounts for the applied reaction forces from the $(i+1)$th to the ith joint.

Since these reaction forces and moments are expressed at the origin of the body frame to include all terms in a common reference frame, they need to be transformed to the location of the joint frame (i.e. offset frame) where the joint has been defined between two consecutive bodies as represented in Eq (4.4) [122].

$$\begin{bmatrix} \mathbf{F}_i \\ \tau_i \end{bmatrix} = \begin{bmatrix} \mathbf{F_o} \\ \tau_\mathbf{o} \end{bmatrix} - \begin{bmatrix} \mathbf{r}^{\mathrm{OJ}_o} \times \mathbf{F}_O \\ \emptyset_{3\times 1} \end{bmatrix} \tag{4.4}$$

The vectors of F_i and τ_i represent the joint reaction force applied to the joint of interest expressed at the ground frame.

4.3 Modeling and Simulations of Assisted Subjects

4.3.1 Modeling of assistive devices.

The kinematics of the exoskeletons were already discussed; in order to model ideal exoskeletons in OpenSim framework, we used the Torque Actuators provided by OpenSim API. Torque actuators of the bi-articular and mono-articular exoskeletons were assigned, as shown in Figure 4.3 and 4.4 in which the blue and red torques represent the action and reaction torques of the assistive actuators on the bodies. As is represented in Figure 4.3, both torque actuators of the bi-articular exoskeleton were assigned to the torso; the reaction forces of the actuators were then applied to the torso, which matches the kinematics and dynamics model of

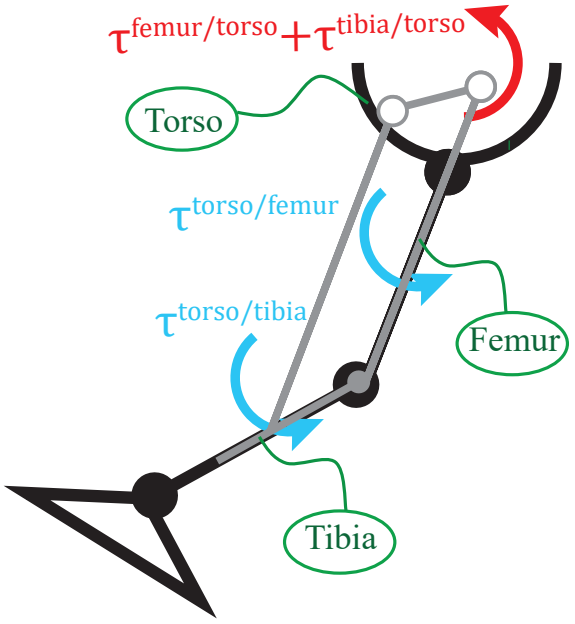

FIGURE 4.3: Bi-articular hip and knee robotics assistive device musculoskeletal modeling.

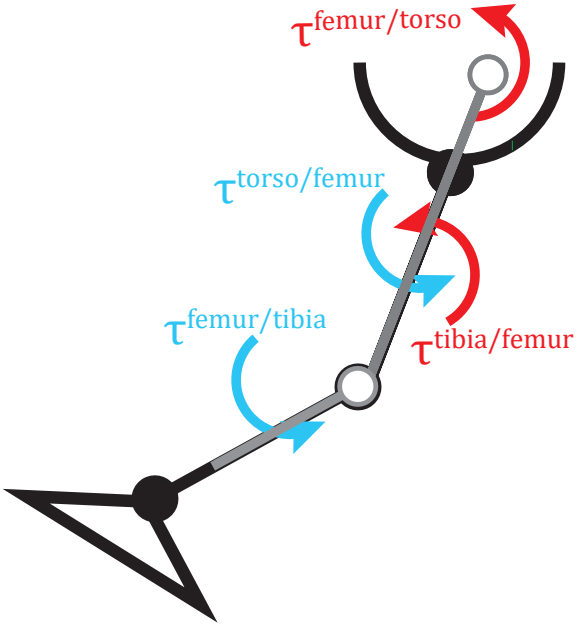

FIGURE 4.4: Monoarticular hip and knee robotics assistive device musculoskeletal modeling.

the bi-articular exoskeleton.

$$\tau^{hip}_{Biarticular} = \tau^{torso/femur} \tag{4.5}$$

$$\tau^{knee}_{Biarticular} = \tau^{torso/tibia} \tag{4.6}$$

The mono-articular exoskeleton (Figure 4.4) was modeled by assigning the hip joint actuator from the torso to the femur body and the knee joint actuator was assigned from the femur to the tibia body at which the reaction torque of the knee torque applied to femur body:

$$\tau^{hip}_{Monoarticular} = \tau^{torso/femur} \tag{4.7}$$

$$\tau^{knee}_{Monoarticular} = \tau^{femur/tibia} \tag{4.8}$$

4.3.2 Computed muscle control adjusted objective function.

To investigate the performance of the assistive devices and their effect on the human musculoskeletal system through the OpenSim simulation framework, we used the CMC algorithm. The computed muscle control algorithm objective function depends on the sum of squared muscle activation and reserve actuators, which compensates for modeled passive structures and potential muscle weakness [15]:

$$J = \sum_{i \in nMuscles} a_i^2 + \sum_{i \in nReserves} (\frac{\tau_{r,i}}{w_{r,i}})^2 \tag{4.9}$$

where w_i determines the weight of reserve actuators, which is generally selected as a small number to highly penalize the use of reserve actuators. By adding assistive device actuators (i.e. Torque Actuators) to the musculoskeletal model of the subject, they are added to the CMC tool objective function.

The adjusted objective function includes the assistive actuators as is expressed in Eq (4.10), and by selecting proper weights for the assistive actuators, they can be chosen by the optimizer as the actuation of the assigned degree of freedom.

$$J = \sum_{i \in nMuscles} a_i^2 + \sum_{i \in nExo} \left(\frac{\tau_{exo,i}}{w_{exo,i}}\right)^2 + \sum_{i \in nReserves} \left(\frac{\tau_{r,i}}{w_{r,i}}\right)^2 \tag{4.10}$$

In the adjusted objective function, $w_{exo,i}$ is torque actuator weights, which is named

optimal force in OpenSim [15] penalizing the usage of torque actuators. By selecting a large number, penalization of the actuators is insignificant and they are selected for actuating the joint between two bodies assigned for the torque actuator. If we select a small optimal force, the optimizer will highly penalize the usage of exoskeleton actuators. To study each configuration of the exoskeleton at their maximum performance, the assigned torque actuator's optimal force was selected as 1000 N-m enabling the optimizer to use the assistive actuators as much as possible during a gait cycle simulation.

4.3.3 Power calculation of metabolics and actuators.

Similar to the unassisted procedure, the instantaneous metabolic power of the subjects was computed using the energetic model of Uchida *et al.* [121]. The metabolic rate of each subject was then derived through integration of the metabolic power over the gait cycle. In order to compute the power consumption of the assistive actuators, the power profiles of the actuators in both sides were obtained and their absolute power profiles were integrated over the gait cycle and normalized to the subject mass. Similar to the power consumption of the exoskeleton procedure, the negative power or regeneratable power through a gait cycle was calculated by obtaining the negative power profile and integrating it over the gait cycle and normalizing it to the mass of the subject. In order to estimate the cost of carrying device without considering the mass of non-actuator components, we obtained the maximum positive power of actuators for each joint in both sides and conducted comparisons among the different devices and different loading conditions.

4.3.4 Joint reaction forces and moments analysis.

We performed a similar joint reaction force analysis to study the effect of the assistive devices on the reaction forces and moments of assisted and unassisted joints. Nonetheless, appending assistive devices to the musculoskeletal system modifies the Newton-Euler equations of motion of bodies to which the Torque

Actuators were appended (i.e., Eq (4.3)), as expressed in Eq (4.11).

$$\begin{bmatrix} \mathbf{F_o} \\ \tau_\mathbf{o} \end{bmatrix} = M_i(q)\,\mathbf{a}_i + \mathbf{F}_{\text{constaints}} - \left(\sum \mathbf{F}_{\text{muscle}} + \sum \mathbf{F}_{\text{assistive}} + \mathbf{F}_{\text{external}} + \mathbf{F}_{\text{gravity}} + \mathbf{R}_{i+1} \right) \tag{4.11}$$

where $\sum \mathbf{F}_{\text{assistive}}$ represents the applied or reaction torques of the assistive actuators.

4.4 Validation of Simulations

OpenSim model and simulations are validated according to the comprehensive procedures detailed by Hicks *et al.* [98] and utilized by Dembia *et al.* [15] to verify simulations of assistive devices.

This study builds upon verified adjusted models, adjusted kinematics, and processed ground reaction forces made available by [15]. Furthermore, the muscular activations resulting from the simulations of unassisted subjects with these data points have been experimentally validated via electromyography studies presented in [15, 98], in which some timing and magnitude discrepancies between simulated and experimentally collected activations of some muscles have been reported due to excessive passive forces in knee and ankle joints.

The *loaded* and *noload* joint kinematics and kinetics have been compared with the results of Huang and Kuo [123] and Silder *et al.* [124] and validated qualitatively. Since our simulations of the unassisted subject for *loaded* and *noload* conditions are the same as those of Dembia *et al.* [15], our results are verified by the reproduction of their simulation results.

Another source of error during simulations is the kinematics error, which has been shown to be within the recommended thresholds in [15]. Since the inverse kinematics stage of the simulation has not been reproduced in this study, the markers error are not examined, and we rely on the previously performed verification of this error source. The analysis in [15] on residual errors indicate that the residual

forces lie below the threshold recommended by Hicks *et al.* [98]; however, the residual moments exceed these thresholds. However, since the joint moments matched with those in [98], it is claimed that these exceeding residual moments do not affect the interpretations [123, 124].

Another error source in these simulations is the additional moments introduced to compensate for any unmodeled passive structures and muscle weakness. These values have been checked to confirm that they are within their recommended thresholds of less than 5% of net joint moments, in terms of peak and RMS values [15].

To ensure that our simulations in both ideal and multi-criteria optimization stages do not deviate from the defined error source thresholds, we have also analyzed the kinematics of all simulations and checked their divergence from the adjusted kinematics resulting from the RRA simulations. Additionally, some simulations of the multi-criteria optimization stage have been selected randomly, and their residual and reserve moments and forces are verified to be within the allowable thresholds.

4.5 Performance Metrics

The main goal of this study is to design an energy efficient untethered wearable assistive device that can reduce the metabolic cost of its users. Following the terminology proposed in [125], the performance requirements for assistive devices can be categorized into four groups as imperative, optimal, primary, and secondary requirements.

Ensuring the safety of physical human-robot interaction and an ergonomic fit are imperative design requirements for exoskeleton type assistive devices. The safety of physical human-robot interaction can be ensured by guaranteeing coupled stability of low-level interaction controllers [], while ergonomic fit can be achieved through the implementation of proper joint alignment mechanisms []. Both of these aspects are out of the scope of this study.

The metabolic cost reduction of its users is an optimal performance requirement that needs to be maximized while designing an assistive exoskeleton. In particular, the assistive devices considered in this study are required to provide assistive torques to decrease the metabolic cost of walking at a self-selected speed, with and without a heavy load. To quantify this metric, the normalized gross whole-body metabolic rate of each subject (for different assistive devices and under two load conditions) are calculated, and the metabolic cost reduction is computed by comparing the metabolic rate of assisted and unassisted subjects. The metabolic cost calculations are repeated for seven subjects in three trials to obtain the average metabolic power expenditure and the metabolic cost reduction for each assistance scenario and load condition.

The energy efficiency of the untethered assistive device is another optimal performance requirement that needs to be maximized. The power consumption is a crucial metric, as it directly affects the battery life and torque output (consequently, the total weight) of untethered devices. To quantify this metric in the simulated exoskeletons, the absolute power consumed by all actuators is computed, considering that power regeneration mechanisms may not be implemented. Additionally, the negative power of the exoskeletons is also computed to analyze the amount of power available for regeneration. This enables an appropriate portion of the negative power to be subtracted from the absolute power consumed to study the effect of regeneration on power efficiency. Finally, to assess the cost of carrying, the average and standard deviation of the maximum positive power of actuators of each device (normalized by subject mass) under different load conditions are calculated, as proposed in [15].

These two optimal performance requirement of metabolic cost reduction and device power consumption are optimized simultaneously to compute a set of non-dominated solutions for each exoskeleton configuration. It should be noted that device power consumption metric indirectly addresses device weight and inertia, as lower power devices can be implemented using smaller actuation and battery modules.

Primary requirements for untethered exoskeleton type assistive devices are considered as low device weight and inertia. Since static optimization based musculoskeletal simulation utilized in OpenSim does not allow for inertial changes to be studied directly, detrimental effects of device weight and inertia are considered as part of primary requirements, such that these effects can be extracted from the relevant human-subject studies in the literature and superposed on the Pareto-front curves to facilitate the design selection process.

Additional primary requirements for assistive exoskeletons may be considered as changes in muscle activities of the key lower limb muscles and the reaction forces and moments at the joints under assistance. Similar to inertial effects, these aspects can be studied for each non-dominated device design computed by the multi-criteria optimization and may help facilitate the design selection process.

Finally, the secondary requirements for the exoskeleton may be considered as ease-of-implementation, robustness, and device cost. These requirements are imposed by the designer based on specific the specific use scenario and implementation approach; hence, are also out of the scope of this study.

4.6 Statistical Analysis

The experiments and their simulations were performed on seven subjects walking in two different loading conditions repeated in three trials. To identify the statistically significant factors and to enable multi-comparisons, relevant statistical analyses are used. In particular, N-way repeated measures analysis of variance (ANOVA) is utilized to identify the statistically significant factors and Tukey post-hoc tests are used for multi-comparisons. As relevant, data is partitioned and a series of one-way ANOVA tests are also utilized to study individual factors. As a tool, SPSS [126] is used to perform the statistical analyses and a significance level of 0.05 is used through the study.

4.7 Biarticular and Monoarticular Untethered Exoskeletons

4.7.1 Device Performance

Both bi-articular and mono-articular configurations of the ideal exoskeleton reduced the metabolic power consumption of subjects walking carrying and not carrying a heavy load at self-selected walking speed. The bi-articular and mono-articular exoskeletons decreased the metabolic rate of subjects carrying a heavy load metabolic rate by 20.49 ± 2.87% and 20.45 ± 2.81%. The mono-articular and bi-articular configurations of the exoskeleton were able to reduce the gross whole-body metabolic cost of the subject in the *noload* condition by 22.38 ± 4.91% and 22.47 ± 4.89%, respectively. These exoskeletons were expected to achieve the same performance on reducing the metabolic power consumption of the subjects due to their kinematic relation, and the results represent an expected performance for these two devices.

TABLE 4.1: Average power and maximum positive power consumption of bi-articular and mono-articular ideal devices.

Loading condition	**Loaded condition**		**Unloaded condition**	
Device	Average power consumption (W/kg)	Maximum positive power (W/kg)	Average power consumption (W/kg)	Maximum positive power (W/kg)
Bi-articular	3.11 ± 0.25	10.52 ± 1.79*	3.00 ± 0.32§	9.76 ± 1.04‡
Mono-articular	2.75 ± 0.55	8.32 ± 1.45*	2.33 ± 0.29§	7.17 ± 0.85‡

Note: equal superscripts indicate a pairwise statistically significant difference ($P < 0.05$).

The assistance of both exoskeletons on subjects carrying a heavy load was able to compensate for their demanding metabolic power to carry the heavy load. As can be seen in Fig 4.5, the assisted subjects in the *loaded* condition have practically the same metabolic rate with unassisted subjects who do not carry any load, meaning that the best both ideal exoskeletons can do is to compensate for the metabolic power demanded by the *loaded* subject to a subject without an additional load. Conducting two-way ANOVA (random effect: subjects; fixed effect: loading condition, devices) shows no significant difference between metabolic demand of the

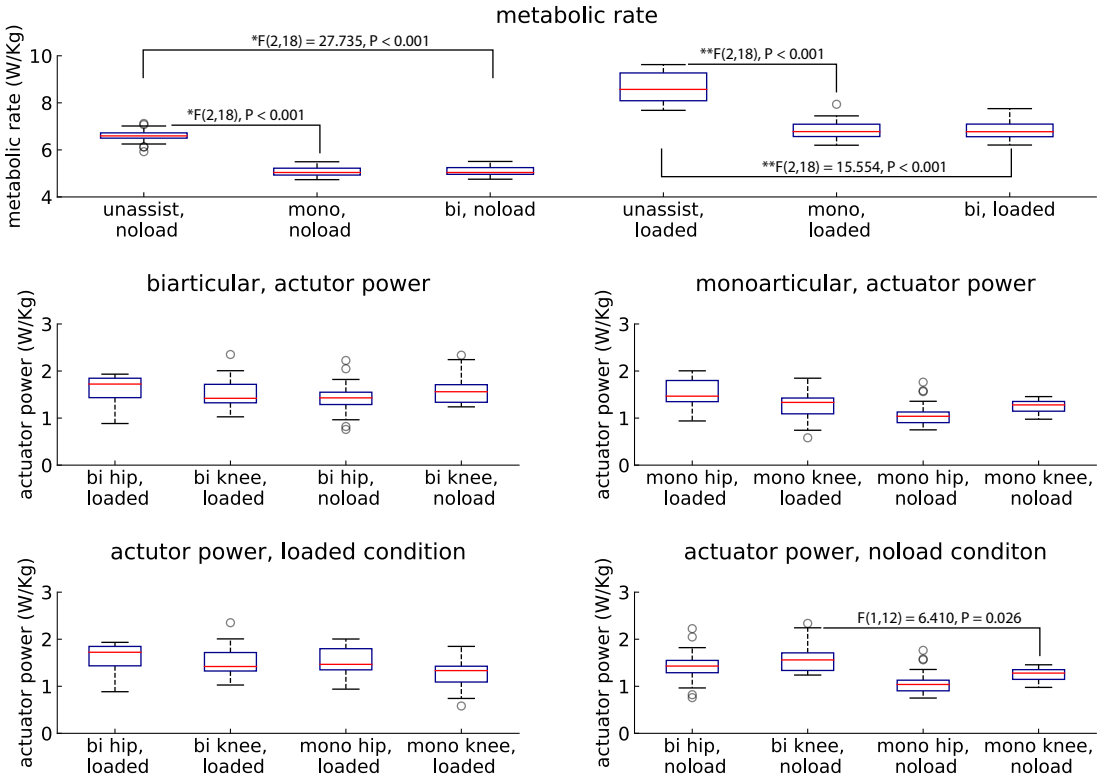

FIGURE 4.5: Assistive devices power consumption and subjects metabolic rate.

assisted *loaded* subjects and unassisted subjects during unloaded walking, which supports our claim.

While the average power consumption of devices was statistically significantly different during the unloaded walking, this difference became statistically insignificant during loaded walking, as shown in Table 4.1. Furthermore, examining the power consumption of actuators of devices in different loading conditions demonstrated a uniform distribution of power consumption between the actuators of both devices. The absence of a significant difference (one-way ANOVA (random effect: subjects; fixed effect: loading condition)) between the load conditions in actuators of both devices indicates that the power consumption of devices was not considerably affected by loading subjects with a heavy load.

In addition to the average power consumption, conducting one-way ANOVA between the bi-articular and mono-articular ideal devices showed that the maximum positive power consumption of devices is significantly different in both loading

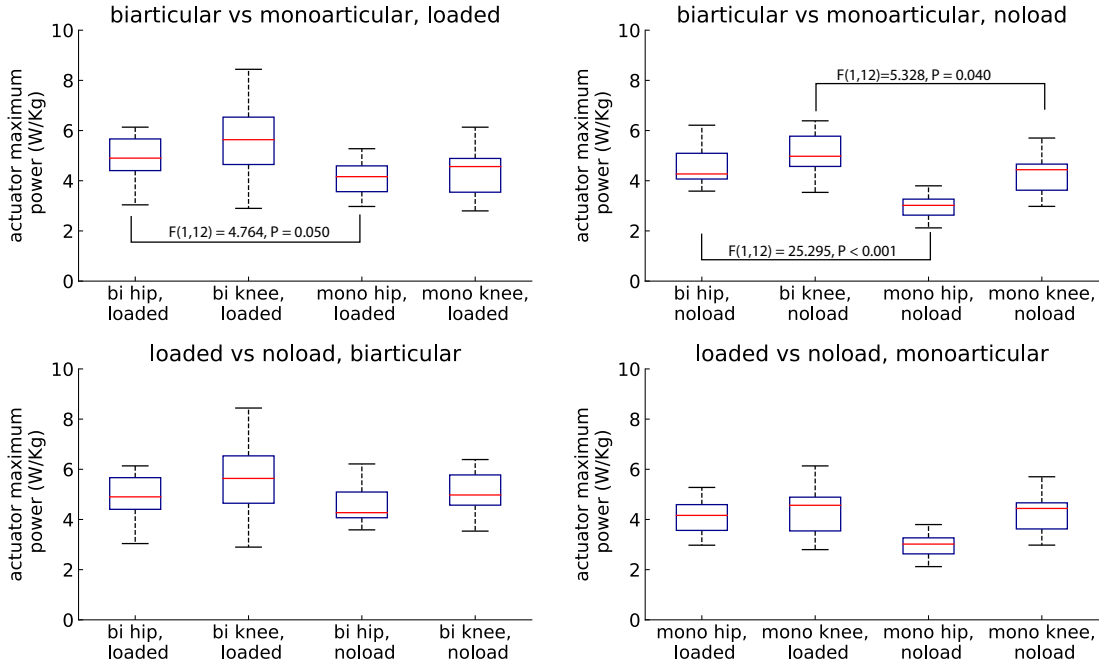

FIGURE 4.6: Assistive devices maximum positive power.

conditions, which indicates that the cost of carrying the mono-articular and bi-articular devices are significantly different (Table 4.1). Analyzing the maximum positive power consumption of actuators in both devices showed that the cost of carrying the hip and knee actuators of the mono-articular device is significantly different during unloaded walking (one-way ANOVA; fixed effects: participants; random effects: actuator type) and the hip actuator of this device has significantly different maximum positive power during loaded walking compared to unloaded walking (one-way ANOVA; fixed effects: participants; random effects: load condition). Moreover, conducting a statistical test between actuators of both devices (i.e., one-way ANOVA, fixed effects: participants; random effects: device type) reveals that the costs of carrying both actuators are significantly different during unloaded walking while this cost is different only at the hip actuator during the loaded walking. The maximum positive power consumption of actuators of both devices are shown in Figure 4.6.

4.7.2 Devices Speed, Torque and Power

One of the main objectives of this section is to validate the kinematic modeling of the proposed exoskeletons on OpenSim. As was already discussed, there is a linear mapping between the mono-articular and bi-articular exoskeletons, and if the modeling of the devices was correct in the musculoskeletal simulator, this kinematics relation must hold. Analyzing the velocity profiles of devices can validate the mapping between two exoskeletons and modeling of them through the OpenSim.

Figure 4.7 represents the velocity profiles of the bi-articular and mono-articular exoskeletons in both load conditions. From Eq (3.7) we were expecting to observe the same angular velocity profiles at the hip actuator, and since the hip actuator in each of the two exoskeletons was supposed to be attached directly to the hip joint, the velocity of the joint and actuators in both devices have practically the same profiles, as is shown in Figure 4.7 for the hip joints in both load conditions in which actuator's velocity for subjects carrying heavy load (dark blue) and without any load (blue), and net joint velocity profile for *loaded* (black) and *noload* (green) conditions are shown for each actuator of the devices.

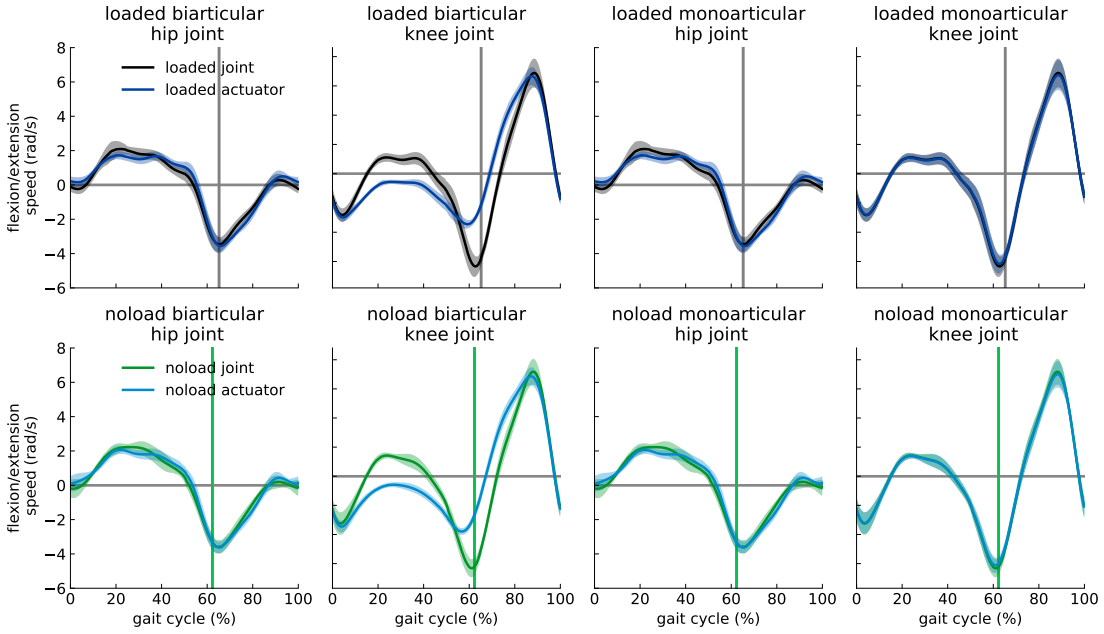

FIGURE 4.7: Assistive devices velocity profiles compared to joint required velocities.

The main difference between the two configurations of the exoskeleton is on the knee joint, in which the bi-articular device assists the joint through a parallelogram mechanism, and the velocity profiles of the knee actuators were supposed to be different according to their jacobian. This difference can be seen in Figure 4.7, in which the mono-articular knee actuator follows the knee joint velocity profile, but the bi-articular actuator shows a different profile from the knee joint profile due to Eq (3.7).

According to the Jacobian between these two devices expressed in Eq 3.8, the knee and hip actuators were expected to exhibit the same and different torque profiles respectively, which is evident in Figure 4.8 for both *loaded* and *noload* conditions. The device actuator torque for subjects carrying heavy load (dark blue) and without any load (blue), net joint moment profile generated by unassisted muscles for *loaded* (black) and *noload* (green) conditions, and the generated moment by assisted muscles for *loaded* (dark rose red) and *noload* (rose red) conditions are shown for each actuator of the devices in Figure 4.8. The curves in this figure are averaged over 7 subjects with 3 trials and normalized by subject mass and the shaded regions around the mean profile indicate standard deviation of the profile. The generated optimal torque profiles of the ideal exoskeletons did not resemble the net moment of the assisted joint, which was also observed by [15] and [2] for the simulation-based study of walking with a heavy load and running, respectively. The torque of assistive actuators in both hip and knee joints exceeded the corresponding net joint moment and resulted in an opposing muscles generated moment and device torque in the joint.

This opposition was more significant on the knee joint than on the hip joint during the mid-stance to the mid-swing phase, with the highest opposition on the onset of the pre-swing phase. The hip joint had significant actuator and muscle torque opposition during the pre-swing to terminal swing phases, indicating that different from the knee joint, in which a major portion of antagonism occurred during the stance phase, the hip entered muscle and actuator torque contraction during the swing phase.

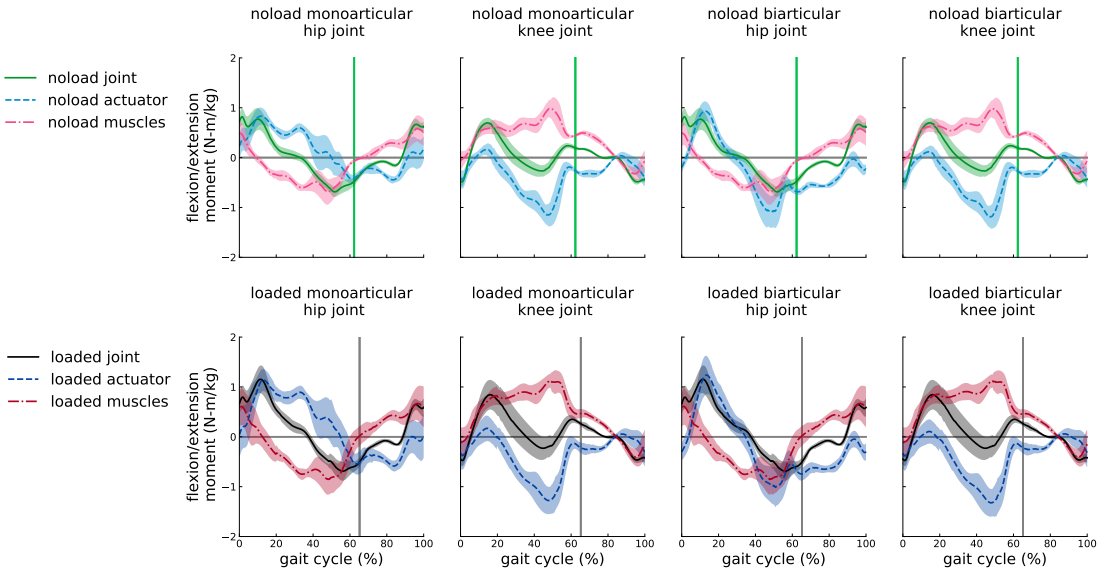

FIGURE 4.8: Assistive devices torque profiles compared to joint and muscles generated moment.

The analysis of the torque profiles of our device in different load conditions, represented in Figure 4.8, indicates that the loading subject with a heavy load does not result in substantial changes in the torque profiles of the assistive devices. The main changes between the *loaded* and *noload* conditions are the timing and magnitude of the profiles, which is due to the change of the kinematics and kinetics of the joints. Nevertheless, the standard deviation of assistive devices and assisted muscles generated torques are considerably greater in the *loaded* condition, and it is more evident in the knee joint, where the net joint moment had a remarkable deviation during the stance phase. This high within-subject deviation of torque profiles indicates that the assistance of subjects carrying a heavy load requires the subject-specific design and control of the exoskeletons [2].

Due to the discussed kinematic differences between two configurations, the power profiles of the exoskeletons were different in both actuators, as is represented in Figure 4.9. The profiles of power consumption of the bi-articular actuators are different during the gait cycle except in the loading response and, partially, mid-stance phases. The load carried by subjects causing different timing and magnitude than subjects walking with no load and the deviation of the profiles are higher for the *loaded* subject, both of which are observed in the torque profiles as well.

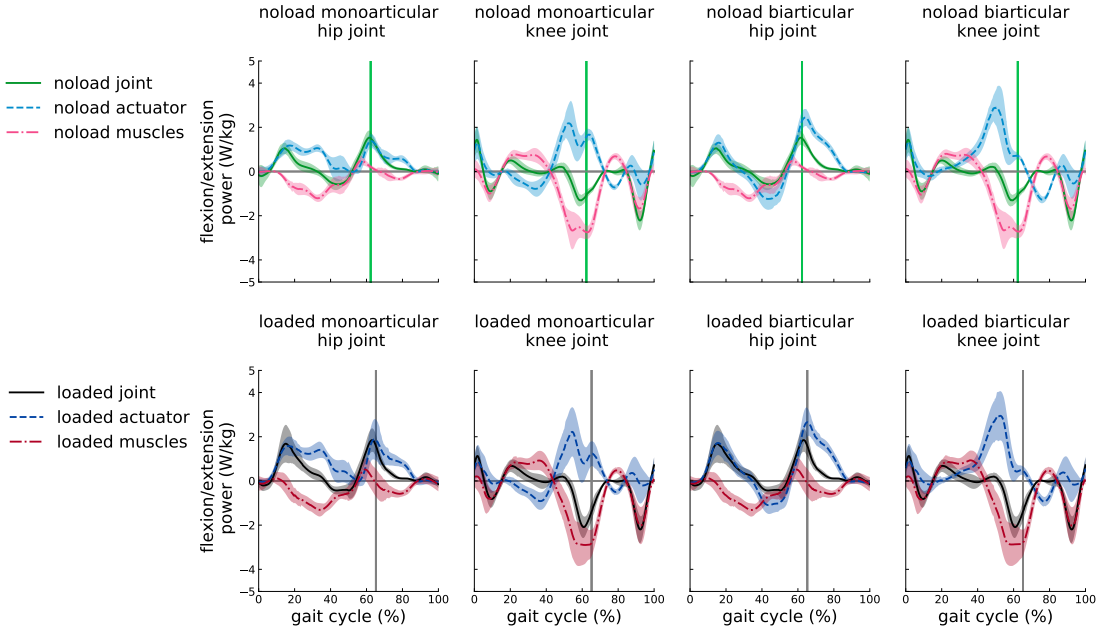

FIGURE 4.9: Assistive devices power profiles compared to joint powers.

Although the power profiles of hip actuators roughly followed the net joint power profile, the knee actuator profiles did not resemble the knee joint power. The mechanical work performed by the assistive devices was mostly positive work for both knee and hip actuators. The negative mechanical work in the bi-articular exoskeleton can be harvested mostly during the initial-swing and mid-swing phases for the knee actuator and terminal phase for the hip actuator. Unlike the bi-articular device, the mono-articular hip actuator performed practically no negative mechanical work, and the regeneratable work of the knee actuator was within both mid-stance and late-swing phases.

4.7.3 Effect of Devices on Muscle Coordination

The muscular activation of the subjects assisted by ideal assistive devices was profoundly adjusted compared to the muscle activation of unassisted subjects. Adding a set of ideal actuators with high optimal force (i.e., low penalization cost) to the musculoskeletal model changes the solution of the optimizer for finding a set of actuators to track the kinetics and kinematics of the joints.

Appending ideal actuators does not necessarily decrease the activity of all muscles, and it can be more economical for the complete set of actuators to increase the activity of specific muscles during some phases of a gait to decrease the activity of less cost-effective muscles. Since the metabolic power of muscles is a function of their activity and their fiber properties [121], the reduction in the activity of the entire set of muscles results in gross whole-body metabolic cost reduction.

Despite the kinematic difference between the two configurations of the assistive device, the torques applied to the joints were practically identical, and it resulted in an identical effect on the muscular activation of the subjects.

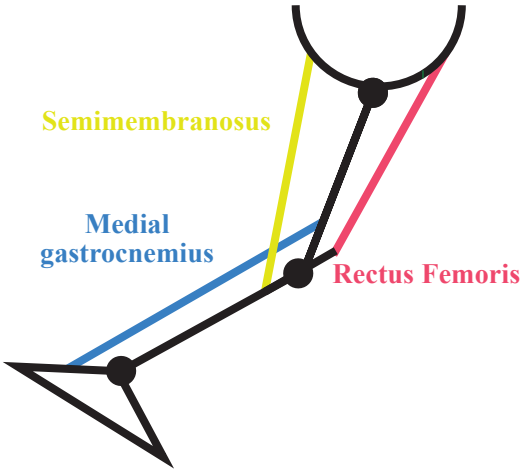

FIGURE 4.10: Biarticular representative lower extremity muscles

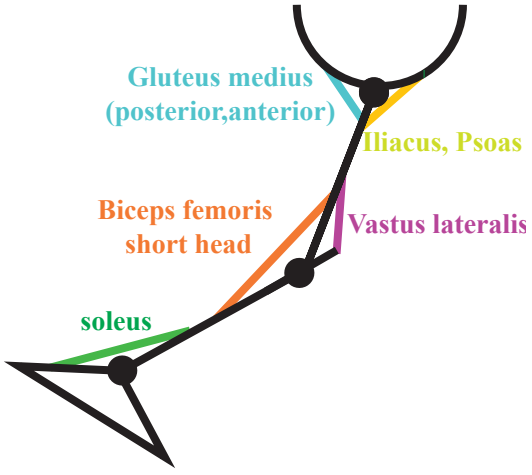

FIGURE 4.11: Monoarticular representative lower extremity muscles

The cause for this effect is rooted in the ideal nature of the actuators and devices, meaning that there are no constraints that the torque actuators can provide, the

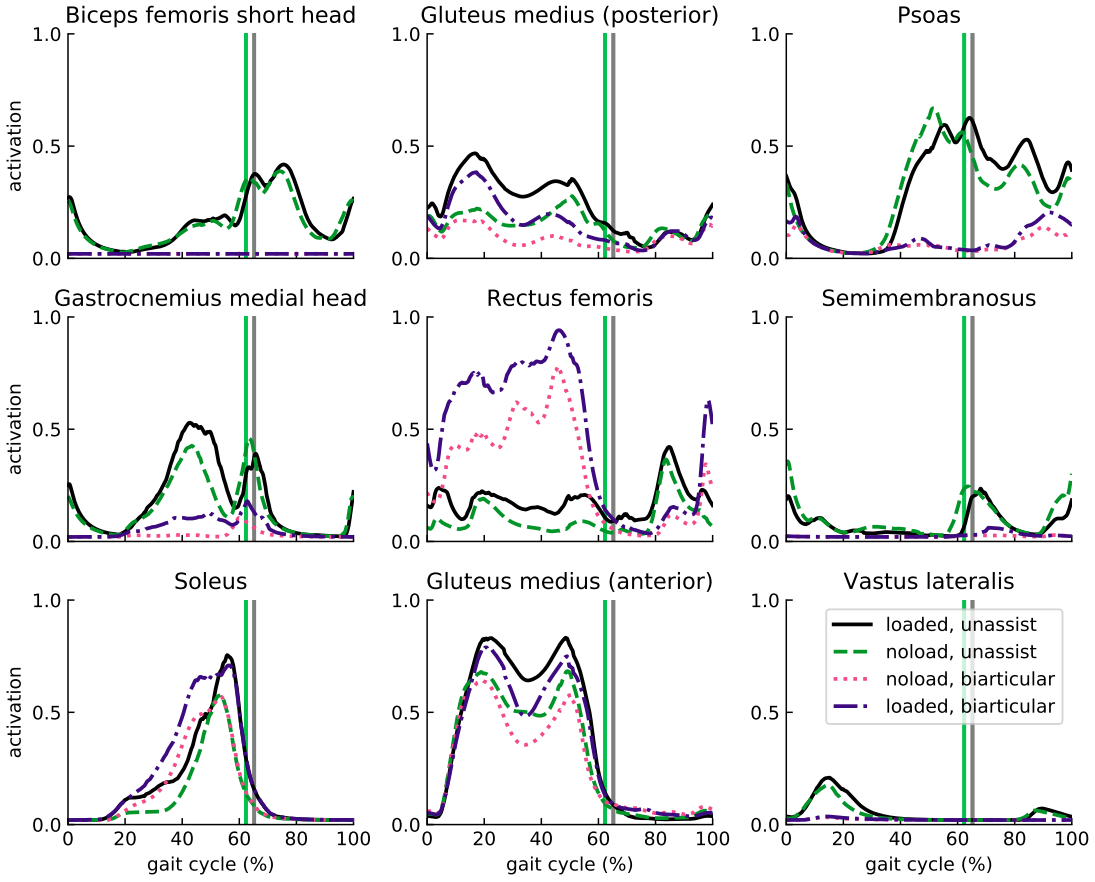

FIGURE 4.12: Activation of representative lower limb muscles of assisted and unassisted subjects.

devices are assumed to be massless, and actuators do not have any reflected inertia effect. The muscle activation in Figure 4.12, which shows the effect of the bi-articular device on the activation of representative muscles, is sufficient and can be generalized for both configurations of the assistive device. In this figure, the activation of unassisted subjects carrying heavy load (black) and without any load (green), and assisted subjects in *loaded* (dark violet) and *noload* (pink) conditions are shown for nine important muscles and the curves are averaged over 7 subjects with 3 trials.

The devices affected the activity of muscles of the lower extremity. This effect was significant on the bicep femoris short head, semimembranosus, and vasti muscles, in which their activation was replaced by another set of actuators, including muscles and ideal actuators. The rectus femoris, which is a large knee extensor and a

hip flexor bi-articular muscle, was considerably increased during the stance phase. This increase occurred so that the optimizer could take advantage of the rectus femoris high force-generating capacity to exert hip flexion and knee extension moments more economically. In the meanwhile, this high muscular activity of the rectus femoris resulted in high knee extension and hip flexion moments exceeding net joint moment of the joints which was neutralized by ideal actuators, which can be extremely economical for applying high torques due to its high optimal force assignments.

This set of activation, in which hip flexion and knee extension required moment could be applied by more cost-effective muscles and actuators, resulted in a substantial reduction in the activity of psoas and iliacus muscles as two major hip flexor muscles and the vasti muscles (vastus lateralis, vastus intermedius, and vastus medialis) as the knee extensor set of muscles. The semimembranous muscle is another bi-articular muscle contributing to hip extension and knee flexion moments, which was affected by the assistive devices, and the new set of actuation practically replaced its activity. The activity of the medial gastrocnemius, as a critical knee flexor and ankle plantar flexor muscle, was substantially reduced by the assistive devices, yet the muscle remained partially active to supply an ankle plantarflexion moment. The reduction of ankle plantarflexion moment was compensated by increasing the soleus activity as another primary ankle plantarflexor muscle. The assistive devices affected the activity of the gluteus medius muscles as well, which not only are responsible for a significant fraction of hip abduction moment, but also contribute to hip motion in the sagittal plane as well as hip rotation.

The anterior and posterior portions of the gluteus medius muscle, besides their primary contribution to hip abduction, supported hip extension and flexion and its lateral and medial rotations. However, the reduction in co-contraction of the hip rotation due to modified muscle coordination of assisted subjects by assistive devices resulting in their muscular activity reduction.

The main differences between the muscular activity of the subjects walking with

no load and subjects walking while carrying a heavy load on the torso were the magnitude and timing of the muscular activations, which had been observed in other profiles as well. This load condition also partially affected some muscles like Semimembranosus, in which the muscles were not entirely replaced by the ideal devices.

4.7.4 Effect of Devices on Reaction Forces and Moments of Joints

The change in the muscle coordination and augmenting assistive device to the subjects affected the reaction forces and moment of both assisted and unassisted joints. This relationship between the muscle activity and joint reaction forces has been established in the literature[127–130]. The modified coordination of muscles in the ankle joint reduces the reaction forces and moments of the ankle in the swing phase while increasing them slightly during the stance stage as shown in Figures A.1 and A.2. The effect of muscle recruitment change was evident in the medial-lateral reaction force and extension-flexion reaction moment of the ankle. The study accomplished by Veen *et al.* [128] shows that an increase in the activation of rectus femoris and gastrocnemius muscles along with a decrease in activation of the soleus muscle can reduce the reaction forces of the ankle joint. Although assistive devices increased the activation of the rectus femoris, the effect of devices on the gastrocnemius and soleus muscles was not favorable in reducing the reaction force, especially during the stance phase. This coordination of muscles explains the behavior of reaction moments and forces of the ankle joint.

The effect of devices and altered muscle recruitment strategy on the reaction moments and forces of the patellofemoral and knee joint was substantial. The reaction forces of the patellofemoral and knee joints decreased during the early stance phase, and increased during the late stance, as shown in Figure A.3 to Figure A.6. The analysis of muscle effect on the tibiofemoral forces showed that the hamstring muscles significantly impact the reaction forces of the knee during the early stance,

while the gastrocnemius, rectus femoris, and iliopsoas muscles affect the reaction forces during the late stance stage [127, 128].

The increase in the activation of the soleus and decrease of the activation of hamstring muscles (i.e., semimembranosus, semitendinosus, and biceps femoris muscles) reduced the reaction force of the knee in the early stance phase. During the late stance, we hypothesize that the substantial promotion and reduction of the rectus femoris and gluteus medius activities, sequentially, became dominant to the reduction of activities of other muscles and resulted in a tibiofemoral reaction force increase. Since the behavior of the other reaction force components in both the patellofemoral and knee joints was practically identical to the tibiofemoral performance, it seems logical that the muscle arrangement had the same effect on other reaction forces. However, since the hip muscles' effect on the knee reaction force is settled in the literature [127, 128], this claim needs to be justified in a more isolated condition, such as assisting a joint condition. Although the reaction moments in both joints roughly followed the reaction forces' behavior, the effect of devices on the reaction moments was slightly different in that the bi-articular exoskeleton was able to reduce the reaction moments and have lower peaks than the mono-articular device on the extension-flexion reaction moment.

Although the reaction forces and moments of the knee joint increased during the late stance phase, the assistive devices were able to reduce most of the maximum or peak reaction forces and moments on the knee joint. Additionally, the modified muscle recruitment effect on the reaction forces and moments during the swing phase was remarkably lower than its effect on the stance phase; nonetheless, the tibiofemoral force experienced considerable reaction force reduction during the swing phase compared to other reaction forces.

The reaction forces of the hip joint were affected by the activity of a group of muscles mentioned in [128], including the gluteus minus, gluteus medius, iliopsoas, and rectus femoris muscles. The increase in the activity of the rectus femoris incorporation with iliopsoas and gluteus medius muscle activity reduction decreased the reaction forces of the hip joint. This reduction was considerable during the

late stance and early swing phases, and subjects in *noload* condition were more substantially affected than the subjects in *loaded* condition, as shown in Figure A.7.

These modifications in the reaction moments and forces of the assisted subjects can improve the health of joint tissues [131]. The large joint loads are identified as an essential factor of onsetting and progressing osteoarthritis [132–134] and joint pain [135] and reduction in the reaction forces and moments can prevent and reduce such joint pain and arthritis onset and development.

4.8 Tethered Hip Exoskeleton

In addition to the hip-knee exoskeletons, we studied torque limited and ideal bilateral hip exoskeleton to experimentally evaluate the performance of simulation-based optimized profiles on our developed tethered hip exoskeleton. We set the peak hip torque on the torque limited hip device to 50 N-m to ensure users and device safety during the experimental evaluations.

4.8.1 Device Performance

The ideal and torque-limited hip exoskeletons improved the unloaded walking economy by 15.185 $\pm$ 2.345 and 13.448 $\pm$ 2.763 and loaded walking economy by 15.769 $\pm$ 3.789 and 12.618 $\pm$ 2.710, respectively.

Both ideal and torque-limited hip exoskeletons were able to reduce the metabolic cost of unassisted subjects significantly in both loading conditions (One-way ANOVA, within-subject factor: subjects, between-subject factor: assistance), as shown in Figure 4.13. However, the metabolic rate of subjects assisted by ideal and torque-limited exoskeletons were not significantly different. This infers that constraining the peak torque of the hip exoskeleton by 50 N-m does not affect the performance of the device on improving both loaded and unloaded walking economy.

While the effect of devices on the metabolic cost of subjects did not significantly change by constraining the peak torque, the power consumption of the device was

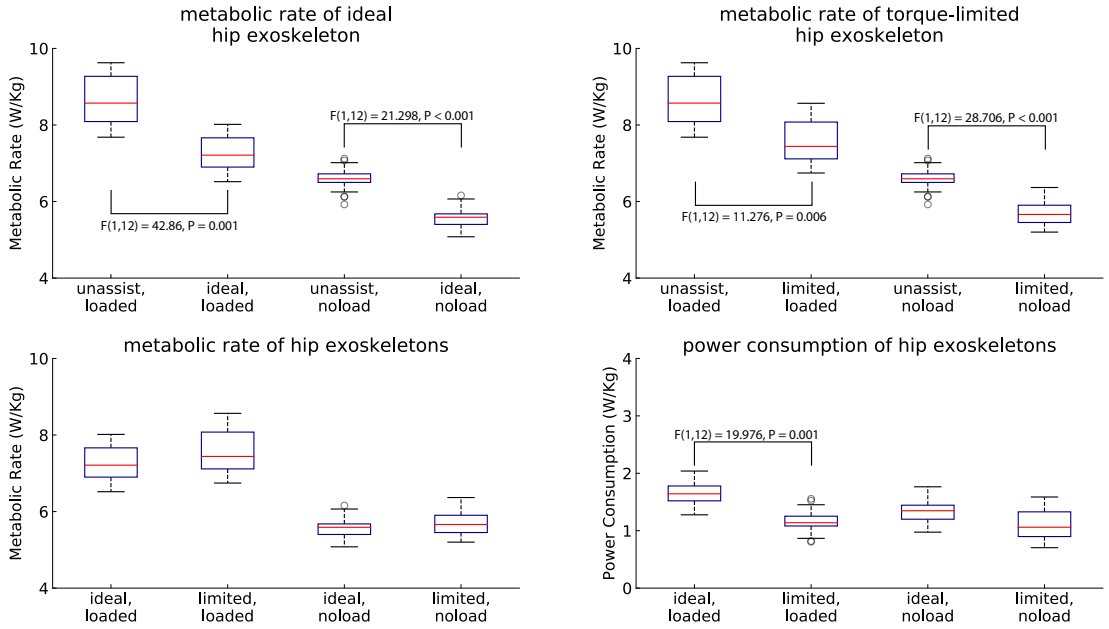

FIGURE 4.13: Ideal and torque-limited hip exoskeleton power consumption and subjects metabolic rate.

significantly reduced during loaded walking, as shown in Figure 4.13. While the effect of devices on the metabolic cost of subjects did not significantly change by constraining the peak torque, the power consumption of the device was significantly reduced during loaded walking, as shown in Figure 4.13. The power consumption of torque-limited hip exoskeleton was not affected significantly by loading subjects with a heavy load, while the change in power consumption of ideal hip device was significant during walking while carrying a heavy load (Figure 4.13).

4.8.2 Device Torque and Power

Similar to the hip-knee exoskeletons, the torque profile of both ideal and torque-limited exoskeletons did not resemble the net moment of the assisted joint. These torque profiles of devices were mostly following the trajectory of the hip joint during mid-stance and terminal stance phases. However, they significantly diverged from the hip joint moment during the swing phase.

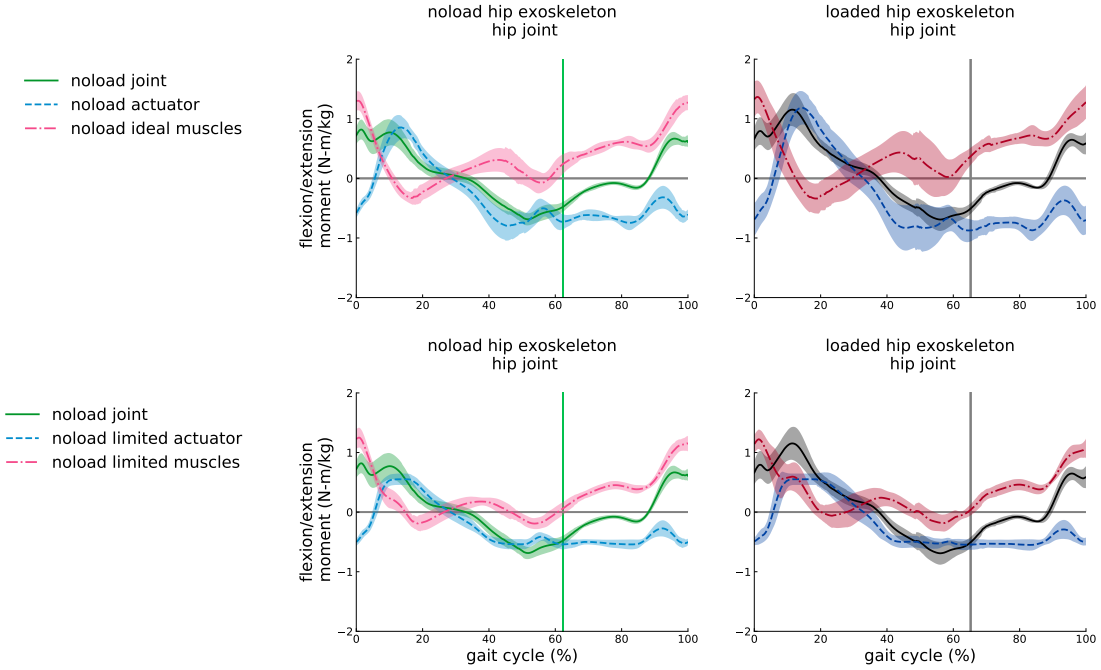

FIGURE 4.14: Ideal and torque-limited hip exoskeleton torque profiles compared to joint and muscles generated moment.

As shown in Figure 4.14, the muscles generated moment increased during the loading response phase while it decreased considerably during the rest of the stance phase and then it opposed to the torque applied by the hip exoskeleton during the swing phase. It can be inferred from Figure 4.14 that constraining the peak torque of the hip joint does not change overall torque trajectory; yet, the muscles generated moment and device torque opposition decreased during mid-stance and swing phases considerably.

The power profile of both toque-limited and ideal hip exoskeleton mostly followed the hip joint power trajectory during the stance phase; however, the magnitude of their power profile increased significantly during the swing phase. Similar to the other ideal exoskeletons, the magnitude was the main variation between the trajectories of the torque limited and ideal device.

Since the bi-articular exoskeleton reflected the reaction torque of both hip and knee actuators to the torso, a close similarity was expected between the torque profiles of the ideal hip exoskeleton and hip actuator of the bi-articular exoskeleton. As shown in Figure 4.16, the hip moment trajectories of the hip device and

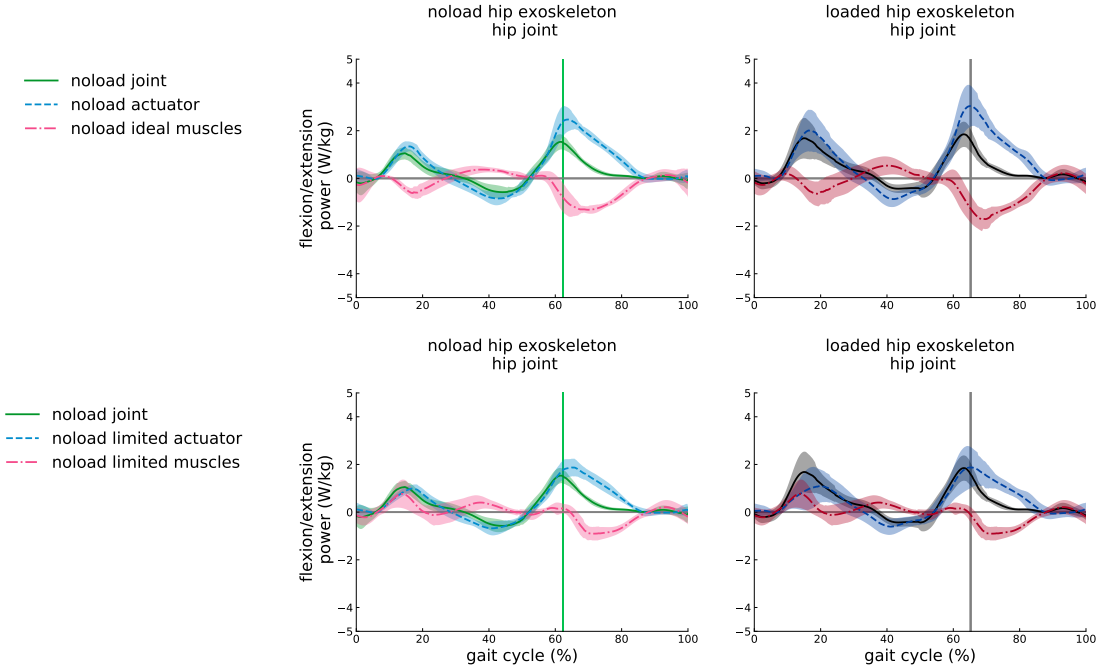

FIGURE 4.15: Ideal and torque-limited hip exoskeleton power profiles compared to joint and muscles generated power.

hip actuator of the bi-articular device have a close match. However, there is a timing difference between these profiles during some phases, which is more evident during the loading support and mid-stance phases. Furthermore, these profiles have different trends during terminal stance and terminal swing phases. In addition to timing, there is a magnitude difference between these torque and power profiles, which becomes more evident in the power profiles of devices during loaded walking.

4.8.3 Effect of Device on Muscles Coordination

The change in muscle coordination of the subjects assisted by the hip device was mostly similar to the changes observed in muscles of subjects assisted by ideal hip-knee exoskeletons. The activation of rectus femoris muscle was increased to take advantage of its high torque generation capacity to reduce the activity of iliopsoas and vasti muscles, as shown in Figure 4.17 and 4.18. Unlike the 2 DOF exoskeletons, the activation of the rectus femoris was mainly increased only during early stance as there is no ideal knee actuator to neutralize the superfluous

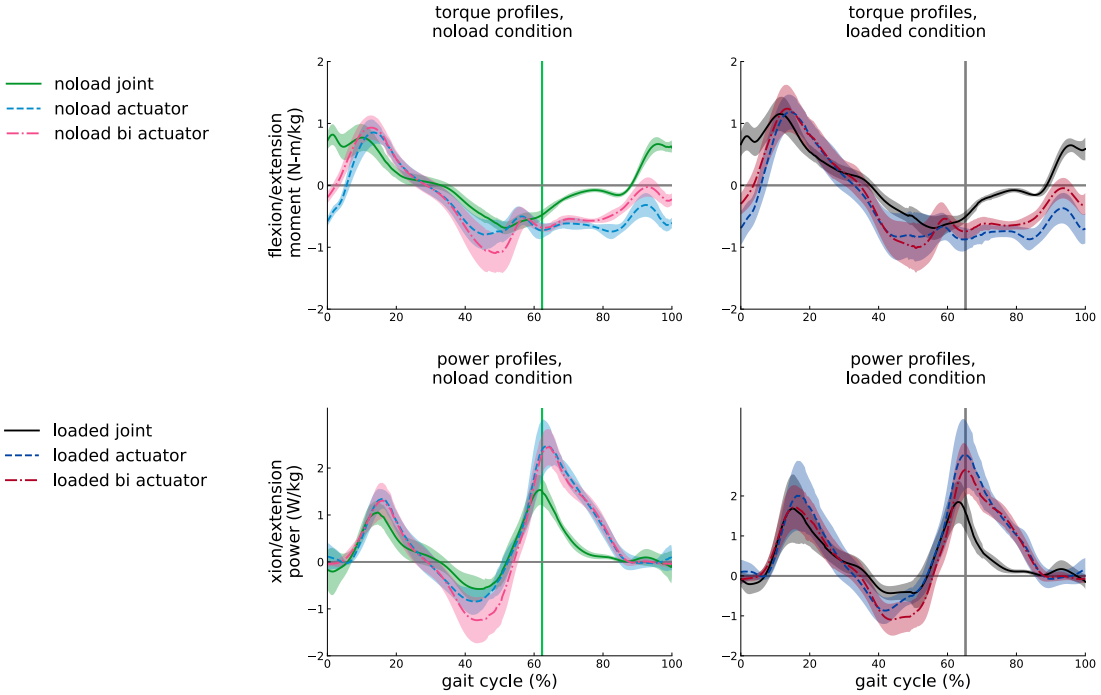

FIGURE 4.16: Torque profile of ideal hip exoskeleton compared to torque profile of hip actuator of bi-articular exoskeleton.

knee extension generated by this muscle. As discussed in [2], the hip device also provides the hip extension moment generated mostly by gluteus maximus muscles resulting in a reduction in their activity. The external rotation moment of the hip joint is also affected by the change in gluteus maximus and iliacus activities, and the co-contraction in the internal rotation is reduced consequently, which affect the activity of the gluteus medius muscles. Since the anterior part of gluteus medius muscle is more economical to generate the internal rotation and abduction moment, it activates more to compensate lack of moment generated by posterior part of gluteus medius muscle.

Similar to the effect of the ideal bi-articular and mono-articular exoskeleton on muscle activity, the activity of the gastrocnemius medial head is reduced, and the lack of its generated moment on the ankle is compensated by increasing activity of soleus muscles; yet, the change in the activity of these muscles are not as significant as we observed in the 2 DOF ideal exoskeletons.

As was expected from the similarity between the torque profiles of the ideal and

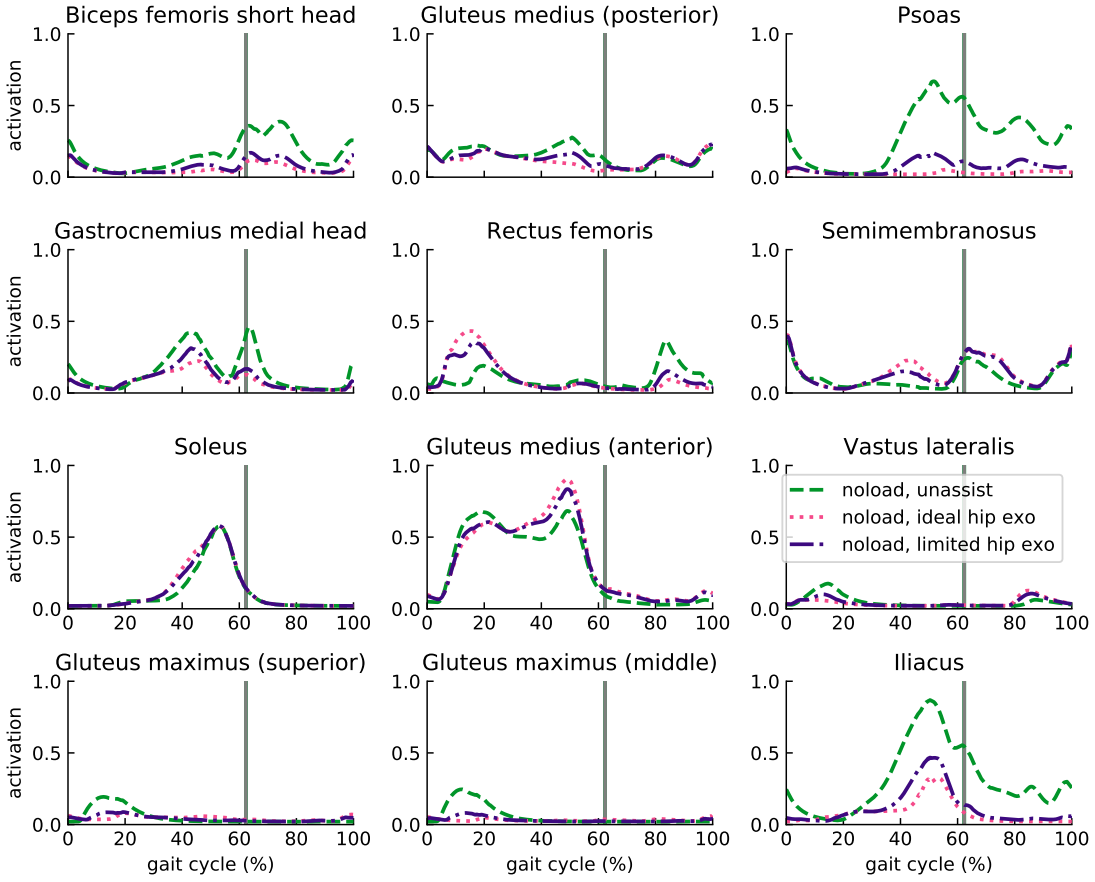

FIGURE 4.17: Activation of representative lower limb muscles of unassisted subjects and assisted subject by ideal and torque-limited hip exoskeleton during unloaded walking.

torque-limited hip devices, their effect on muscle activation was also similar. The main difference in the effect of these two devices could be observed on rectus femoris, iliopsoas, and gluteus maximus muscles.

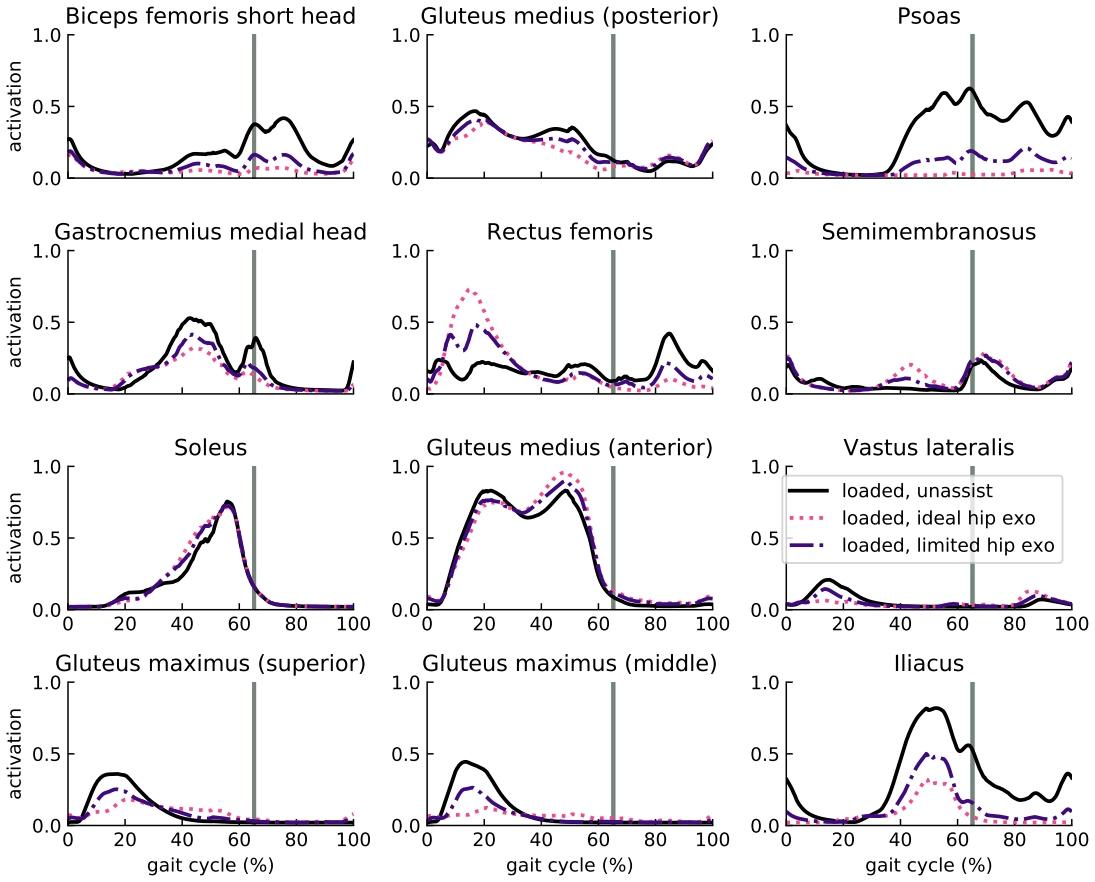

FIGURE 4.18: Activation of representative lower limb muscles of unassisted subjects and assisted subject by ideal and torque-limited hip exoskeleton during loaded walking.

Chapter 5

Simulation-Based Multi-criteria Optimization

The CMC algorithm resolves muscle redundancy by applying static optimization to the weighted sum of squares objective function to solve it in a least-square sense at each instant of time, to track the captured data of the subject with the lowest cost [98]. While studying ideal exoskeletons, the weights assigned for assistance torques are selected in such a way that, these actuators are promoted to be utilized as much as possible. However, this approach does not take any physical limitations of such devices into account.

Although musculoskeletal simulations of ideal assistive devices provide insights into the maximum assistance that can be provided to the human musculoskeletal system, in real life applications, the exoskeletons are constrained by the power that can be supplied to their actuators and the maximum assistive torque that the actuation modules can provide to the joints of interest. Furthermore, kinematics and inertial distribution of exoskeletons are other aspects that need to be taken into account.

In general, there exist trade-offs among the power consumption, the metabolic cost reduction, and the inertia of assistive devices. One the one hand, high metabolic cost reduction necessitates large torque capacity and large power consumption,

and on the other hand, power-efficient and lightweight exoskeleton designs require compact and efficient actuator units that cannot provide high assistance torques.

Taking energy efficiency of exoskeletons into consideration together with their beneficial effects on the metabolic burden of subjects introduces another optimization criterion to be studied while optimizing the performance of devices. Hence, a multi-criteria design optimization problem needs to be addressed to study the trade-off between the energy efficiency and the metabolic cost reduction.

One way to address the multi-criteria design optimization problem is to use a weighted sum of the cost functions. Assigning predetermined weights to define a single aggregate objective function, such a scalarization approach enables the original multi-objective problem to be formulated as a single criterion optimization problem. The drawback of this approach is that the preferences between objectives need to be assigned a priori, before having a complete knowledge on the trade-off involved.

We advocate the use of Pareto methods for musculoskeletal simulation based multi-criteria design optimization of assistive devices. Given a multi-criteria optimization problem, there exist multiple solutions that reflect optimal designs for different preferences among the selected metrics. All such *non-dominated* solutions constitute the Pareto front [136–138]. Unlike one-shot scalarization-based optimization methods, Pareto methods fully characterize the trade-off among objectives. Once the Pareto front is computed, the designer can study these solutions to get an insight of the underlying trade-offs and make an informed decision to finalize the design by selecting an *optimal* solution from the Pareto set. Secondary constraints or new design criteria that have not been considered during the original optimization can be introduced at the design selection stage. Consequently, Pareto methods allow the designer to choose alternative optimal solutions under different conditions.

The Pareto optimization approach is rewarding as it not only leads to musculoskeletal simulation based design of optimal assistive devices, but also enables

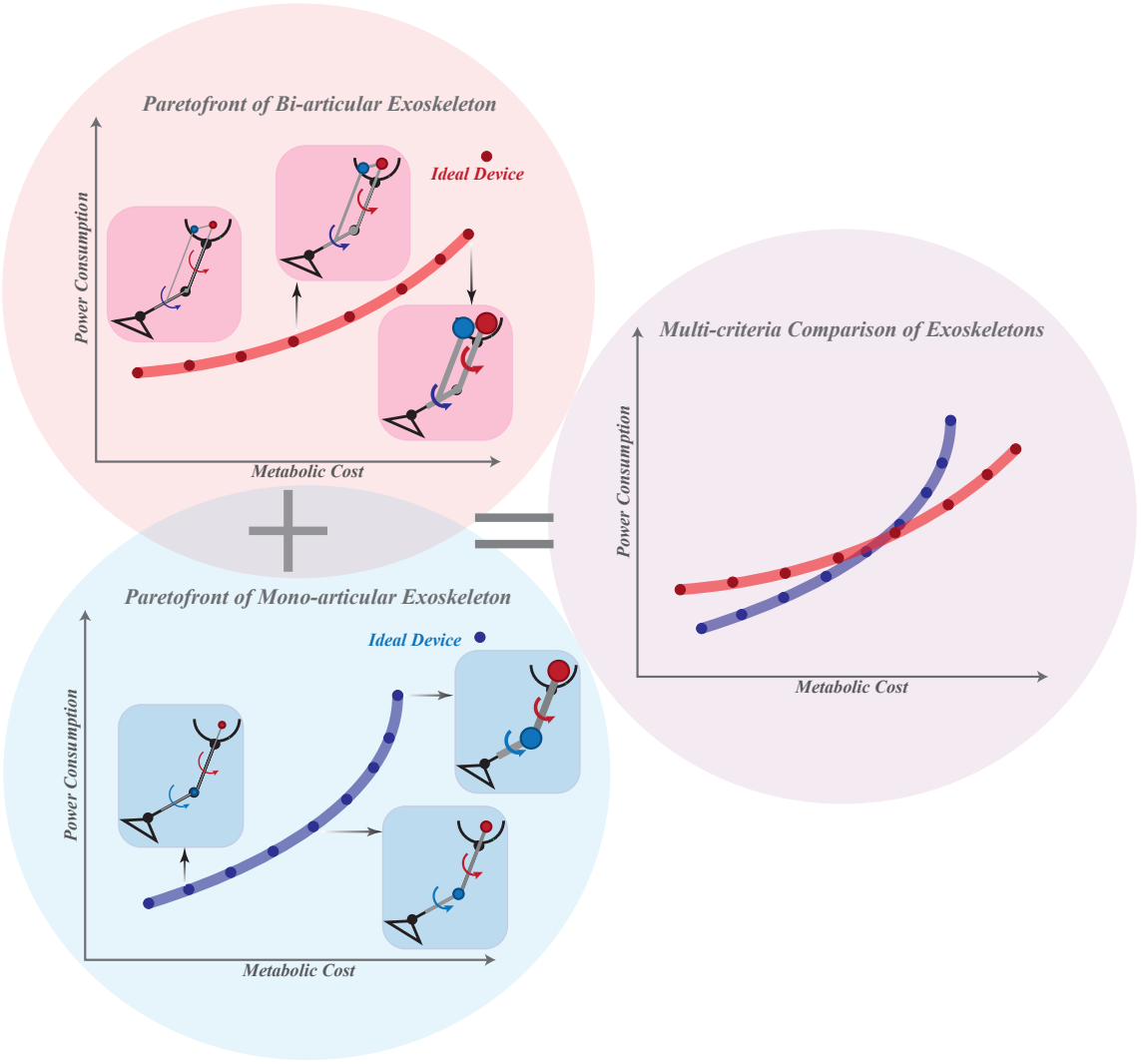

FIGURE 5.1: Multi-criteria comparison of bi-articular and mono-articular exoskeletons

fair comparisons among various assistive devices, possibly with different underlying kinematic, dynamic, actuation and loading properties [139–141]. Given that the Pareto front for each assistive device characterizes the best performance of that exoskeleton for all possible preferences of the designer, fair comparisons become possible by studying the Pareto front of each exoskeleton. Hence, for any given designer preference, the best possible performances of each exoskeleton can be compared to the best possible performances of other exoskeletons, as depicted in Fig 5.1, leading to a fair and systematic comparison methodology.

Pareto optimization approaches consist of three main stages: i) selection and evaluation of performance metrics, ii) computation of the Pareto front, and iii) selection

of an optimal solution among all non-dominated solutions.

5.1 Computation of the Pareto front

Since optimal performance requirements of metabolic cost reduction and device power consumption constitute two objectives that conflict with each other, there exists no unique solution that simultaneously optimizes both objectives. Furthermore, the trade-off between these objectives is not entirely apparent; hence, assigning a relative importance to these objectives is not trivial. Instead of a computing a unique solution that optimizes both objectives simultaneously, multi-criteria design optimisation aims at computing a set of mathematically equivalent solutions, called non-dominated solutions. A non-dominated solution is an optimal solution such that an improvement in one objective requires the degradation of another objective. The set of all non-dominated solutions forms a Pareto front.

There exists a wide range of techniques for multi-objective optimization [142–144]. Simultaneous maximization of metabolic cost reduction and minimization of device power consumption are performed using an ϵ-constraint method, as this method can solve for both the convex and non-convex regions of the Pareto front.

The ϵ-constraint method computes optimal solutions on the Pareto front by optimizing one of the objectives, while the other objective is systematically expressed as an inequality constraint. In this way, the ϵ-constraint method transforms a multi-objective optimization problem into a series of single-objective problems [145–147]. Through a systematic variation of the constraint bounds, the set of Pareto optimal solutions are obtained. Unlike the commonly employed weighted sum approach, this method can also solve for non-convex regions of the Pareto front.

To implement the ϵ-constraint within the OpenSim musculoskeletal simulation framework, we systematically constrained the peak torque of assistive actuators. Limiting the maximum assistance torques that can be provided during a gait cycle directly affects the redundancy resolution of the CMC algorithm; hence, the

muscle recruitment and the metabolic cost reduction caused by the assistance. Furthermore, given that the user kinematics is kept constant throughout the musculoskeletal simulations, actuator saturation provides a systematic upper bound on the device power consumption metric. Along these lines, a systematic variation of the maximum torque that assistive actuators can provide over a discrete range results in optimal solutions in the objectives space. After filtering these solutions to select the non-dominant ones, a Pareto front curve is calculated for each configuration of the exoskeleton under different loading conditions.

In this study, a symmetry constraint between the left and right leg actuators is imposed and the maximum torque that the actuators can provide to the hip and knee joints are varied between 30 Nm to 70 Nm with a step size of 10 Nm, to study all combinations for both the bi-articular and the mono-articular exoskeletons. The algorithm is shown in the following pseudo-code.

Algorithm 1 Simulations of Multi-criteria Optimization Algorithm

```
for i = [70, 60, 50, 40, 30] do
    for j = [70, 60, 50, 40, 30] do
        Set {−i, i} : hip actuators constraint: {MinControl, MaxControl}
        Set {−j, j} : knee actuators constraint: {MinControl, MaxControl}
        Update exoskeleton model by the new constraints
        Perform CMC Simulation
    end for
end for
```

5.2 Multi-criteria comparisons and selection of an optimal solution among all non-dominated solutions

Once Pareto front curves are calculated for each exoskeleton configuration under different loading conditions, different exoskeletons can be compared to each other and an optimal solution may be selected among all non-dominated solutions. To facilitate the design selection, several metrics can be computed to quantify primary and secondary requirements for the non-dominated solutions.

5.2.1 Effect of Device Inertial Properties on Subject Energetics

Effect of device inertial properties on subject energetics is studied based on the metabolic model studied by Browning *et al.* [16]. The mass and inertia of the proposed bi-articular and mono-articular exoskeletons affect the waist, thigh, and shank segments of the body. Since the bi-articular exoskeleton enables placement of the knee actuation module to the waist instead of the thigh, the inertial properties of the mono-articular and bi-articular exoskeletons differ significantly.

To quantify the effect of the inertial properties of the exoskeletons on the metabolic rate of assisted subjects, rigid links with identical inertial properties are considered at the hip, thigh and shank of the users. The center of mass (CoM) locations are chosen based on the mean lengths of the thigh and shank segments, under the assumption of uniform distribution of link weight [148]. The inertial properties used for the numerical simulations are represented in Table 5.1.

Actuation modules with identical mass are assigned to both exoskeletons. However, both the placement of the actuator units on the body and the transmission ratio assigned to each module to ensure the require maximum torque level result in significantly different inertial properties for each exoskeleton. A maximum direct drive motor output torque of 2 Nm is considered and the proper transmission ratio to achieve the required peak torque at each joint is calculated accordingly. The reflected inertia of the actuation unit is then computed using this transmission ratio. The inertia of the moving segments (i.e., thigh and shank segments) are computed about the hip joint in the body frame by considering the distal mass effect on the inertia, reflected inertia of the actuation module, and the leg inertia

TABLE 5.1: Inertial properties considered for the bi-articular and mono-articular exoskeletons.

Configuration	**Waist**	**Thigh**		**Shank**		**Actuator**
	mass (kg)	mass (kg)	CoM (m)	mass (kg)	CoM (m)	inertia ($kg.m^2$)
bi-articular	4.5	1	0.23	0.9	$0.18 + l_{thigh}$	5.06×10^{-4}
mono-articular	3	2.5	0.30	0.9	$0.18 + l_{thigh}$	5.06×10^{-4}

provided in [16]. Eq (5.1) presents the inertia calculation of the moving segments.

$$\begin{aligned} I_{Exo,segment} &= I_{reflected} + m \times CoM^2 \\ I_{loaded\,leg} &= I_{Exo,segment} + I_{noload\,leg} \end{aligned} \tag{5.1}$$

While Browning *et al.* [16] characterizes the metabolic rate of the subject with loaded segments, for this study, it is more informative to capture the change in the metabolic rate due different reflected inertia levels of various exoskeletons. Along these lines, the change in the metabolic rate due to inertial effects is extracted from [16], by characterizing the change from unloaded conditions to loaded ones. Eq (5.2)–(5.3) present the metabolic model used to analyze the effect of the inertial properties of the exoskeletons on the metabolic rate.

$$\begin{aligned} \Delta MC_{Waist} &= 0.045 \times m_{Waist} \\ \Delta MC_{Thigh} &= 0.075 \times m_{Thigh} \\ \Delta MC_{Shank} &= 0.076 \times m_{Shank} \end{aligned} \tag{5.2}$$

$$\begin{aligned} I_{ratio} &= \frac{I_{Exo,segment} + I_{unloaded\,leg}}{I_{unloaded\,leg}} \\ \Delta MC_{Thigh} &= ((-0.74 + (1.81 \times I_{Thigh,ratio})) \times MC_{unassisted}) - MC_{unassisted} \\ \Delta MC_{Shank} &= ((0.63749 + (0.40916 \times I_{Shank,ratio})) \times MC_{unassisted}) - MC_{unassisted} \end{aligned} \tag{5.3}$$

During the multi-criteria comparisons and the selection of an optimal solution among all non-dominated solutions, the detrimental effects of the mass and inertia of the exoskeletons on the metabolic cost of the subjects are reflected on the Pareto solutions according to Eq (5.2)–(5.3). Then, these solutions are filtered to obtain the Pareto front curves with the effect of the exoskeleton inertial properties on the metabolic expenditure.

5.2.2 Modified Augmentation Factor

To facilitate the design selection among the solutions on the Pareto front curves, the augmentation factor (AF) is utilized as another primary metric to enable systematic analysis of the performance of devices under the effect of their inertial properties, for both *loaded* and *noload* conditions. The augmentation factor has been proposed by Mooney *et al.* [17] to measure the relationship between the device applied positive power and the change in metabolic power consumption. The augmentation factor estimates the metabolic power change due to carrying the exoskeleton, balancing the mean positive power resulting in a metabolic improvement and the net dissipated power and device weights causing metabolic detriment.

Although the augmentation factor introduces a general factor for predicting the performance of assistive devices, it does not address the effect of reflected inertia due to the actuation units and mass attached to moving segments. On the other hand, Browning *et al.* [16] note the importance of the inertial effects on the metabolic burden of subjects, advocating for the necessity of including this factor to any performance measurement of exoskeletons. Consequently, we introduce a modified augmentation factor (MAF) to augment the augmentation factor with such inertial effects.

In order to include the inertial effects into the augmentation factor, the detrimental effects of the mass and inertia of the exoskeletons on the metabolic cost of the subjects are modeled as in Eq (5.2)–(5.3) and the device location factor γ_i is computed for the inertia applied to each segment, according to Eq (5.4). It is noteworthy to mention that γ_i is obtained considering the device inertia in addition to the inertia of the unloaded leg. Furthermore, the mass of each segment is verified to be within the range of weights of the exoskeletons studied by Mooney *et al.* [17] for calculating the augmentation factor.

$$\gamma_i = \frac{A_i \times m_{subjects} \times MC_{unloaded}}{I_{unloaded}} \qquad i \in \{1, 2, 3\} \tag{5.4}$$

In the inertia position factor in Eq (5.4), A_i are the multipliers of I_{ratio} in Browning metabolic models [16] for the foot, thigh and shank segments, while $I_{unloaded}$, $m_{subjects}$, and $MC_{unloaded}$ represent the inertia of a leg without any external load, the mean weight of subjects, and the metabolic rate of subjects walking without any load on their segments, respectively. The modified augmentation factor (MAF) is obtained by adding the effect of inertia on the metabolic detriment part of this factor, as in Eq (5.5).

$$MAF = \frac{p^{+} + p^{disp}}{\eta} - \sum_{i=1}^{4} \beta_i m_i - \sum_{j=1}^{3} \gamma_j I_j \tag{5.5}$$

$$p^{disp} = \alpha(p^{-} - p^{+}) \qquad \alpha = \begin{cases} 1 & p^{+} < p^{-} \\ 0 & p^{+} \geq p^{-} \end{cases} \tag{5.6}$$

In Eq (5.5), p^{+}, p^{-}, and p^{disp} represent the mean positive, negative, and dissipated power calculated through Eq (5.6). The symbol β_i in MAF stands for the location factors of the device mass, which are taken as 14.8, 5.6, 5.6, and 3.3 W/kg from the foot to waist, respectively [16, 17]; the symbol γ_j represent the location factors of the device inertia, which are set to 47.22, 27.78, and 125.07 W/kg.m^2 from the foot to thigh, respectively. Consistent with augmentation factor, MAF uses a muscle-tendon efficiency of $\eta = 0.41$ to convert the mechanical assistive power to metabolic power, as empirically determined by Sawicki and Ferris [149] and Malcolm *et al.* [28]. Finally, MAF is normalized by the weight of each subject.

5.2.3 Effect of Regeneration on Efficiency

The regeneratable power of the optimal exoskeletons can be acquired by capturing the negative power profiles of the assistive actuators and obtaining the dissipated power from the negative power profile. This dissipated power is normalized by the mass and the gait duration of each subject during each trial and multiplied by the efficiency factor of the power electronics. The effect of regeneration on

optimal devices and their trade-off curves can then be studied by subtracting the regeneratable power from the total power consumption of the devices.

The regeneration performance of optimal devices are studied using various efficiency factors. While the maximum reported efficiency of harvesting dissipated power ranges between 30% to 37% for the lower limb assistive devices [150], custom power electronics of MIT Cheetah robot [151] and the biomechanical power harvester developed by Donelan *et al.* [152] report experimentally verified regeneration efficiencies up to 63%. Along these lines, a maximum efficiency of 65% is considered in this study.

5.2.4 Root mean square error of profile in gait phases.

To establish quantitative and systematic comparisons between two profiles of selected optimal devices, we obtained the root mean square error (RMSE) between overall and phases of profiles. The phases of a general gait cycle were adopted from [153, 154] and customized for each subject and trial according to their toe-off timing, as represented in 5.2. The gait cycle of each subject and trial was then partitioned to its phases, and we used the root mean square error (RMSE) method to compute the difference between the two profiles in each phase of the gait cycle and reported them by their mean and standard deviation over the subjects.

5.3 Optimal devices performance

The analyzed assistive devices in the previous section and their effect on metabolic cost and muscular activation of the subjects in two different load conditions were studied under the assumption that the assistive actuators have no bounds on the amount of the moment they can supply to the musculoskeletal model. However, this assumption is not a descriptive assumption for the real-time designing and controlling of assistive devices because these devices, and especially untethered exoskeletons, have some constraints on the amount of moment that their actuation unit can provide to assist the joint of interest, and the power suppliable from the battery for untethered exoskeletons is limited by the battery life.

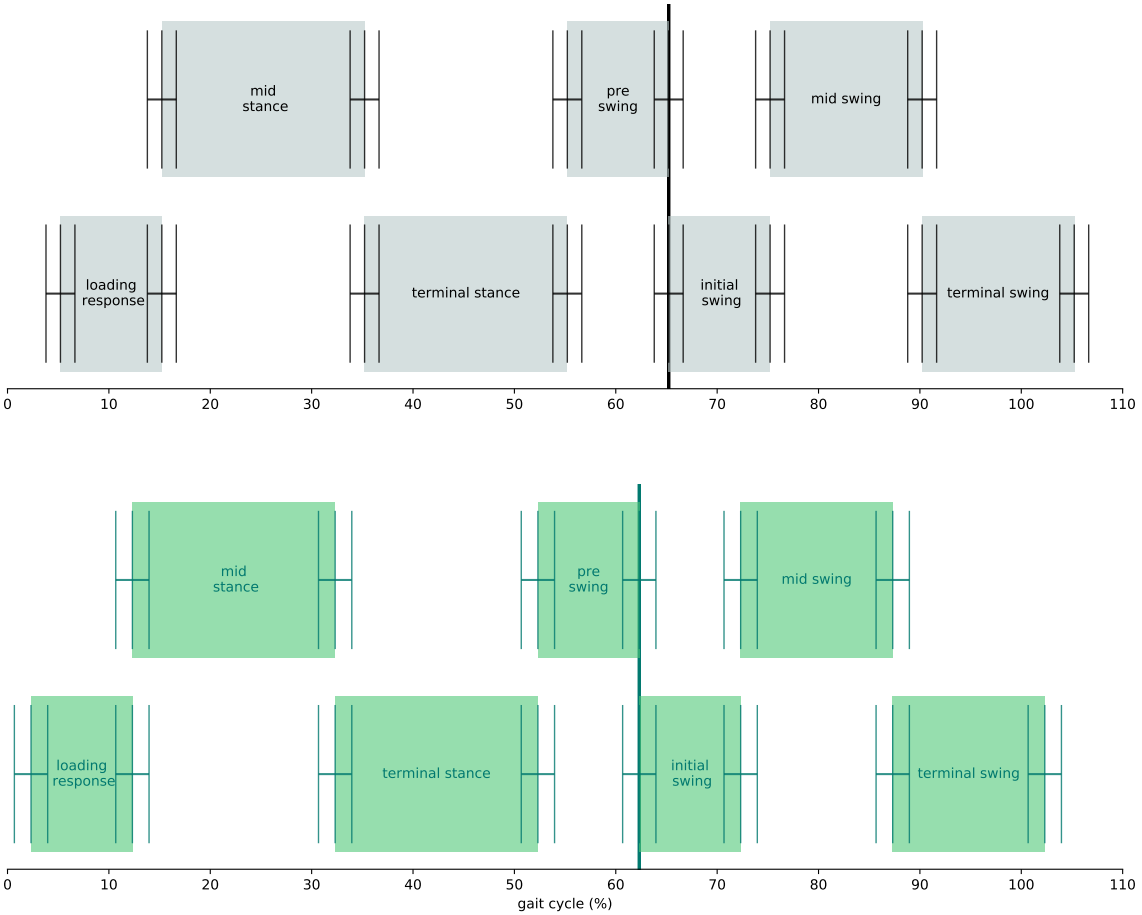

FIGURE 5.2: Phases of loaded and unloaded walking gait cycle

One of the main intentions of simulation based multi-criteria optimization was to address the mentioned limitation through a simulation-based study in which we can analyze the performance of assistive devices under the limitation of their actuators on providing torque to the joints. The study was accomplished by constraining the maximum torque the assistive actuators can provide, and the optimal trade-off between the metabolic cost reduction and power consumption of the devices was obtained. The average Pareto front for the bi-articular and mono-articular exoskeletons for both loading conditions of the subjects are represented in Figure 5.3; the label on each marker is denoted to results from different peak torque constraints. The hip and knee constraints are labeled from A to E and a to e respectively. The A, a to E, e labels represent for 70 N.m to 30 N.m constraints respectively, and each marker, which stands for a specific configuration of a device, is labeled by the hip and knee constraints labels. The optima points on Pareto

fronts are resulted from averaging over 7 subjects.

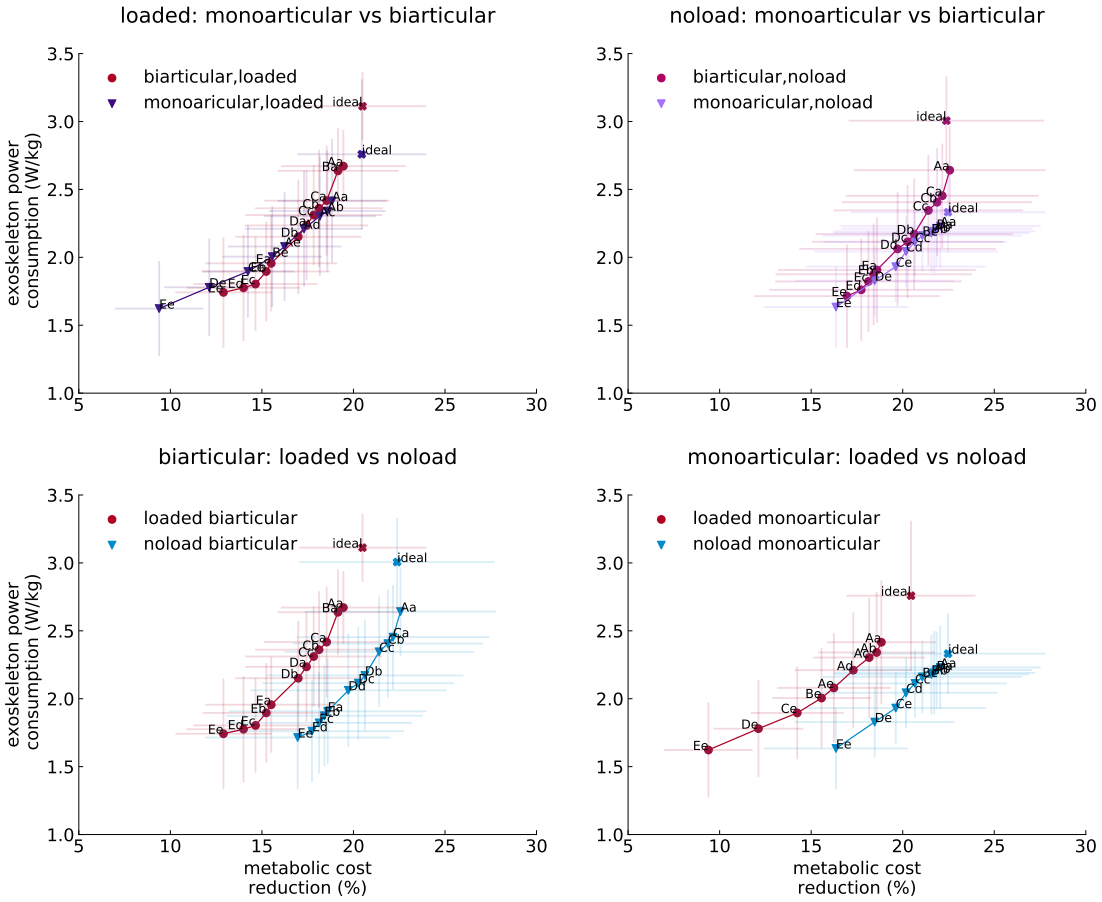

FIGURE 5.3: Optimal trade-offs between metabolic cost reduction and device power consumption.

One of the immediate indications provided by the Pareto front curves was that the torque-limited devices with sufficiently large torque bounds at the hip and knee actuators could provide nearly the same level of assistance that was provided by the ideal exoskeletons with significantly lower power consumption in both load conditions (Table 5.2). In particular, selected torque-limited devices from Pareto front curves of both devices were able to provide nearly the same assistance to the subjects that were provided by the ideal exoskeletons, whereas the power consumption in the exoskeletons was reduced compared to their ideal devices, which was supported by statistically significant differences between the power consumption of ideal and torque limited devices. Although the total power consumption of the torque limited and ideal devices demonstrated significant differences, the

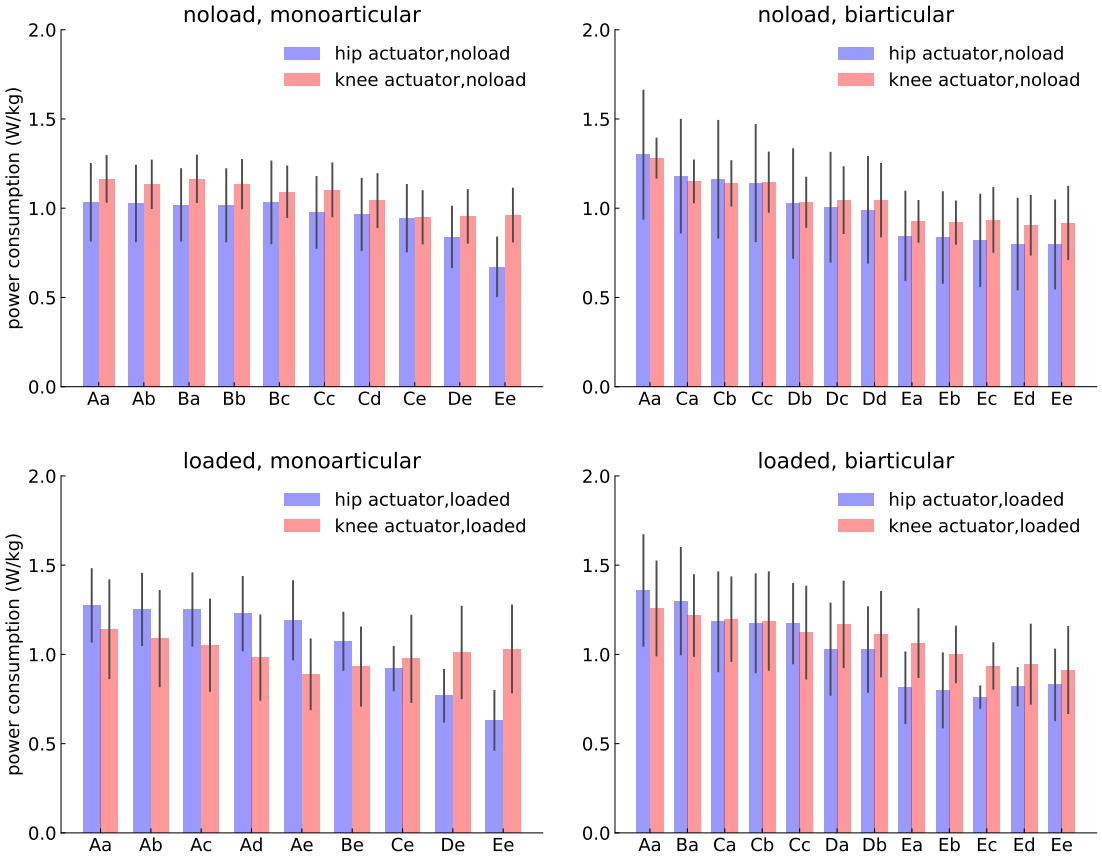

FIGURE 5.4: Power consumption of optimal assistive actuators

power consumption of some actuators did not demonstrate a significant pairwise difference. The same as the average power consumption, the cost of carrying both devices was reduced significantly (one-way ANOVA; within-subjects factor: subjects; between-subjects factor: peak torque constraint) in both loading conditions.

The performance of devices under peak torque limitation and comparison with the ideal devices implies that the comparison of assistive devices with ideal actuation units is not a legitimate comparison and it just conduct a comparison between shadow points of two different type of devices. These results suggesting that the comparison between assistive devices should be conducted using optimal trade-off points of devices in which a device has its optimal performance in both the power consumption and metabolic cost reduction criteria.

The bi-articular and mono-articular exoskeletons show practically similar performance in assisting subjects in both *loaded* and *noload* conditions. Nevertheless,

TABLE 5.2: Power consumption and metabolic cost reduction of ideal and torque limited actuators.

Configuration	Device type	Condition	Hip power consumption (W/kg)	Knee power consumption (W/kg)	Metabolic cost reduction (%)
bi-articular	ideal	*noload*	1.42 ± 0.32	1.58 ± 0.30*	22.38 ± 4.91
	ideal	*loaded*	1.58 ± 0.29†	1.52 ± 0.29‡	20.49 ± 2.87
	Torque limited "Db"	*noload*	1.03 ± 0.31	1.03 ± 0.14*	20.36 ± 5.39
	Torque limited "Db"	*loaded*	1.03 ± 0.24†	1.11 ± 0.24‡	16.99 ± 3.44
mono-articular	ideal	*noload*	1.09 ± 0.24	1.24 ± 0.13$^{\gamma}$	22.47 ± 4.89
	ideal	*loaded*	1.52 ± 0.28§	1.24 ± 0.27	20.45 ± 2.81
	Torque limited "Ce"	*noload*	0.98 ± 0.20	1.10 ± 0.15$^{\gamma}$	20.67 ± 5.01
	Torque limited "Be"	*loaded*	1.07 ± 0.17§	0.93 ± 0.22	15.56 ± 2.71

Note: equal superscripts indicate a pairwise statistically significant difference (7 subjects, 3 trails, Tukey Post-hoc, $P < 0.05$).
$*$: $F(1,12) = 6.284$, $P = 0.028$; §: $F(1,12) = 11.889$, $P = 0.005$; ‡ : $F(1,12) = 4.747$, $P = 0.050$; † : $F(1,12) = 12.313$, $P = 0.004$.
γ : $F(1,12) = 13.591$, $P = 0.003$.

TABLE 5.3: Maximum positive power of ideal and torque limited actuators.

Configuration	Device type	Condition	Hip power consumption (W/kg)	Knee power consumption (W/kg)	Metabolic cost reduction (%)
bi-articular	Ideal	noload	4.65 ± 0.75*	5.10 ± 0.81**	22.38 ± 4.91
	Ideal	loaded	4.90 ± 0.76†	5.62 ± 1.55‡	20.49 ± 2.87
	torque limited "Db"	noload	3.54 ± 0.87*	3.07 ± 0.43**	20.63 ± 5.39
	torque limited "Db"	loaded	3.06 ± 0.54†	3.26 ± 0.68‡	16.99 ± 3.44
mono-articular	Ideal	noload	2.92 ± 0.44§	4.24 ± 0.74	22.47 ± 4.89
	Ideal	loaded	4.08 ± 0.69$^{\gamma}$	4.24 ± 0.97$^{\gamma\gamma}$	20.45 ± 2.81
	Torque limited "Ce"	noload	2.29 ± 0.39§	3.97 ± 0.83	20.67 ± 5.01
	Torque limited "Be"	loaded	2.67 ± 0.45$^{\gamma}$	3.19 ± 0.59$^{\gamma\gamma}$	15.65 ± 2.71

Note: equal superscripts indicate a pairwise statistically significant difference (7 subjects, 3 trails, Tukey Post-hoc, $P < 0.05$).
$*$: $F(1,12) = 5.863$, $P = 0.032$; § : $F(1,12) = 8.361$, $P = 0.014$; ‡ : $F(1,12) = 13.491$, $P = 0.003$; † : $F(1,12) = 20.082$, $P = 0.001$.
γ : $F(1,12) = 22.015$, $P = 0.001$; $**$: $F(1,12) = 39.441$, $P < 0.001$; $\gamma\gamma$: $F(1,12) = 5.944$, $P = 0.031$

analyzing the power consumption of the devices on the Pareto front reveals that the mono-articular device was considerably affected by the load condition of subjects in that the performance of the mono-articular exoskeleton became practically identical with the bi-articular device when subjects were in *loaded* condition, whereas the mono-articular device with larger torque limits had a slight superior performance in *noload* condition.

The detailed analysis of the mono-articular device shows that both actuators of this device were affected by loading subjects with a heavy load (Figure 5.3 and 5.4), and unlike the *noload* condition where the power consumption of the knee actuator was dominant to the hip in all optimal devices, loading subjects increased the amount of mechanical work performed by the hip actuator. In contrast, the power

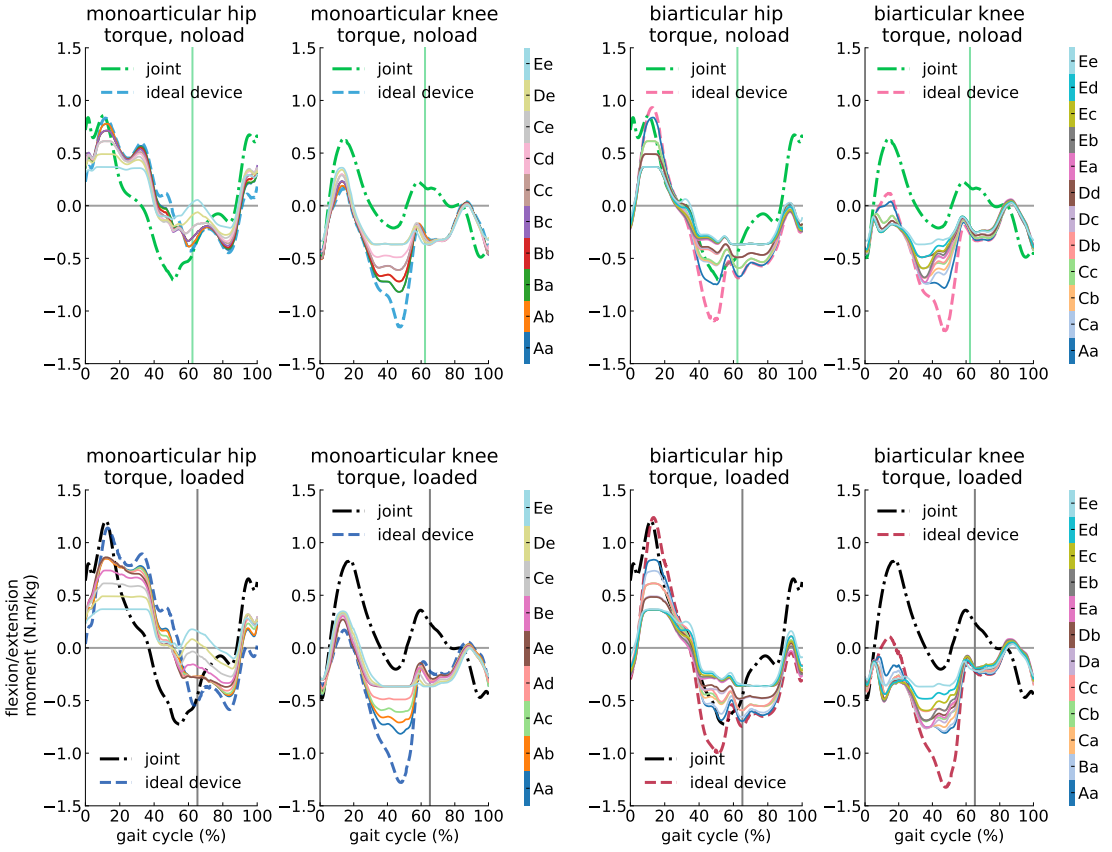

FIGURE 5.5: Optimal assistive devices torque profiles compared to joint moments.

consumption of the bi-articular knee and hip actuators was not affected noticeably by loading subjects, as seen in Figure 5.4, representing the power consumption of optimal devices. Additionally, the optimal configurations of the bi-articular exoskeleton were mostly similar in the subjects walking while carrying a heavy load and walking with no load, whereas the mono-articular exoskeleton had different configurations in both load conditions. The practically similar configurations and performances of the bi-articular exoskeleton in both load conditions can facilitate the design of a bi-articular device and development of a generic controller to assist subjects in different load conditions.

5.4 Optimal device torque and power profiles

The torque profiles of torque limited optimal devices differed from the net joint moments of the hip and knee joints, and the general torque trajectories of these actuators were mostly similar to the torque profiles of the devices with ideal actuators. The ideal and torque limited torque profiles of bi-articular hip actuators had magnitude differences mostly during mid-stance and terminal-stance to terminal-swing phases. In contrast to the hip actuator, the knee actuator had practically the same profile as the ideal knee actuator during the swing phase, but the path and magnitude of the knee actuator were mostly different from those of the ideal device. This comparison between the ideal and torque limited devices is mostly valid when subjects were walking without carrying any load, and the only difference was the magnitude of the torque limited profiles. The torque profiles of torque limited devices are shown in Figure 5.5 in which each line represents the torque profile of a different optimal device defined in the color bar. The label on each marker is denoted to results from different peak torque constraints. The hip and knee constraints are labeled from A to E and a to e respectively. The A, a to E, e labels represent for 70 N.m to 30 N.m constraints respectively, and each marker, which stands for a specific configuration of a device, is labeled by the hip and knee constraints labels. The profiles are averaged over 7 subjects with 3 trials normalized by subject mass.

Both actuators of the torque limited mono-articular device demonstrated differences that were more remarkable in comparison with the profiles of the ideal device. The hip actuators had a significant magnitude difference during the load response phase, and most of the optimal torque limited hip actuators were saturated during the mid-stance and terminal stance phases, which affected their trajectories as well. The difference between hip actuators became significant during the pre-swing to mid-swing phases, during which the torque trajectories of the torque limited hip actuator not only were different from the ideal actuator, but also exhibited high variations among optimal torque limited actuators. The mono-articular knee had

greater resemblance to the ideal knee actuator torque profile when the torque limited and ideal actuators had practically identical profiles during the swing phase, and the differences between them were the higher torque magnitude during the mid-stance and lower magnitude during the pre-swing phases.

The bi-articular knee actuator demonstrated a direction change during the early stance phase in comparison with the torque limited optimal devices (e.g. *noload* "Aa" versus "Ea" devices) and ideal exoskeleton. The reason for this direction change is that the muscle generated moment was exceeded from the knee joint moment during the early stance phase, and the knee actuator opposed the muscle generated moment to follow the knee joint moment trajectory, as shown in Figure B.1 demonstrating the torque profiles of the bi-articular "Aa" versus "Ea" devices in the *noload* condition. The reduction of the torque capacity of the hip actuator decreased the activity of the rectus femoris, soleus muscles, and increased the activity of gastrocnemius, iliopsoas, and vasti muscles, respectively, as shown in Figure B.2 which shows the muscle activity of subjects in the *noload* condition assisted by bi-articular "Aa" and "Ea" devices. The increase in the activity of the vasti muscles as the knee extensor muscles, along with the excessive activity of rectus femoris, causes a higher extension moment during the early stance on the knee joint, compensated by the assistive knee actuator by changing the direction of its trajectory during the early stance phase.

Similar to the bi-articular knee actuator, the hip actuator of the mono-articular exoskeleton showed a considerable variance during the pre-swing and initial swing phases. The reason for this significant variance is rooted in the muscular activities of assisted subjects and the torque capacity of mono-articular hip actuators. Conducting a comparison between mono-articular *loaded* "Ae" and "Ee" exoskeletons shows that by reducing the torque generation capacity of the hip actuator, the activity of rectus femoris reduced and, consequently, the activity of iliopsoas muscles increased during the pre-swing and initial swing phases as shown in Figure B.3. This modified muscle coordination resulted in a muscle-generated moment profile exceeding the net joint moment profile during the pre-swing and initial swing

phases, which was neutralized by the hip actuator of the mono-articular exoskeleton, as can be seen in Figure B.4.

Unlike the bi-articular exoskeleton, in which the load condition only affected the magnitude of the profiles and there was a close similarity between the torque trajectories in *loaded* and *noload* conditions, the torque profiles of the hip actuator of the mono-articular device assisting the subjects walking without carrying any load had considerable differences with the same device in the *loaded* condition. The hip torque profiles of the device in different load conditions exhibited two mostly different trajectories and magnitudes during all phases of a gait cycle, and their differences were more unambiguous during load response to mid-swing phases.

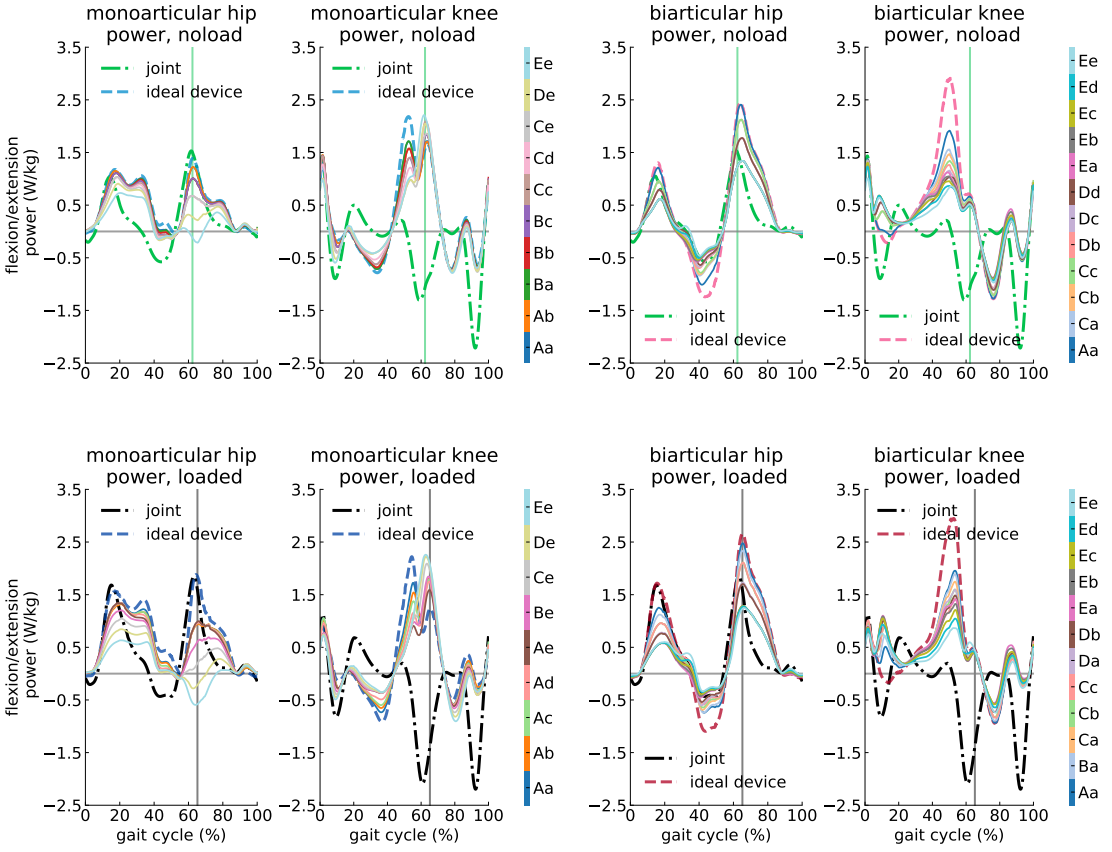

FIGURE 5.6: Optimal assistive devices power profiles compared to joint power.

The power profiles of the torque limited bi-articular and mono-articular devices, which are shown in Figure 5.6 resembled those of the ideal devices, similar to the torque profiles. The bi-articular hip actuator had mostly a similar power

trajectory for the hip in both load conditions with considerably lower magnitude for all optimal devices where this magnitude difference is more substantial during mid-stance and initial swing to mid-swing phases. While the knee actuator had a high correlation with the ideal actuator, the loading response and mid-stance phases of the torque limited knee actuator was different from the ideal actuator, like the torque profile. The torque limited mono-articular hip actuator had a high variation within optimal devices, and most of the optimal configurations had their unique power profile; nevertheless, the optimal devices with the highest peak torque limitations showed a close resemblance to the ideal device. In contrast to the hip actuators, the power trajectories of the knee actuator in both load conditions were similar to those of the ideal device with a difference during the pre-swing to mid-swing phases when the peak power consumption occurs about the toe-off in the torque limited knee actuators.

The power and torque profiles of optimal bi-articular and mono-articular devices reveal that although the optimal mono-articular exoskeletons have a lower power consumption compared to the optimal bi-articular devices, the variation of the torque and power profiles within optimal configurations of the mono-articular device is higher than that of bi-articular devices and the load condition of the subjects can considerably affect the profiles of assistive actuators. These variations within optimal mono-articular devices indicate that achieving a generalized design and control policies for assisting subjects in different load conditions, different actuation, and battery life limitations would be genuinely challenging with mono-articular exoskeletons.

We conducted comparisons between devices and load conditions to analyze the torque and power profiles of selected solutions from the Pareto front of devices in different load conditions qualitatively and quantitatively (using the root mean square method) in each phase of a gait cycle and discussed them comprehensively. Through these comparisons, we showed that even though two devices can have the same performance on the defined objectives space, they can have different power and torque profiles for delivering the assistance, and these differences also affect the muscle coordination of the assisted subject in whom some muscles like

rectus femoris and psoas demonstrated slightly different activation profiles. These comparisons also showed that the bi-articular exoskeletons have approximately the same effect on the subjects in different load conditions comparing optimal devices with about the same power consumption.

5.5 Effect of optimal Devices on Reaction Forces and Moments

The profiles of reaction forces and moments of subjects assisted by the torque limited optimal devices mostly resembled the profiles of reaction forces and moments of subjects assisted by the ideal exoskeletons, and the difference on their maximum suppliable torque did not considerably affect the profiles of the reaction forces and moments. The reaction moments and forces at the ankle joint closely followed the profiles of the ideal devices, indicating that the optimal bi-articular and mono-articular devices had practically the same effect on the muscles contributing to the reaction loads and moments of the ankle joint, as represented in Figures A.8 and A.9. Similar to the ankle joint, the reaction loads of the hip joint also followed the trajectories of the subjects assisted by the ideal devices. Nevertheless, there was a magnitude difference between the ideal and torque limited trajectories, especially during the stance phase of a gait cycle, as shown in Figure A.10.

The devices had a different effect on the reaction forces and moments at the knee and patellofemoral joints. Unlike the ideal bi-articular device, in which the peak reaction moments and forces were reduced in the loading response and increased in late stance phase, the torque limited optimal exoskeletons were not able to reduce the peak reaction loads and moments at the loading response phase. Nonetheless, they demonstrated a better performance than the ideal bi-articular device in the late stance phase and did not increase the reaction forces as ideal devices (Figure A.11 and Figure A.14). It may be reasonable to deduce that this different behavior was due to the changes in the activation of the rectus femoris, iliopsoas, and hamstring muscles, which was shown in the case studies for selected configurations.

The torque limited optimal mono-articular exoskeletons had better performance on reducing the reaction moments and forces. The reaction moments and forces in this assistive device more closely resembled the trajectories of the reaction moments and forces in the ideal assistance scenario during the loading response, and the torque limited devices were able to reduce the peak moments and forces during the late stance phase better than during their ideal configuration (Figure A.11 and Figure A.14). The optimal torque limited devices had more within device variations in the reaction moments and forces trajectories, which may be due to high within device deviations of their torque profiles. Similar to the differences between the profiles of ideal and torque limited bi-articular exoskeletons, the differences between the torque limited mono-articular and bi-articular exoskeletons also might be due to the discrepancy in their effect on the muscular activation of assisted subjects.

5.6 Regeneration Effect

The significant power requirement of the untethered exoskeletons and the finite density of the power source of the proposed assistive devices constrain their assisting duration and make them dependent on their battery life [150]. The review published by Young and Ferris [24] reported that the maximum functioning duration of portable exoskeletons is 5 hours indicating several recharging requirements in a day. Harvesting the dissipated power of assistive devices can address this issue on mobile exoskeletons and help users to be more independent by prolonging the device battery life [150, 155, 156]. Regenerating and harvesting power has been utilized in different assistive devices to improve the efficiency of the device, which has been excellently reviewed in several papers [150, 155, 156].

The power harvesting with the reported highest efficiency (i.e. 65%) had a positive effect on the devices, enabling some new configurations in both devices to become optimal solutions in the amount of power consumption for delivered assistance, as shown in Figure 5.7 and 5.8. Analyzing the performance of both devices throughout the reported efficiency range demonstrates that the performance of the

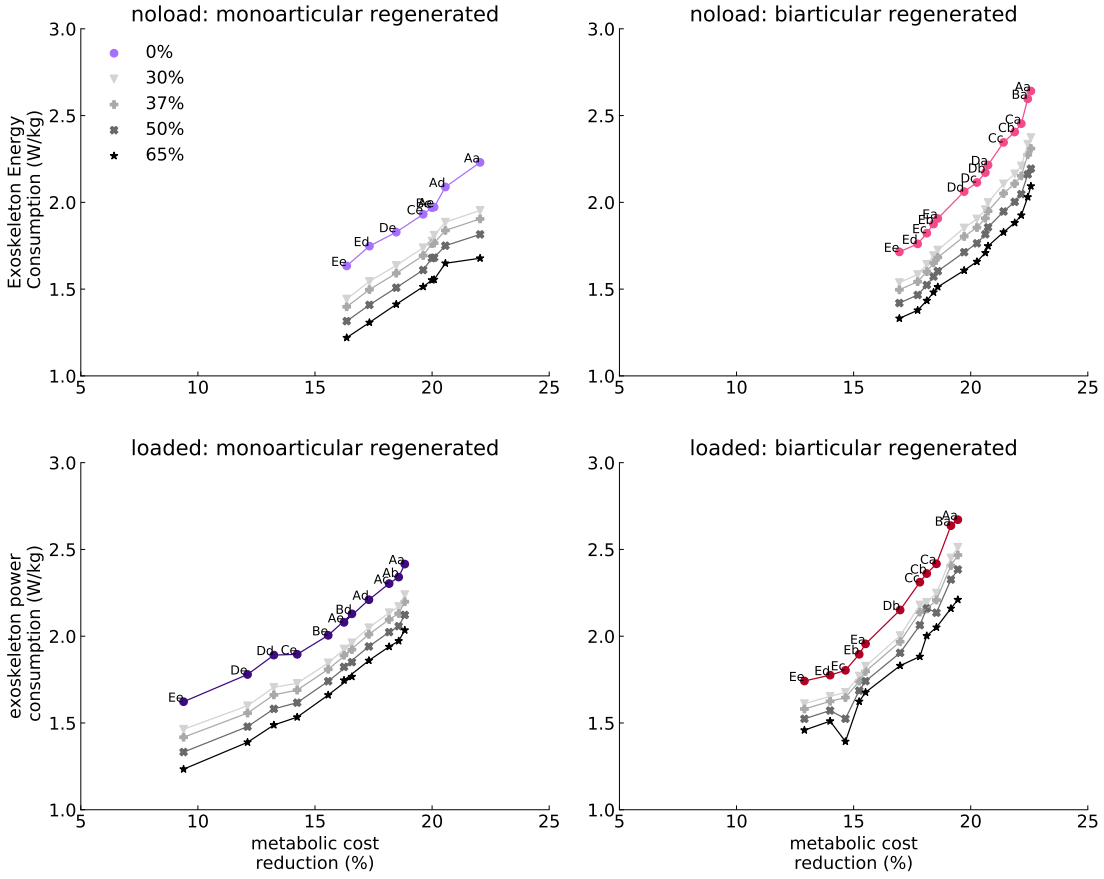

FIGURE 5.7: Pareto fronts of devices under regeneration effect with different harvesting efficiency.

system can be improved, even with a low power harvesting efficiency. Although designing an assistive device with a regeneration mechanism can be challenging from both mechanical and electrical perspectives, this result, shown in Figure 5.7, indicates that the performance and independence of the assistive device can be significantly improved, even with a relatively weak performance of a regeneration mechanism. Additionally, this power requirement reduction can enable the battery and mechanical designers to reduce the load of the battery and device on the musculoskeletal system of subjects, which is causes metabolic power consumption increase in an individual being assisted and requires the device to compensate for this increase ahead of providing assistance to the subject.

Conducting comparisons between the devices and load conditions showed that the

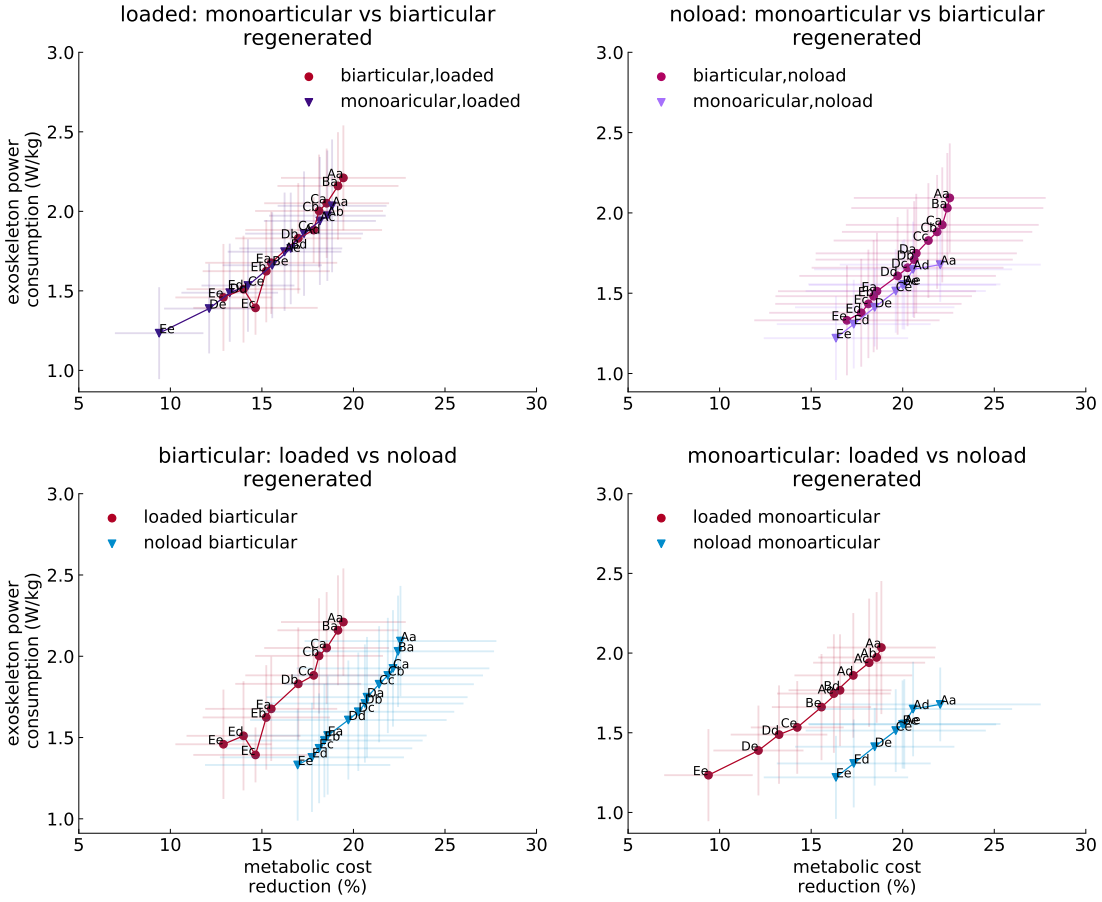

FIGURE 5.8: The main Pareto fronts of devices under regeneration effect with 65% harvesting efficiency.

knee actuator of the torque limited mono-articular exoskeletons has a large regeneration capacity, indicating the inefficient power profile of the knee actuator of the mono-articular devices. Unlike the mono-articular exoskeleton in which the regenerable power of the knee actuator was significantly larger than the hip actuator, both actuators of the bi-articular exoskeleton had similar regeneration capacity. In addition to this property of the bi-articular device, the regenerable power of this device was significantly decreased by loading subjects with a heavy load. Although the low regenerable power capacity reduces the effect of the regeneration on the device power consumption, this shows that the power profiles of the bi-articular exoskeletons are more efficient in delivering the positive power to the musculoskeletal system in *loaded* condition compared to the mono-articular exoskeletons. The regeneration additionally changed the slope of the bi-articular

Pareto front curves and enabled this configuration to achieve more optimal solutions on the higher torque requirement regions, while the performance of the mono-articular exoskeleton was not affected considerably in high peak torque regions, as shown in Figure 5.8.

5.7 Effect of Optimal Device Inertial Properties on Subject Metabolics

One of the main challenges with designing mobile exoskeletons is the effect of their mass and inertia, augmented to the extremities of assisted subjects on the metabolic rate of subjects. The effect of mass and inertia on the metabolic cost has been studied by several researchers [16, 157]. It has been shown that the metabolic rate of the subject changes considerably by adding mass and inertia [16, 157, 158].

The proposed exoskeletons in this study have different inertial properties due to their kinematic designs and this difference results in a different effect on the metabolic power consumption of subjects. Since the current neural control algorithm of OpenSim is not able to simulate any variations in the musculoskeletal model that has not been captured by experimental data [98], we estimated the effect of the mass and inertia offline using the model proposed by Browning et al.[16] for the effect of mass and inertia on the metabolic cost of subjects.

The study by Browning *et al.* [16] proposed a linear model for the effect of adding mass and inertia on each segment of the lower limb by experimentally capturing and analyzing the effect of adding mass to different segments of the lower extremities and their inertia on the metabolic power expenditure of the subjects. In this study, subjects walked at 1.25 m/s without carrying any heavy load on their torso, which is similar to the data captured from the subjects in the walking with *noload* condition at their self-selected speed [15]. This qualitative match between the data and experimental protocols of [16] and [15] enabled us to employ the developed model of [16] to study the effect of mass and inertia added by assistive devices

through offline simulations for the subjects walking at free speed without carrying any external load (i.e.*noload* condition).

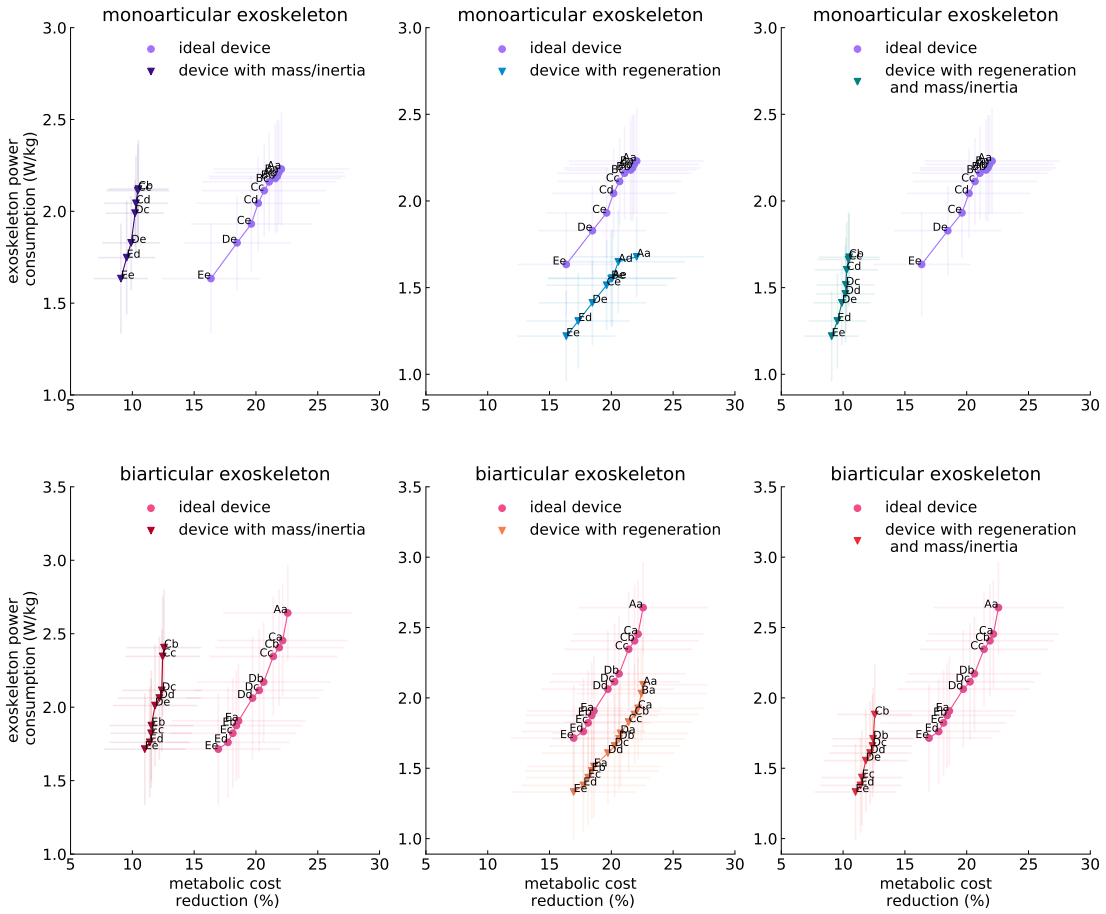

FIGURE 5.9: Pareto fronts of devices in ideal condition and under regeneration and device mass and inertia effects.

The effect of inertial properties of devices on the simulated devices was significant, changing most of the solutions on the optimal trade-off curve, as represented in Figure 5.9. The highest peak torques in both mono-articular and bi-articular exoskeletons are 60 N.m for the knee and 50 N.m for the hip joint. Since the inertia of devices was affected by altering the peak torque, these results indicate that the reflected inertia has a considerable effect on the optimality of a device, and power consumption of a mono-articular exoskeleton with large peak torques is not efficient in comparison to the assistance it provides.

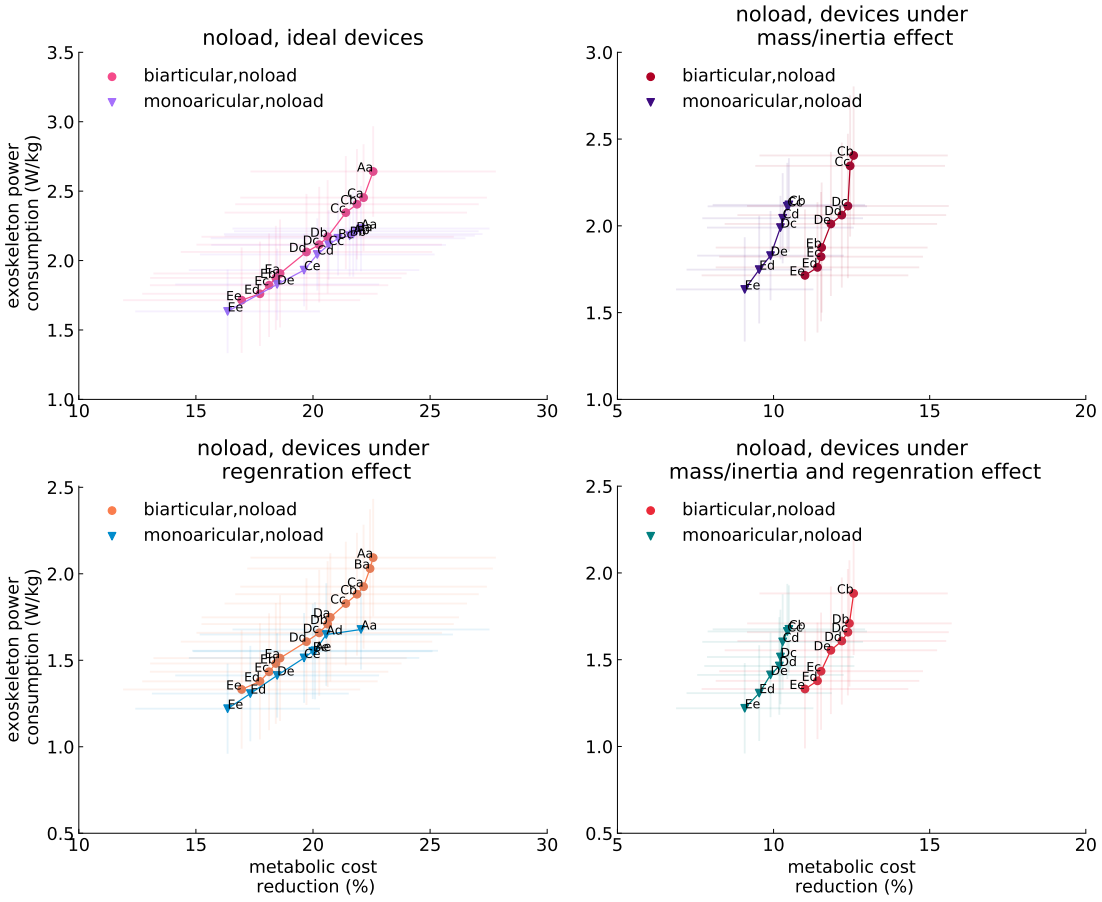

FIGURE 5.10: The comparison of the Pareto fronts of devices in different metabolic and device power expenditure conditions. The bi-articular and mono-articular exoskeletons have been compared in (a)ideal condition, (b)under devices mass/inertia effect on metabolic power consumption, (c)under dissipated power regeneration effect on power consumption of devices, and (d)under the effect of (b) and (c).

While the bi-articular exoskeleton showed a better performance than the mono-articular exoskeleton when the inertial properties of exoskeletons were considered (Figure 5.10), the slope of Pareto front for both exoskeletons indicates that devices with higher torque capacity does not considerably change the amount of assistance that the device can provide to the subjects due to the inertia effect, which can be seen more obviously for the mono-articular device.

The analyses accomplished for the effect of the regeneration and device inertial characteristics on the performance of assistive devices can provide a qualitative perspective for mechatronic systems designers for designing assistive devices. The

general outcome of these analyses shows that selecting an actuator with a high torque density is essential to reduce the reflected inertia effect of gear train on the power expenditure of subjects. The active inertia compensation methods through controller design also can be helpful in reducing the impact of inertia on the metabolic expenditure increase of subjects, which has been used by [159] for controlling a one degree of freedom knee exoskeleton to compensate its inertia; however, this method comes with some coupled stability issues [159–161] that need to be addressed while designing the controller.

The results also showed that keeping the actuator mass near proximal joints and assisting the joint of interest distally has a considerable impact on the metabolic power consumption of subjects. As we discussed previously, this mechanical design conclusion was already studied on the human musculoskeletal system, and it was shown the bi-articular muscles enable human musculoskeletal structures to keep muscle volume near to the trunk and transfer power to the distal joints to reduce the inertia and mass of the leg. Consequently, the bio-inspired bi-articular and multi-articular configurations of the assistive devices can provide a promising improvement in their performance.

Although assistive design with highly effective regeneration requires system-level optimization and complicating the design of assistive devices [150], even a qualitative comparison between devices with regeneration and without regeneration shows a remarkable difference in power consumption. This implies the necessity of regeneration, especially for untethered devices, to improve their independence and their operational duration.

As was discussed, the main difference between the inertial properties of the exoskeletons was the location of augmenting the knee actuator affecting the performance of the mono-articular exoskeleton significantly. According to the developed model, the performance of the mono-articular exoskeleton can be improved by embedding the knee actuator to the upper part of the shank or thigh while its kinematic remains constant. Therefore, we examined the performance of the mono-articular exoskeleton with two different inertial characteristics.

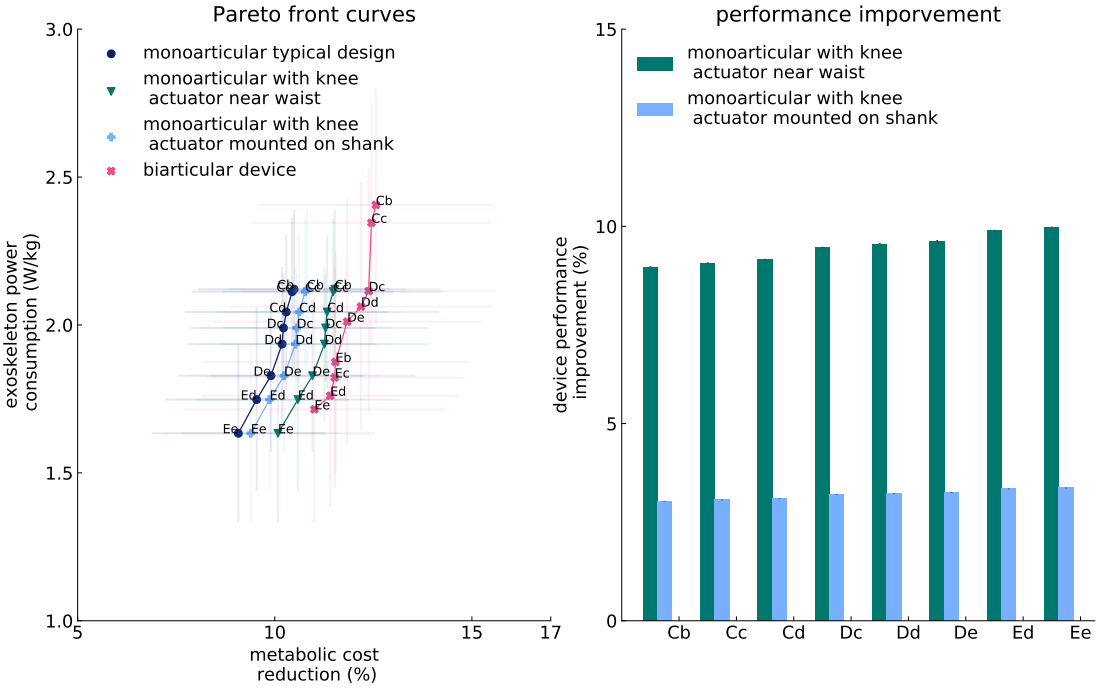

FIGURE 5.11: The comparison of Pareto fronts of the mono-articular devices with different inertial characteristics.

As can be seen in Figure 5.11, both proposed alternative locations for embedding the knee actuator can improve the performance of the mono-articular exoskeleton under their mass and inertia effect. Among these configurations, attaching the knee actuator proximal to the waist performs better than the other configurations of the mono-articular exoskeleton. The proposed alternative mono-articular configurations can be used to design a mono-articular exoskeleton that enables designers to avoid bi-articular device design complexities while achieving performance superior to that of the typical mono-articular exoskeleton design.

5.8 Study Limitations

This simulation-based study of an assistive device has some limitations that need to be considered for any interpretation of the results. One of the main limitations is kinematics and ground reaction forces for the assisted subjects; Although experimental studies reported that an exoskeleton could make minor [14, 29, 32, 162–164] and significant [87, 165–167] changes on assisted subjects kinematics and joint

moment, the OpenSim current neural algorithm (i.e., CMC algorithm) does not capture these changes and it was assumed that unassisted and assisted subjects have the same kinematics, ground reaction force, and joint moment. Nonetheless, it has been reported that metabolic cost may not substantially be affected by kinematics changes [168]. This limitation recently has been addressed by employing dynamic optimization methods for performing simulations, which can capture the changes in the kinematics and dynamics of the assisted subjects.Yet, since altered kinematics can have several side effect such as increasing joint loads, the kinematic adaptation may not be desirable in some conditions [15].

Secondly, as was earlier stated, the assistive devices that we modeled were assumed to be massless without any actuator and link mass and inertia; however, in practice, exoskeleton actuation modules mass and their reflected inertia on the links are large and one of the main challenges on mechanical design of exoskeletons; it was also proven that adding mass to the lower limbs can considerably change metabolic cost of the subjects [16]. Although we addressed this limitation of OpenSim by developing a metabolic model for adding mass and inertia, our model does not capture the effect of inertial properties of devices on the profiles and power consumption of devices. The attachment of exoskeletons to the limbs is also one of the central performance limiting factors of assistive devices [169], which is not modeled in ideal exoskeletons.

Additionally, conducting simulations to obtain the optimal trade-off curve of each exoskeleton comes with a discretization of the problem, which needs to be considered for any interpretation of these Pareto front curves. Another significant limitation of this study is limitations on musculoskeletal modeling. Some influential restrictions on muscles modeling affect assistive device simulation results. One of these restraints is extortionate passive force generated by the muscles [15, 98], which can result in extortionate muscular activities, which was observed in similar work [15] comparing simulation and experimental muscular activities. Another critical issue in Hill-type muscles modeling is that it does not take into account muscle fatigue, which is an effective factor in muscle recruitment strategies [98]. Rectus femoris, which is more vulnerable to fatigue due to its fiber properties [170]

experienced extreme activations in all of the assistance scenarios, which in practice may cause subjects muscle fatigue [171]. Tendon modeling, constant force enhancement, short-range muscle stiffness, training effect, and other factors [98] are limiting factors of the muscles and models that affect the musculoskeletal models and simulations results which need to be considered for any interpretation of this study's results. Additionally, conducting simulations to obtain the optimal trade-off curve of each exoskeleton comes with a large discretization of the problem, which needs to be considered for any interpretation of these Pareto front curves.

Apart from all these general limitations, the dataset and models of unassisted subjects used in this study, had some inconsistency with the experimentally collected data affecting some of the results. One of the specific limitations of these simulations is the excessive passive force at the knee joint due to excessive activity of the knee extensor muscles, which affects the metabolic saving of the studied devices. Another limitation of this dataset is the inconsistency between the experimentally measured and simulation-based estimated metabolic cost of carrying a heavy load in which the simulation-based predicted metabolic cost underestimated the increase in metabolic cost of carrying a load; this underestimation also indicates that the metabolic savings of the simulation-based assisted subjects were also underestimated. We would refer to [15] in which these limitations were discussed more comprehensively.

Furthermore, [98] provides comprehensive information about all aspects of the OpenSim simulations and proposes some recommendations for any interpretation and validation of the simulation results, which can be beneficial in obtaining an accurate interpretation of our results. It is not reasonable to expect to obtain a close quantitative match between the results of our simulations and experiments without acknowledging the discussed limitations and other practical matters.

Chapter 6

Case Studies

We conducted four different case studies to gain more insight into the performance of assistive devices that include studying both assistive devices in a particular load condition or an assistive device in two different load conditions with the same effect on the metabolic power expenditure or the same power consumption of assistive actuators. Investigating these specific configurations of the optimal devices helped us to understand how the profiles of devices with the same performances change in a load condition more systematically. These cases can also help us to gain insight into the effect of load condition on assistive device profiles, and clarify how a particular device can be affected by loading assisted subjects with a heavy load. The selected optimal solutions of each configuration in each of both loading conditions are shown in Figure 6.1.

6.1 Case 1: Devices Performance in Loaded Condition

It was shown that the optimal trade-offs of both exoskeletons are practically the same in the *loaded* condition. To study the performance of each actuator of the devices and their effect on the muscle activity of assisted subjects, we selected two devices on the Pareto front that had nearly the same performance in both

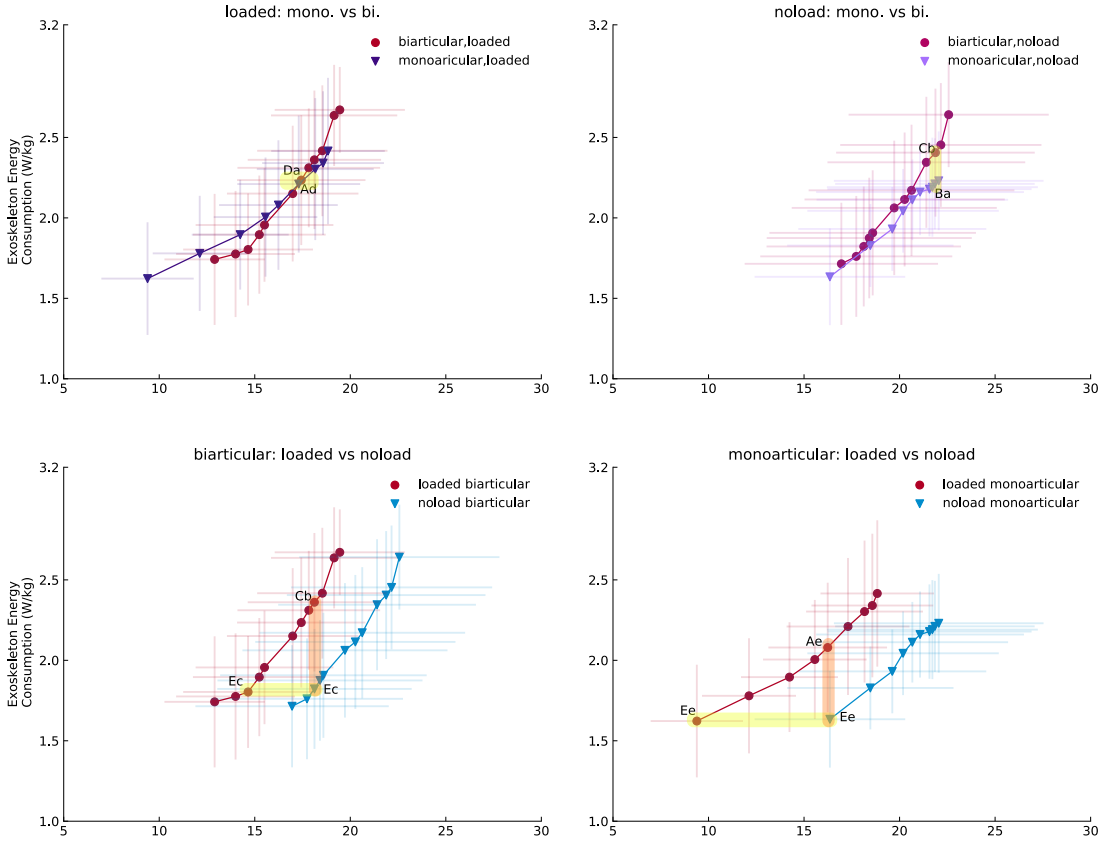

FIGURE 6.1: Studied cases chosen from the Pareto front curves.

metabolic cost reduction and power consumption. The chosen device for the mono-articular exoskeleton has 70 N-m hip peak torque and 40 N-m knee peak torque, which is represented by "Ad" on the Pareto front (Figure 6.1), and the peak torques of the bi-articular device are 40 and 70 N-m on the hip and knee actuators, respectively, represented by "Da " on the Pareto front. As can be inferred from the configurations of devices, although these two chosen devices have the same performance on defined objectives, they have a completely different arrangement on hip and knee actuators. The metabolic rate of assisted subjects with bi-articular and mono-articular devices shows no significant difference between the level of assistance delivered by these devices, which was expected from the Pareto front. While the total power consumptions of these two devices were practically identical on the Pareto front, the power consumptions of the hip and knee actuators between the bi-articular and mono-articular devices were not identical, as represented in Figure 6.2. This dissimilarity indicates that while the devices deliver the same

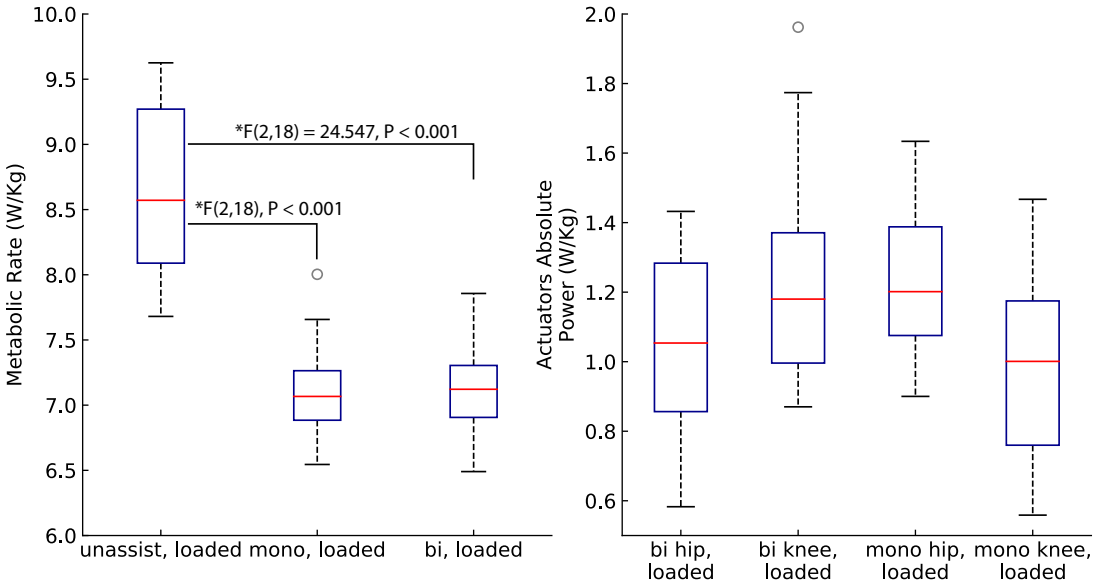

FIGURE 6.2: Assistive devices power consumption and their effect on the metabolic rate.

assistance to the subjects carrying a heavy load, their assistance strategies are different; this claim can be more illuminated by analyzing the profiles of actuators.

Although the selected mono-articular and bi-articular exoskeletons had the same effect on the metabolic rate of *loaded* subjects, it was shown that their assistive actuator configurations were different, resulting in different power consumptions of the actuators. This variation in the configuration of their actuators affects their mechanical design, especially their required gear train and reflected inertia. We employed the developed modified augmentation factor to assess the performance of the bi-articular and mono-articular exoskeletons under the effect of device inertial properties. The computed modified augmentation factors for the mono-articular and bi-articular devices were 0.66 ± 1.00 and 1.98 ± 0.71 W/kg, respectively, which indicates that both exoskeletons would be able to deliver assistance to the subjects even under the inertial properties of the devices, causing a greater metabolic burden on the subject. Additionally, the MAF values show that the bi-articular device had superior performance to the mono-articular exoskeleton, and the reason for this is rooted in the mass distribution and gear train of the mono-articular device. The inertia calculations show that the mono-articular device had nearly

three times more inertia on the thigh than the bi-articular device, and according to the inertia location factor of the thigh, the effect of inertia on the thigh is expensive in terms of the metabolic rate increase, which results in a lower MA factor for the mono-articular exoskeleton.

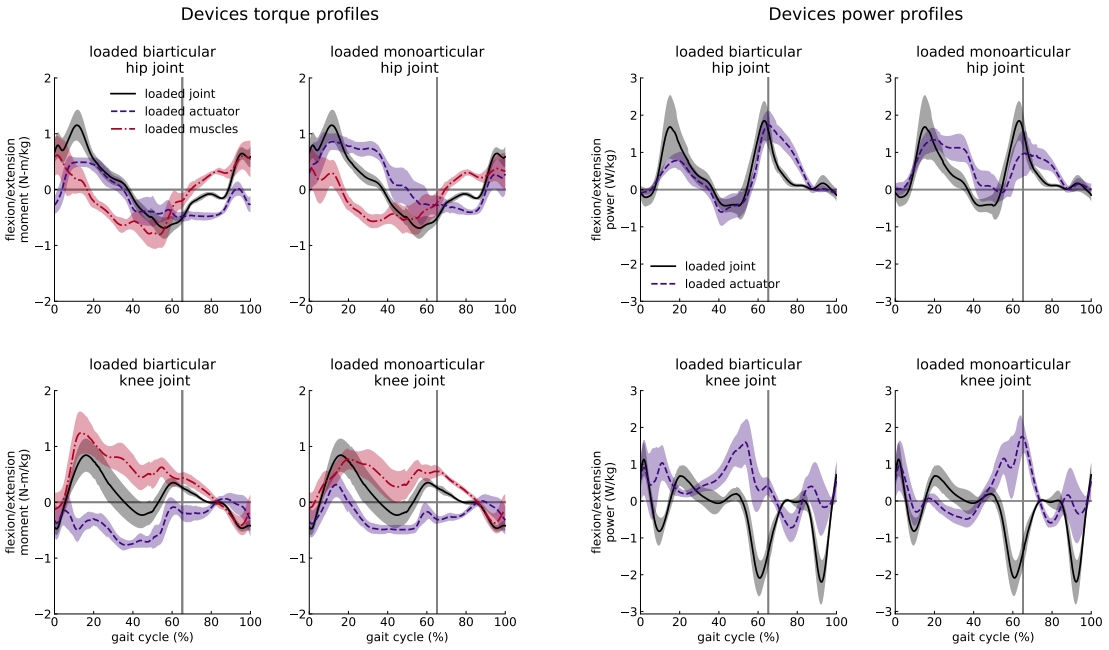

FIGURE 6.3: Assistive devices torque and power profiles.

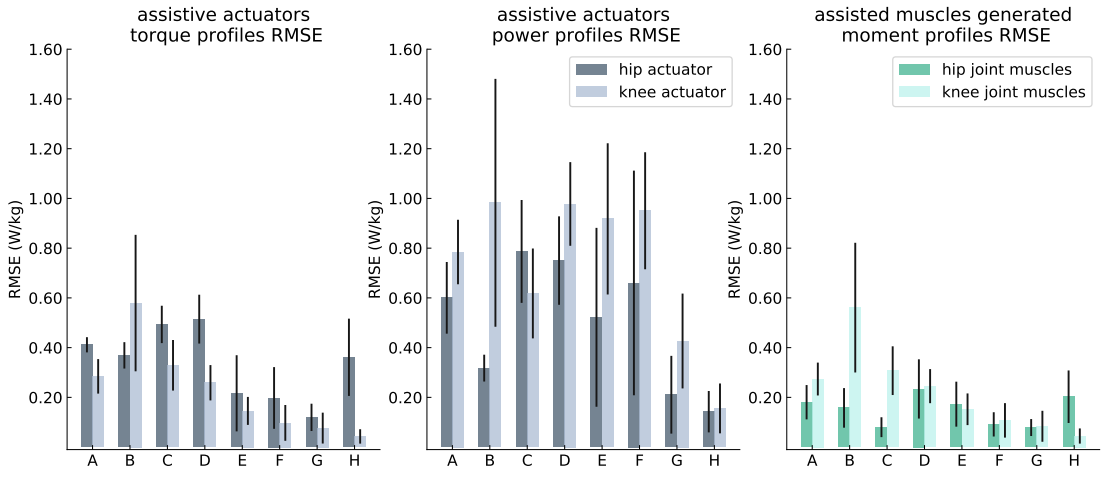

FIGURE 6.4: Assistive devices torque, power, and muscles generated moment profiles root mean square error.

The overall trend between the torque profiles of the mono-articular and bi-articular devices was similar, which can be seen in Figure 6.3 qualitatively, and the root

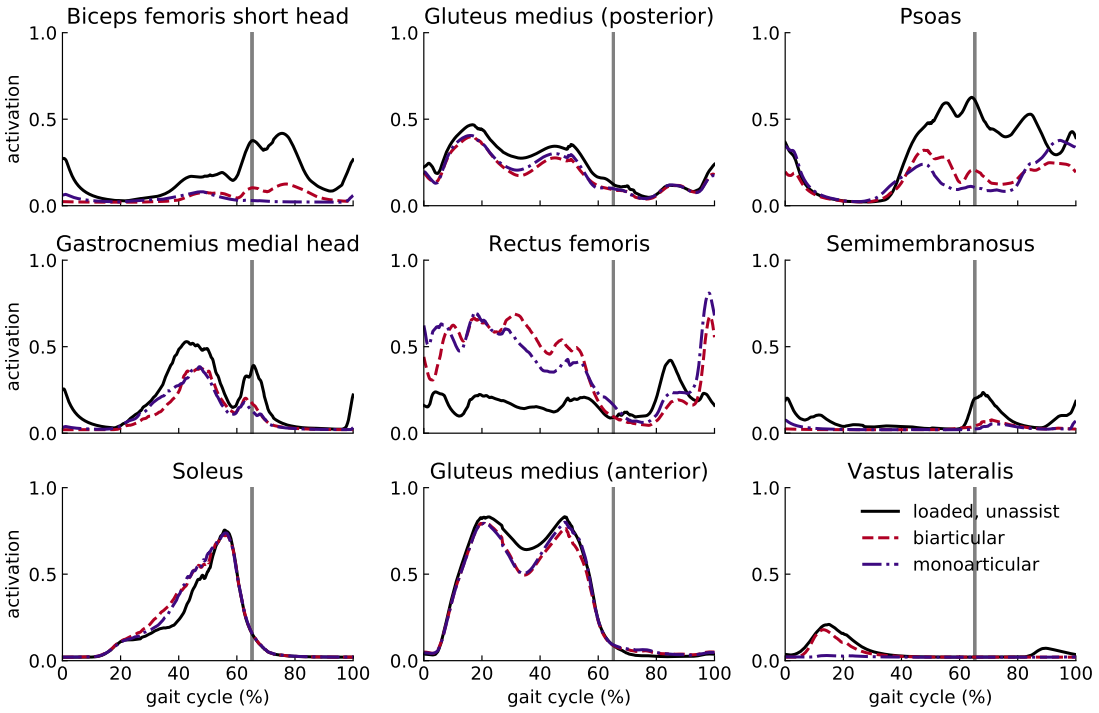

FIGURE 6.5: Activation of representative lower limb muscles of assisted and unassisted subjects.

mean square error between the profiles of the selected devices during a gait cycle also supports this claim quantitatively, as shown in Figure 6.4 in which the RMSE was calculated during a total gait cycle (A), loading response (B), mid stance (C), terminal stance (D), pre swing (E), initial swing (F), mid swing (G), and terminal swing (H) phases. A detailed analysis of the gait cycle shows that the main difference between the torque profiles of the hip actuators occurred during the stance phases, and the mono-articular device delivered hip extension torque greater than the bi-articular device, especially during the mid-stance and terminal-stance phases (Figure 6.3 and 6.4). Although the difference between the profiles of the hip actuators followed similar trajectories during the swing phase, the terminal-swing phase of these actuators was considerably different in that the mono-articular exoskeleton delivered extension while the bi-articular one provided flexion torque to the joint.

Although the bi-articular and mono-articular knee actuators had almost identical trajectories during the swing phase, as their RMSE shows in Figure 6.4, there

were some significant differences between these two actuators during the stance phases. While the bi-articular knee actuator opposed the torque generated by muscles around the knee joint during the all stance phase, the mono-articular knee actuator assisted torque generated by the knee muscles during the loading response and mid-stance phases.

These remarkable differences between the torque profiles of the two devices affected the torque trajectories generated by muscles around the knee and hip joints, indicating muscular activation differences between subjects assisted by the mono-articular and bi-articular exoskeletons; nevertheless, according to the root mean square error between torque trajectories generated by hip and knee muscles, the differences were not substantial except on the loading phase of the knee joint.

The comparison between the muscular activation of the *loaded* subjects assisted by ideal devices and constrained devices indicates substantial differences in some muscles. The activation of rectus femoris and psoas as two primary muscles on the hip and knee was considerably different in the ideal and constrained devices. The constrained bi-articular and mono-articular exoskeletons also had different impacts on these two muscles (Figure 6.5). The difference between the activation of rectus femoris and vasti muscles of subjects assisted by the constrained optimal bi-articular and mono-articular devices during the loading response phase explains the difference between the muscles generated moments of subjects assisted by the bi-articular and mono-articular devices. Another difference between the ideal and torque limited devices was in the gastrocnemius medial head muscle; the activation of this muscle increased during the loading response to terminal stance phases. Due to the higher activation of the gastrocnemius muscle, it provided a greater moment on the ankle joint. Consequently, the activation of the soleus muscle did not increase considerably to compensate for the inadequacy of the moment generated by gastrocnemius at the ankle joint. The differences between the muscular activation of subjects assisted by mono-articular and bi-articular constrained devices were not limited to the rectus femoris and psoas muscles. The other representative muscles also demonstrated some differences, as shown in

Figure 6.5; nevertheless, the differences between them were not as considerable as those of the rectus femoris and psoas muscles.

Unlike the moment profiles of devices in which the difference was significant only in some specific phases, the power profiles of the bi-articular and mono-articular devices had significant differences, as shown qualitatively and quantitatively in Figures 6.3 and 6.4, respectively. The difference between the power profiles of these two devices was notable in the knee actuator in which the devices followed different trajectories during the gait cycle. Similar to the knee actuators, the hip actuators had roughly different power profiles, and their maximum power consumption occurred in two completely different phases, similar to the knee actuators. The difference between the trajectories and magnitudes of the power profiles also explains the difference observed between the power consumption of the mono-articular and bi-articular exoskeletons (Figure 6.2).

Studying the selected mono-articular and bi-articular devices proves that devices with the same total power consumption can have different power consumption in different joints. Additionally, we showed that optimal devices with the same performance could follow different moment and power profiles, even under kinematic similarities due to the arrangement of the actuators. Although the devices were selected from the ideal Pareto front with the same performance, employing the modified augmentation factor for the mono-articular and bi-articular devices with different mass and inertia characteristics indicated the superior performance of the bi-articular device. This emphasizes the discussion held in the ”Effect of Optimal Device Inertial Properties on Subject Metabolics” section in that the bi-articular device could deliver the same amount of assistance to the subjects more effectively than the mono-articular configuration.

6.2 Case 2: Devices Performance in Unloaded Condition

In the second case study, we selected two devices with similar power consumption and the same effect on the metabolic rate of subjects walking without any external load, which are shown as "Cb" and "Ba" on the Pareto front curves of the bi-articular and mono-articular devices, respectively, in the *noload* condition. Similar to the first case study, while the total performance of these two bi-articular and mono-articular devices was similar in mean values on the trade-off curves, the actuators had different power consumptions.

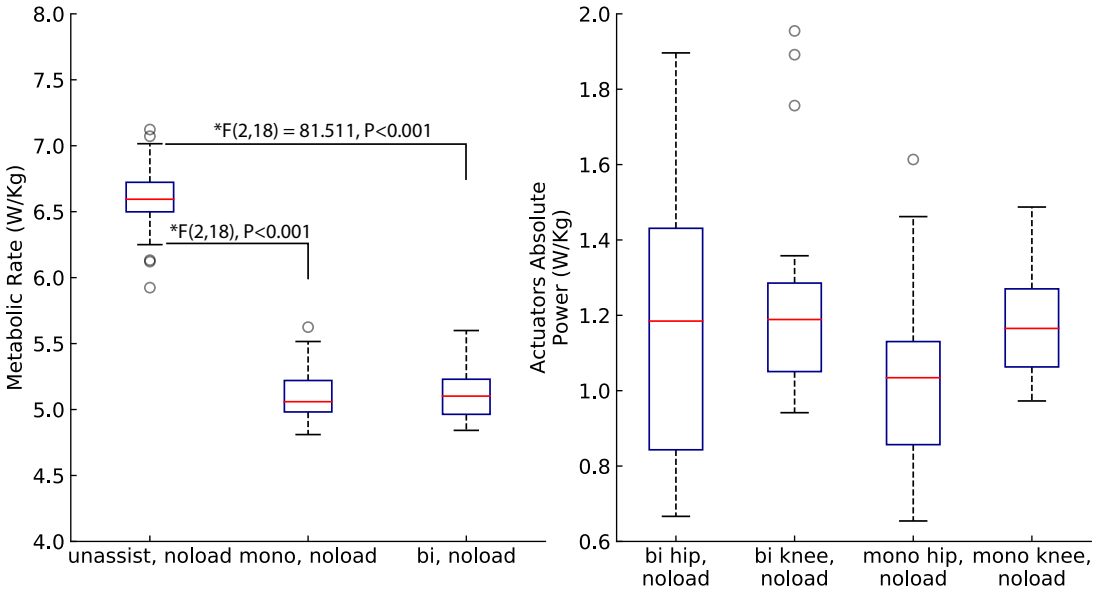

FIGURE 6.6: Assistive devices power consumption and its effect on the metabolic rate.

The power consumption of the hip actuators in both exoskeletons had a high within-subject deviation, as shown in Figure 6.6, which explains the absence of statistically significant differences between the actuators. Additionally, the metabolic rate of subjects assisted with the mono-articular and bi-articular devices had no significant differences. However, the metabolic cost reduction caused a significant difference between the metabolic expenditure of unassisted and assisted subjects, as represented in Figure 6.6.

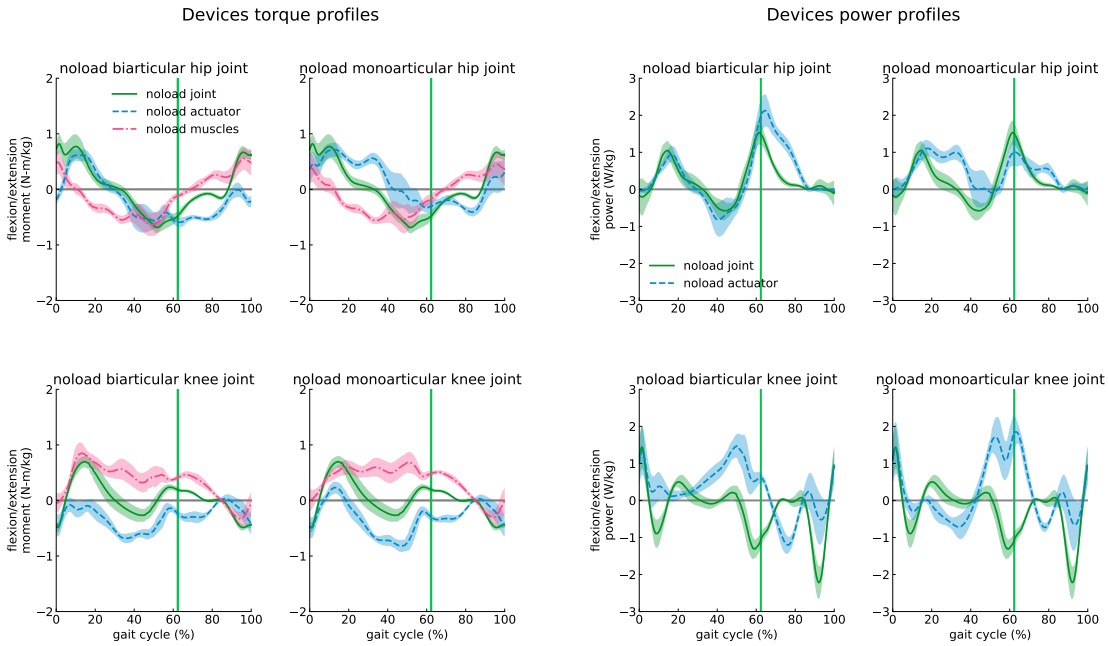

FIGURE 6.7: Assistive devices torque and power profiles.

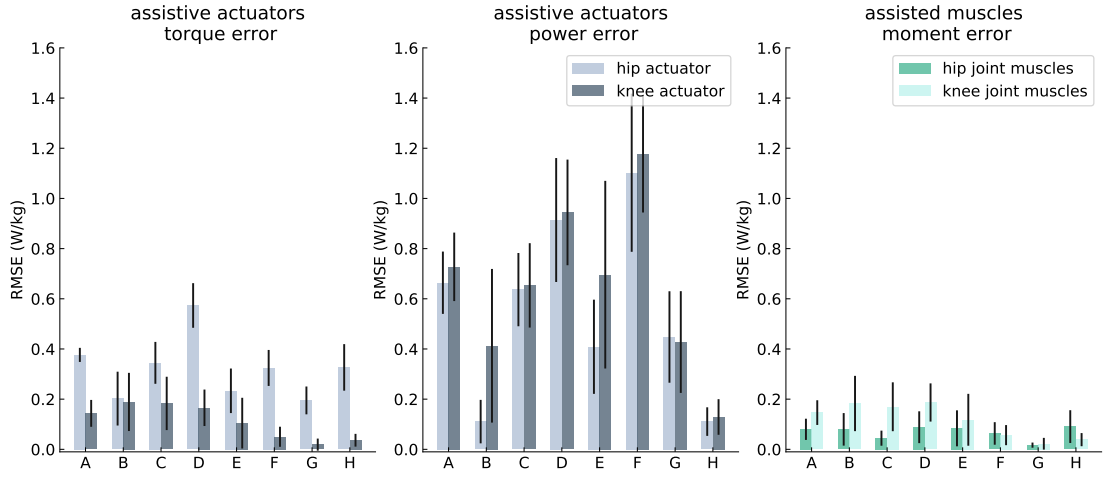

FIGURE 6.8: Assistive devices torque, power, and muscles generated moment profiles root mean square error.

Despite the large variation between the devices' power consumption and the absence of significant difference among their actuators, employing the modified augmentation factor indicates the different performance of the mono-articular and bi-articular exoskeletons delivering assistance to the subjects. The selected devices had a different design in the actuators in which the bi-articular device could provide maximum 50 and 60 N-m torque in the hip and knee actuators, respectively,

while the maximum moments in the hip and knee actuators of the mono-articular device were 60 and 70 N-m, respectively. The computation of MAF under the mentioned configurations of these two devices resulted in 1.57 ± 0.72 and 0.42 ± 0.85 W/kg for the bi-articular and mono-articular devices, respectively, indicating the superior performance of the bi-articular device similar to the first case. The performance of these two devices can also be discussed based on the Pareto front of devices under inertia and mass effect, as shown in Figure 17 in the paper. According to this analysis, the studied configuration of the mono-articular device became a dominated solution in Pareto simulations under the inertial properties of devices, while the chosen bi-articular device could maintain its efficiency under the negative effect of its inertial properties on the metabolic rate of subjects. This analogy between the Pareto front under the effect of the inertial properties of the devices and MAF can also confirm the extension of the augmentation factor.

The analysis of moment profiles of assistive devices in the *noload* condition shows that the differences between these two devices were similar to the difference between the bi-articular and mono-articular devices in the *loaded* circumstance, which is represented in Figure 6.7. Nevertheless, the variations of moment generated by muscles of the assisted subjects were negligible in the *noload* condition (Figure 6.8), which signals similar muscular activation of subjects assisted by these two exoskeletons. Unlike the moment profiles, the devices' power profiles were different in the *noload* condition. It can be seen from the power profiles that the devices followed remarkably different trajectories during a gait cycle to deliver assistance to the subjects and these profiles in the hip actuators, similar to those in the knee actuators, had the highest contrast during the pre-swing phase, according to their RMS error, as shown in Figure 6.8.

Studying specific optimal mono-articular and bi-articular exoskeletons in two load conditions, chosen from the Pareto fronts, shows that even though the devices had practically the same performance in the optimal trade-off between the device total power consumption and metabolic cost reduction curves, their provided moments during a gait cycle had considerable differences, which could cause a different effect on the muscular activation of assisted subjects as well. These two case studies

also show that the power profiles of mono-articular and bi-articular devices are considerably different, while they have a similar total power consumption.

The study on the performance of selected devices in both loading conditions by developed MAF factor supports the discussion in the "Effect of Optimal Device Inertial Properties on Subject Metabolics" section on the effect of mechanical design on the performance of devices and also showed that the performance of the mono-articular exoskeleton was highly affected by the inertial properties of the device. Although the mechanical design of a bi-articular device can be complicated, its performance under the device inertial properties seems promising in both loading conditions, according to the performance of the studied cases. The studied cases and general Pareto front of the mono-articular device under the effect of its inertial characteristics show that this type of device needs to be designed thoughtfully to reduce the effect of inertia and mass effect of the device on the metabolic burden of subjects, complicating the design procedure, and ignoring the mechanical design results in delivering no assistance to the subject, or increasing their metabolic burden.

6.3 Case 3: Bi-articular Exoskeleton Performance

To study how the performance of a bi-articular exoskeleton changes by loading subjects with a heavy weight on torso more specifically, we chose two cases in which the bi-articular exoskeletons had the same effect on the metabolic rate of subjects in one case and had the same power consumption in another case.

The selected configuration of the bi-articular exoskeleton in the *noload* condition was "Ec" with 30 and 50 N-m peak torque in the hip and knee actuators, respectively, and it was compared to the same configuration (i.e., "Ec") in the *loaded* condition in which they had practically the same power consumption. In order to conduct a comparison with the similar metabolic burden reduction, the same configuration of the device in the *noload* condition (i.e., "Ec") was compared to the bi-articular exoskeleton with 50 and 60 N-m peak torque in the hip and knee

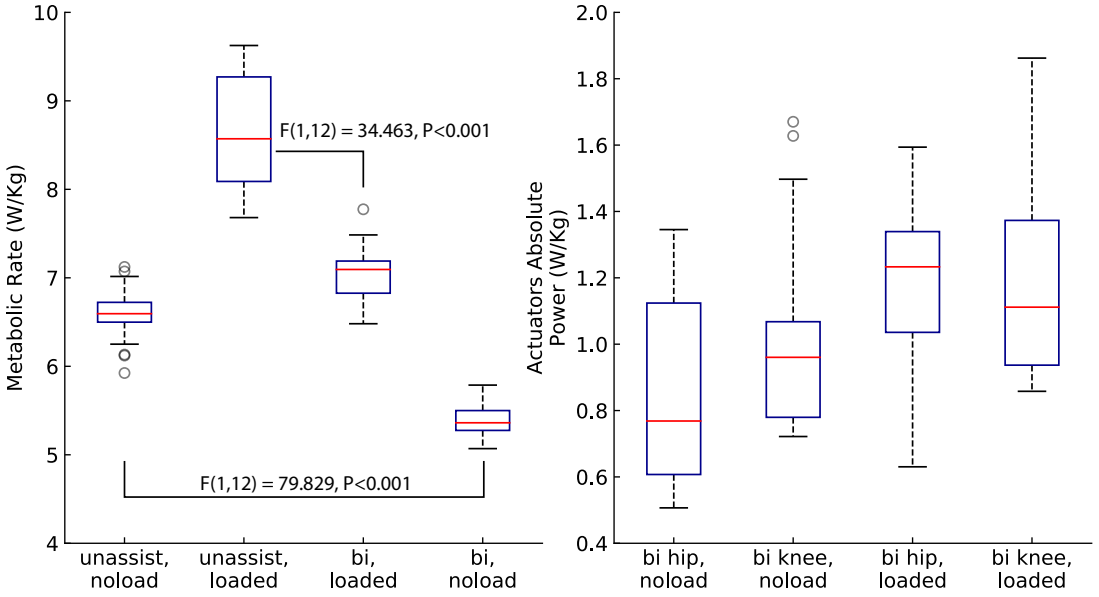

(a) Bi-articular exoskeleton with the same effect on the metabolic consumption of subjects

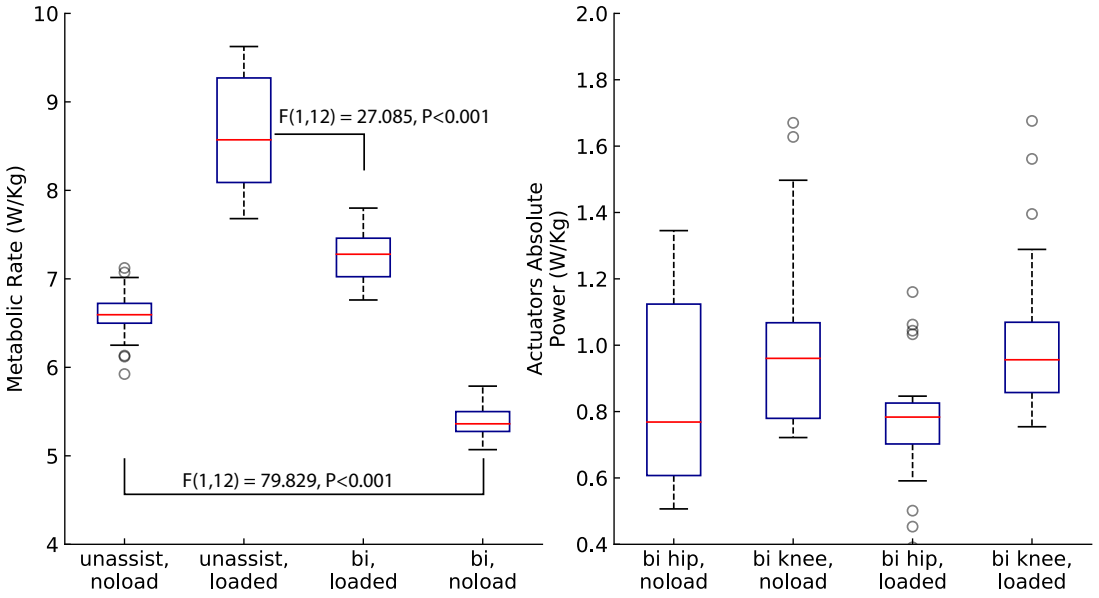

(b) Bi-articular exoskeleton with the same total power consumptions

FIGURE 6.9: Bi-articular exoskeleton power consumption and its effect on the metabolic rate in different load conditions.

actuators represented by "Cb" on the Pareto front of the *loaded* bi-articular exoskeleton.

Comparing the metabolic rate of assisted subjects by the bi-articular devices in two conditions, which were similar metabolic cost reduction conditions and the same power consumption condition, were represented in Figure 6.9. The metabolic

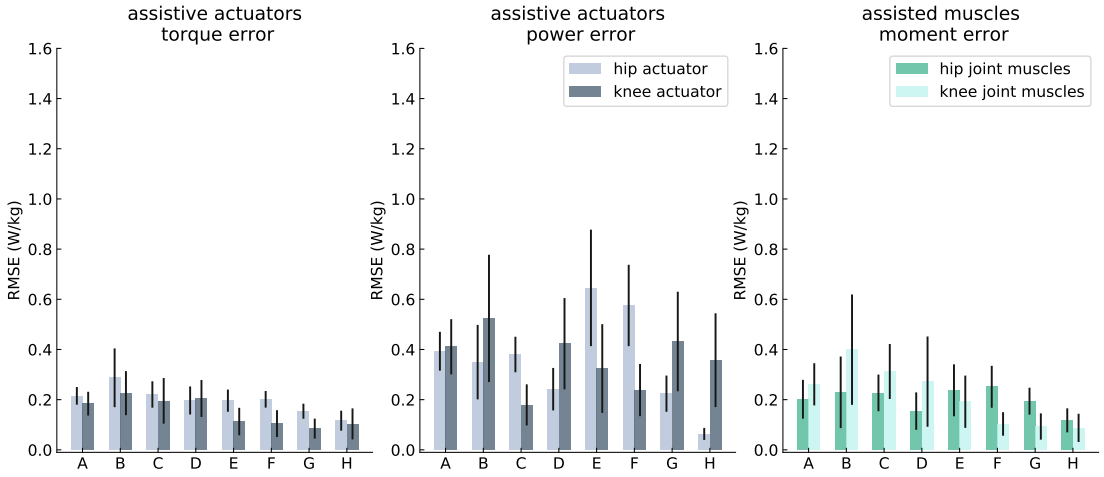

(a) Bi-articular exoskeleton with the same effect on the metabolic consumption of subjects

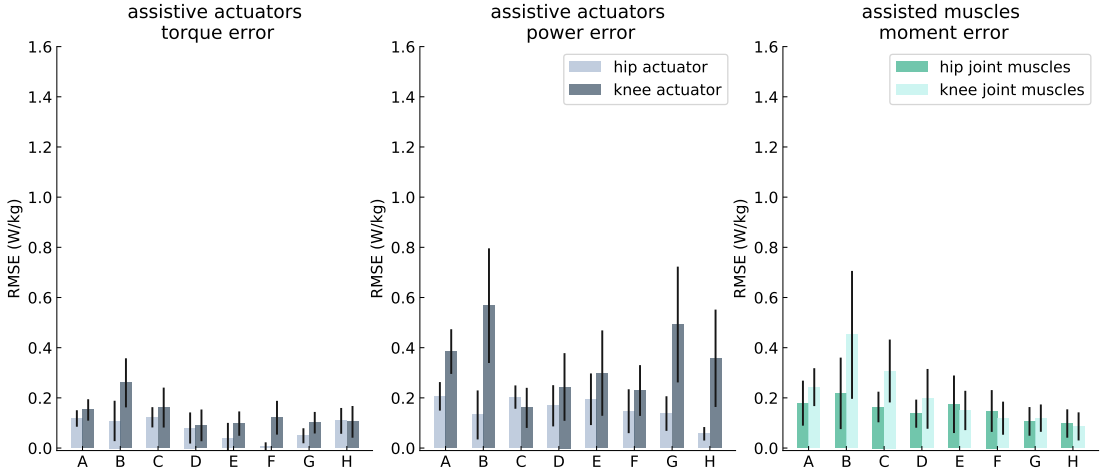

(b) Bi-articular exoskeleton with the same total power consumptions

FIGURE 6.10: Bi-articular exoskeleton torque and power and muscles generated moment profiles root mean square error in different load conditions.

rates of subjects in both conditions show that the metabolic rate of the *loaded* subjects was reduced considerably, and there was no significant difference between subjects walking with no load and the *loaded* subjects assisted by the bi-articular device. The power consumption of the hip actuators and knee actuators showed no significant differences when the selected device consumed a similar amount of the power in different loading conditions. Additionally, a similar performance in power consumption of two different configurations of the bi-articular exoskeleton delivering a similar amount of assistance in different load conditions was observed, which is represented in Figure 6.10(a).

The absence of a significant difference between the two devices with different configurations and different load conditions can facilitate designing a battery with a robust performance to the different load conditions. This performance can also help to achieve a general mechanical design for an exoskeleton to assist subjects in different load conditions and assistance levels. Nevertheless, the high within-subject deviations and outliers of power consumption indicate high contrast within-subjects, which can complicate obtaining general power profiles for the device.

The performance assessment of the same bi-articular configuration in two different load conditions by employing MAF showed that the performance of the bi-articular exoskeleton in the *loaded* condition was improved (1.40 ± 0.80 W/kg) in comparison with the *noload* condition, in which the MAF value was 1.01 ± 0.70 W/kg. Although the increase in the device's positive power in the *loaded* condition was expected, improvement of the MAF value shows that this increase in positive power was delivered to the subjects effectively. In the meanwhile, comparing the devices with the same effect on the metabolic cost reduction of subjects in different load conditions showed the superior performance of the bi-articular device in the *loaded* condition in which devices in the *loaded* and *noload* circumstances had 2.08 ± 0.69 and 1.01 ± 0.69 W/kg MAF values, which can indicate the inefficiency of noload device power profiles in general.

The quantitative and qualitative analyses of power and moment profiles between the pair of selected devices not only show a moderate variation between the torque profiles of the compared bi-articular devices; the power profiles also demonstrated considerably low diversity in different load conditions, as shown in Figure 6.10(a), 6.10(b). Additionally, Figure in 6.11 supports our claims regarding the high resemblance between profiles of the bi-articular exoskeletons in the *loaded* and *noload* conditions. As shown in Figure 6.11, the difference between the power and moment profiles of the pair of devices in *load* and *noload* conditions were nearly limited to the magnitude and timing based on the toe-off difference except on the pre-swing and initial-swing phases of knee profiles in which the trajectories had differences between bi-articular devices with the same effect on the metabolic power consumption of assisted subjects.

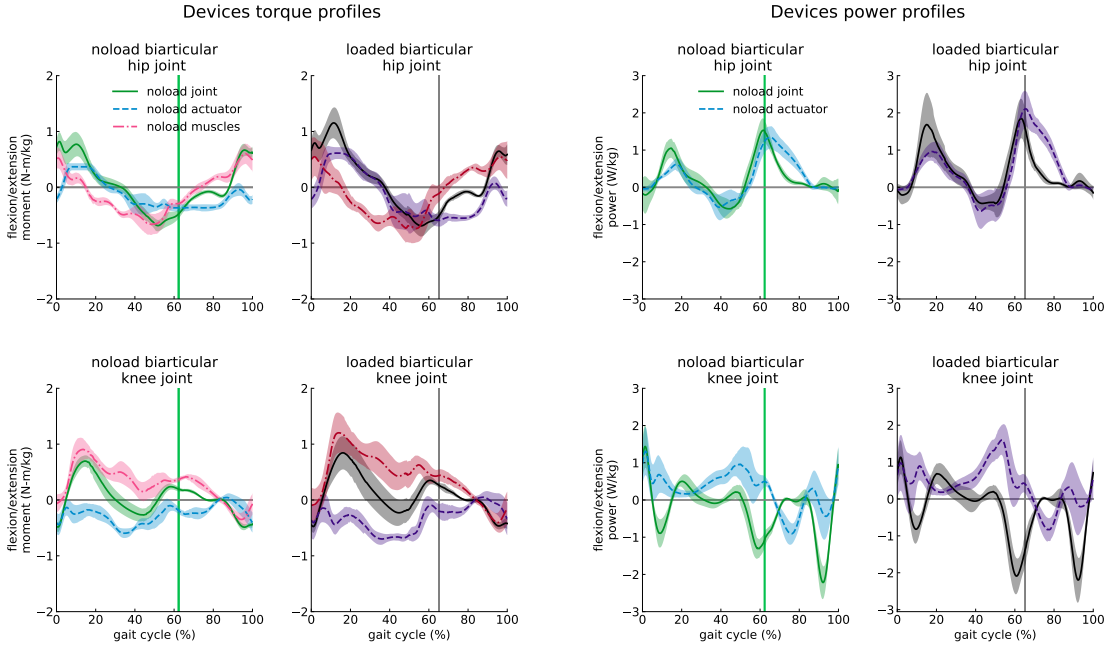

(a) Bi-articular exoskeleton with the same effect on the metabolic consumption of subjects

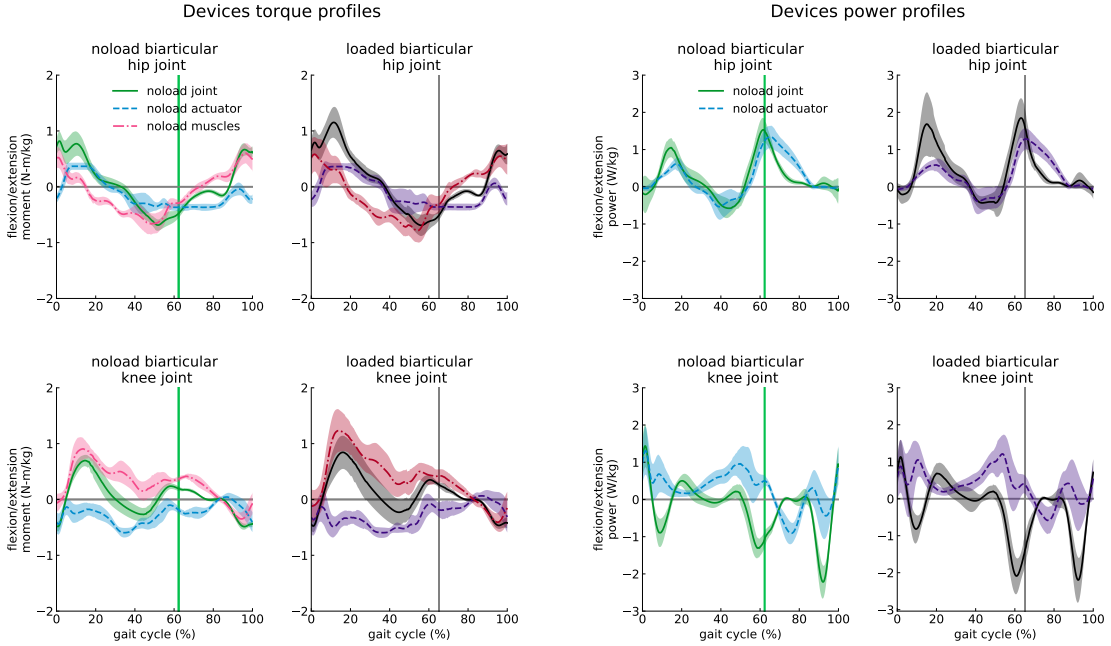

(b) Bi-articular exoskeleton with the same total power consumptions

FIGURE 6.11: Bi-articular exoskeleton actuators torque and power profiles and muscles generated moment of assisted subjects.

6.4 Case 4: Mono-articular Exoskeleton Performance

The same analyses on the bi-articular exoskeleton, discussed in the previous case study were performed on the mono-articular exoskeleton to gain an in-depth insight into this type of exoskeleton. To conduct the comparisons between a pair of mono-articular devices with a similar effect on the metabolic cost or with similar power consumption, we chose the "Ee" configuration of the mono-articular device in the *loaded* and *noload* conditions and the "Ae" mono-articular exoskeleton from the Pareto front of the mono-articular device in the loaded condition. The selected "Ee" and "Ae" configurations have 30 and 30 N-m, and 70 and 30 N-m peak torque constraints on the pair of hip and knee actuators, respectively.

The comparison of actuators power consumption between the "Ae" *loaded* and "Ee" *noload* devices, which have a similar metabolic cost reduction, showed a statistically significant increase in power consumption of the *loaded* hip actuator. Despite the reduction in the knee power consumption of the *loaded* knee actuator, the difference between the pair of knee actuators was not significant. One of the observed critical issues was that even though the within-subject variation of mono-articular devices was generally low, the deviation of actuator power consumptions between the load condition and between the configurations was considerable. As shown in Figure 6.12(a) along with Figure 6.12(b), while the power consumption of the knee actuator in the low torque availability (i.e., "Ee") was higher than that of the hip actuator, this was changed in higher torque constraints, and the hip actuator became dominant power consumer indicating considerable changes in the power profile of the mono-articular device in different arrangements of its actuators.

Despite the similar percentage of the metabolic rate reduction, the metabolic rate of assisted subjects in the *loaded* condition has a significant difference with that of the unassisted *noload* subjects, which indicates that the mono-articular device was not able to sufficiently compensate the cost of carrying a heavy load. Comparing the metabolic rate of subjects assisted by two mono-articular devices with a similar

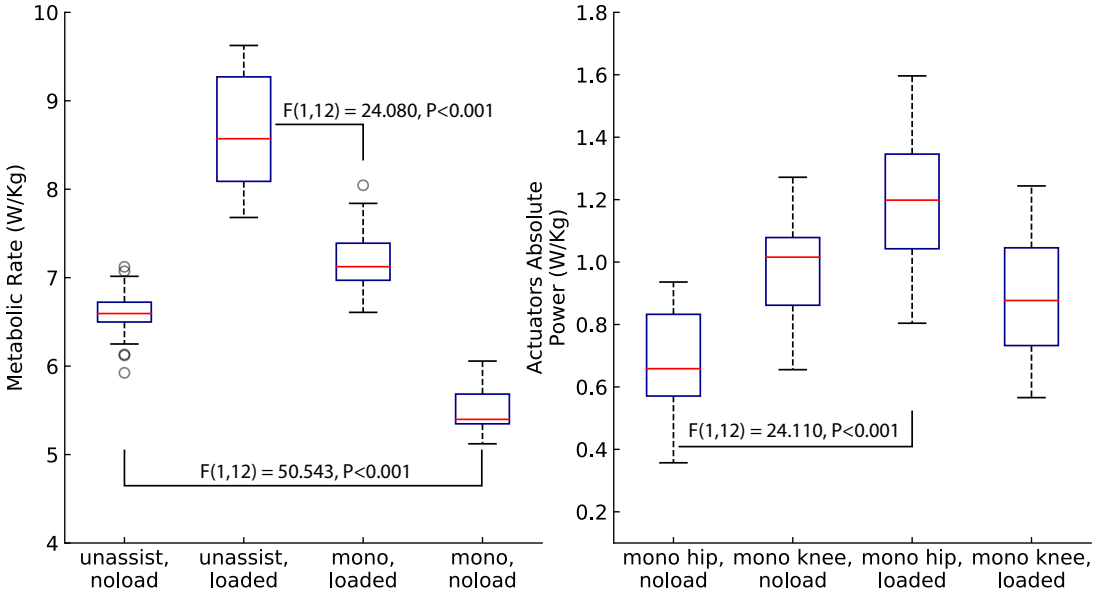

(a) Mono-articular exoskeleton with the same effect on the metabolic consumption of subjects

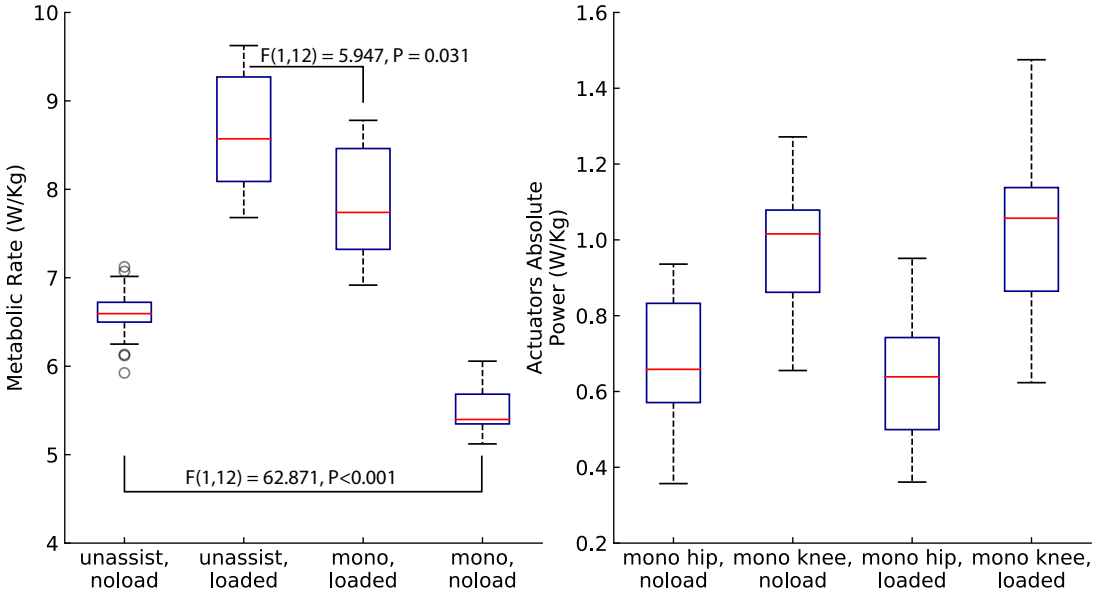

(b) Monoarticular exoskeleton with the same total power consumptions

FIGURE 6.12: Mono-articular exoskeleton power consumption and its effect on the metabolic rate in different load conditions.

power consumption also shows that compensating additional load is more costly for mono-articular devices. The metabolic rate of the compared pairs of mono-articular devices is shown in Figures 6.12(a) and 6.12(b).

The pair of devices selected for conducting the comparisons were evaluated by the

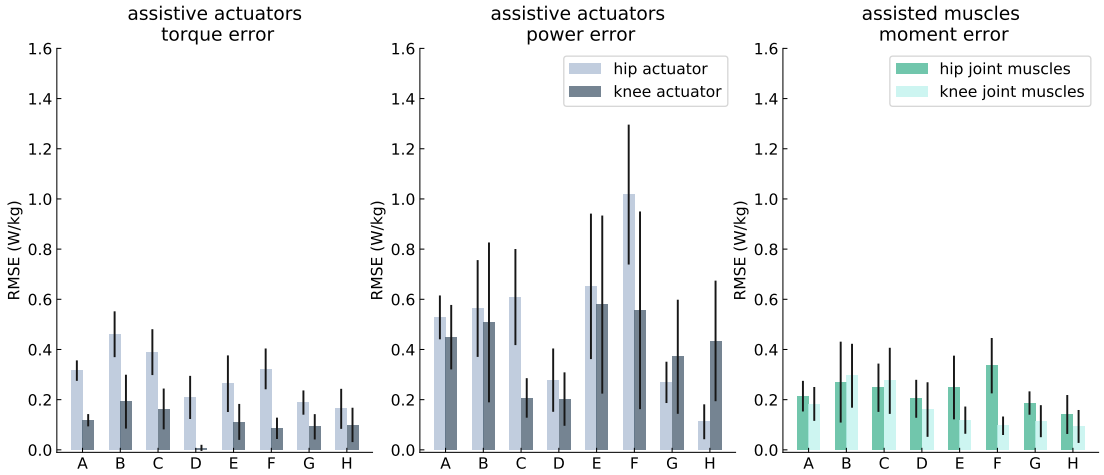

(a) Mono-articular exoskeleton with the same effect on the metabolic consumption of subjects

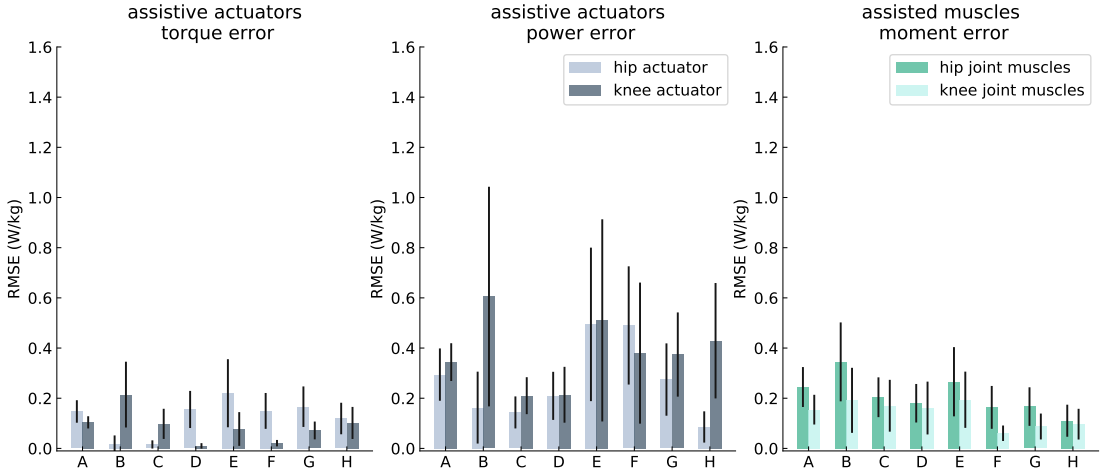

(b) Mono-articular exoskeleton with the same total power consumptions

FIGURE 6.13: Mono-articular exoskeleton torque and power and muscles generated moment profiles root mean square error in different load conditions.

modified augmentation factor to assess their performance under their mass and inertia effect. Unlike the other case studies in which all evaluated bi-articular and mono-articular devices delivered a positive power to the human musculoskeletal system, the mono-articular exoskeletons evaluated in this case study both caused an increase in the metabolic expenditure of subjects according to MAF performance factor. The modified augmentation factor of the mono-articular device with 30 N-m peak torque constraints in both hip and knee actuators showed -0.20 $\pm$ 0.43 W/kg in the *noload* condition while it increased to -0.15 $\pm$ 0.56 W/kg

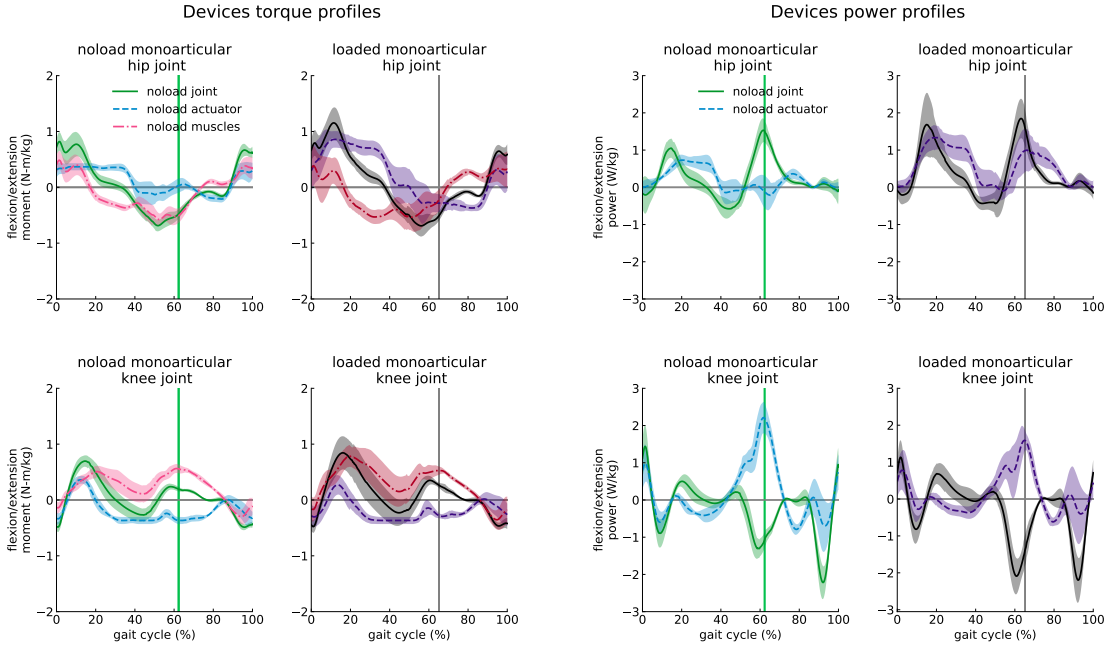

(a) Mono-articular exoskeleton with the same effect on the metabolic consumption of subjects

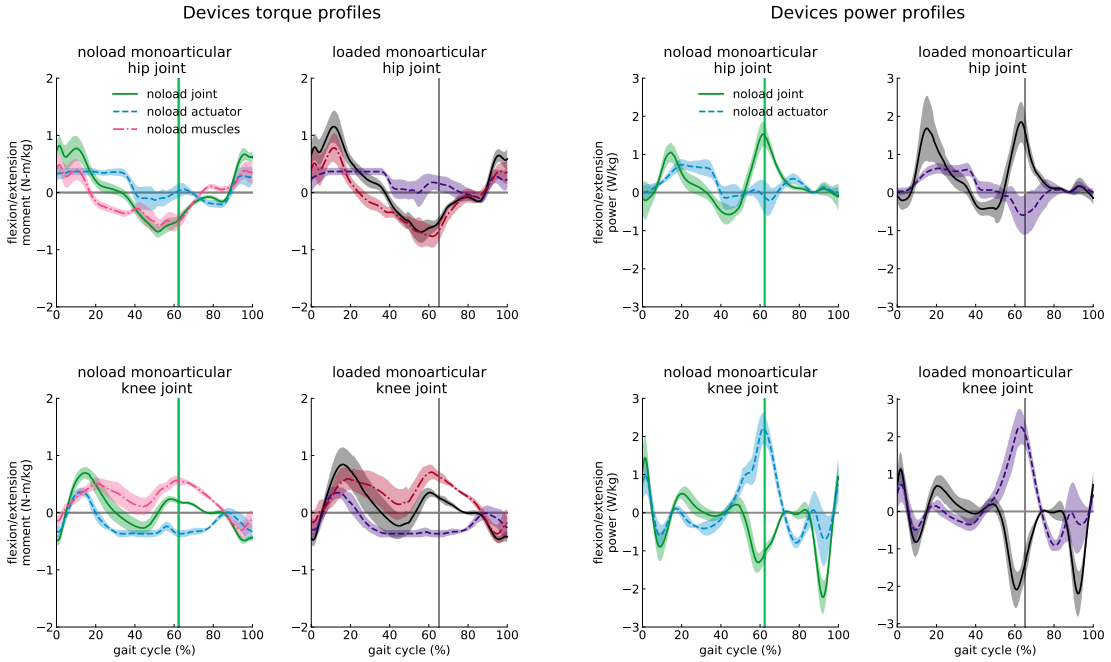

(b) Mono-articular exoskeleton with the same total power consumptions

FIGURE 6.14: Mono-articular exoskeleton actuators torque and power profiles and muscles generated moment of assisted subjects.

when subjects were loaded. These MAF values of the "Ee" mono-articular device represent a high variation of device effect on the subjects and improvement of the device performance by loading subjects, which was also observed in the

bi-articular exoskeleton. Even with the improvement of device performance in the loaded condition, the device in both loading conditions would cause subjects to consume more power due to wearing these devices. The same analysis on the mono-articular device "Ae" configuration (70 N-m hip 30 N-m knee) in the *loaded* condition showed relative improvement compared to the "Ee" device.

According to the MAF value, the mono-articular exoskeleton requires a large torque capacity at the hip actuator to deliver assistance to the subjects. According to the slope of the Pareto front of the mono-articular device under the devices inertial properties effect, we claimed that it might be beneficial to keep the torque capacity of the mono-articular exoskeleton more moderate, yet, we observe in this case study that the mono-articular device cannot inject positive power to the human musculoskeletal system in low torque capacity. According to the MAF value and our previous observations, it might be reasonable to conclude that designing an optimal mono-articular exoskeleton that can be used for different assistance levels and load conditions is complicated.

The moment and power profiles of the selected mono-articular exoskeleton did not show a similar resemblance that we observed in the bi-articular device between the pair of actuators. The hip actuators of devices with the same metabolic reduction effect followed completely different trajectories, and it was not surprising that their power profiles had significant differences. Although the moment profiles of the knee actuators had a higher resemblance than the hip actuators, their power profiles showed relatively different paths during pre-swing and initial swing phases. The comparison of the same device (i.e., "Ee") profiles in different load conditions showed a considerable divergence between the profiles of the hip actuator after the mid-stance phase of the gait cycle and their maximum difference occurred during the pre-swing and initial swing phases. Although the knee actuators showed similar torque profiles in different load conditions, their power profiles demonstrated remarkable differences during pre-swing and initial swing phases. These described moment and power profiles; their quantitative differences, using the RMSE, in both comparison cases are represented in Figures 6.14 and 6.13.

This case study confirms our discussion about mono-articular exoskeleton in which we claimed that obtaining a generic control policy for this device would be challenging. Also, designing an optimal battery under its life and weight considerations highly depends on the selected configuration, and a generic battery would not perform optimally for the mono-articular device at different assistance levels and in different load conditions.

Chapter 7

Conclusion and Future Work

7.1 Conclusions

This study proposed a simulation-based design approach to conduct a rigorous and fair comparison of different configurations of exoskeletons systematically. This design approach was used to simultaneously optimize and compare the metabolic cost reduction of assisted subjects with and power consumption of bi-articular and mono-articular hip-knee exoskeletons.

In this study, we introduced a biarticular configuration of an exoskeleton assisting hip and knee joints. The proposed exoskeleton is motivated by human bi-articulation, which is known to improve human bipedal locomotion efficiency. The presence of biarticular muscles in the human musculoskeletal system advances locomotion performance by enabling power transformation from proximal to distal joint and power regeneration between adjacent joints, facilitating joint movement coupling resulting in the distribution of muscle weight and reduction of leg inertia. The monoarticular exoskeleton, which assists each joint directly by mounting an actuator to the joint of interest, is motivated by its simplicity in design and is commonly employed by researchers.

The introduced multi-criteria optimization and comparison method also subsumes single objective optimization cases. One of these cases is optimizing metabolic rate

reduction of devices without considering their power consumption; these types of devices are called ideal exoskeletons in the literature [2, 15]. We have conducted simulations using ideal exoskeletons and showed that both devices could reach the same level of metabolic rate reduction and total power consumption. We also showed that the assistances could considerably reduce the metabolic rate and the peak reaction forces and moments at the knee, patellofemoral, and hip joints. In addition to the direct effect of devices on the muscular activities of the hip and knee joints, we confirmed that these devices could also indirectly affect the activity of muscles at the ankle joint and hip abduction. Furthermore, these simulations showed that loading subjects with a heavy load changes the assistant profiles by magnitude and time shift.

Although studying the ideal exoskeletons provides handy erudition about these devices, it is necessary to analyze and compare them in more physically practical conditions applied in real-time applications. Consequently, we compared the performance of devices on metabolic cost reduction and their power consumption simultaneously using a multi-criteria optimization method, which is necessary for a fair comparison of different devices. To implement Pareto optimization and obtain a set of optimal solutions for each of both devices to conduct a fair comparison between them, we performed simulations for both devices in both loading conditions by introducing the peak torque limitation on actuators at different levels.

Through the multi-criteria optimization of devices, we showed that introducing sufficiently large torque limits to both devices' actuators does not have a large impact on the provided assistance, while it causes a considerable reduction of their power consumption. Additionally, we showed that both devices could reach similar performance levels but for different peak torques assignments. In particular, we showed that larger peak torque limits are required for mono-articular exoskeletons compared to bi-articular devices. Despite the similar assistance levels of both devices, monoarticular exoskeletons demonstrated better performance in reducing the peak reaction moments and forces. By analyzing the Pareto front curves of both devices in different load conditions, we showed that the power consumption of bi-articular exoskeletons is less affected by loading subjects than mono-articular

devices. Lastly, analyzing power and torque profiles of both devices laid on their Pareto front curves explicated that the effect of loading subjects on the profiles of bi-articular devices is more uniform than the profiles of mono-articular exoskeletons.

We studied the effect of regeneration on the power consumption of devices and how it affects the trade-off curves in Pareto comparisons. We then showed that regeneration could improve the power consumption of devices from $6.54 \pm 2.60\%$ to $25.76 \pm 4.34\%$ depending on the efficiency of regeneration, configuration, and torque limitation, and it should be considered in designing exoskeletons. Additionally, the analysis of each device's actuators revealed that the knee actuator of mono-articular devices has more potential for a generation while both actuators of the bi-articular device showed large regeneration capacity.

We started with torque limited device multi-criteria comparisons, and to make them even more realistic comparisons, we superimposed the effect of device inertial properties to these Pareto front curves. We studied the effect of the mono-articular and bi-articular exoskeletons' inertial properties on the metabolic rate of subjects through modification of augmentation factor and adaptation of the model developed by Browning *et al.* [16] which estimates the effect of adding inertia and mass on metabolic rate of subjects. Our study showed that optimal monoarticular devices lose their efficiency by $42.51 \pm 0.17\%$ to $55.51 \pm 0.11\%$, whereas optimal biarticular devices are affected by $35.12 \pm 0.21\%$ to $49.67 \pm 0.21\%$. By adding inertial properties' effect on the metabolic rate, we showed that Pareto optimal solutions of the biarticular device are not significantly affected, whereas a different set of Pareto solutions needs to be considered for the monoarticular device. Since the monoarticular configuration in which the knee actuator was attached to the lower thigh exhibited a weaker performance compared to the biarticular device, under their inertial properties effect, we proposed two alternative monoarticular configurations. We achieved maximum 9.96% and 3.36% improvement on their provided assistance using these two alternative designs of monoarticular exoskeletons.

7.2 Future work

On of the main future work is evaluating our results using human subject experiments. Based on results of the simulations, we have developed several hypotheses to test on hip exoskeleton (i.e., AssistOn Gait Device) and mono-articular hip-knee exoskeleton (i.e., AssistOn Walk Device) and then we will conduct a comparison between the results of experiments and the results of this thesis.

In consideration of our study limitations, the mono-articular and introduced bi-articular exoskeletons can be modeled in simulators with dynamic optimization neural algorithms [101–103, 107] by considering their inertial properties to study their effect on the power expenditure of subjects muscles activity and how adding inertia can affect the torque and power profiles while performing different tasks. Simulations based on the Pareto front had limitations as highlighted in the previous section, which should be addressed in future work. The large discretization might well be addressed using the normal boundary intersection method [172], which is designed to resolve these issues on computationally expensive problems, resulting in a more accurate Pareto front with fewer discretization problems.

Simulation outcomes are beneficial as prior information to assist the subjects, and they can be used on the human in the loop (HIL) optimization [173] as a prior profile to start optimization with the torque profiles of simulations which may result in less optimization time by increasing the convergence rate of the optimization. We are planning to establish experimental setups and partially validate our results using the outcomes of the experiments. Although we do not anticipate to obtain a quantitative match between the results of the simulations and experiments due to the discussed limitations, we expect obtaining qualitative matches between these results. Along with these confirmations, muscle fatigue, muscle activities, and training effects that could not be addressed through simulations can be assessed through the experiments.

Appendix A

Joint Reaction Forces and Moments

The reaction forces and moments of the ankle, knee, patellofemoral and hip joints for assisted subjects are shown in the following sections. The first section represents the reaction force and moments of joints of subjects assisted with ideal exoskeletons in both loaded and unloaded conditions. The second section of this appendix presents the joint reaction forces and moments for subjects assisted by torque-limited devices. These figures include three columns representing the reaction forces and moments in all spatial directions.

A.1 Ideal Devices Effect on Joint Reaction Forces and Moments

The black and green profiles represent the reaction forces of unassisted subjects in *loaded* and *noload* conditions, respectively. The curves are averaged over 7 subjects with 3 trials and normalized by subject mass; shaded regions around the mean profile indicate standard deviation of the profile.

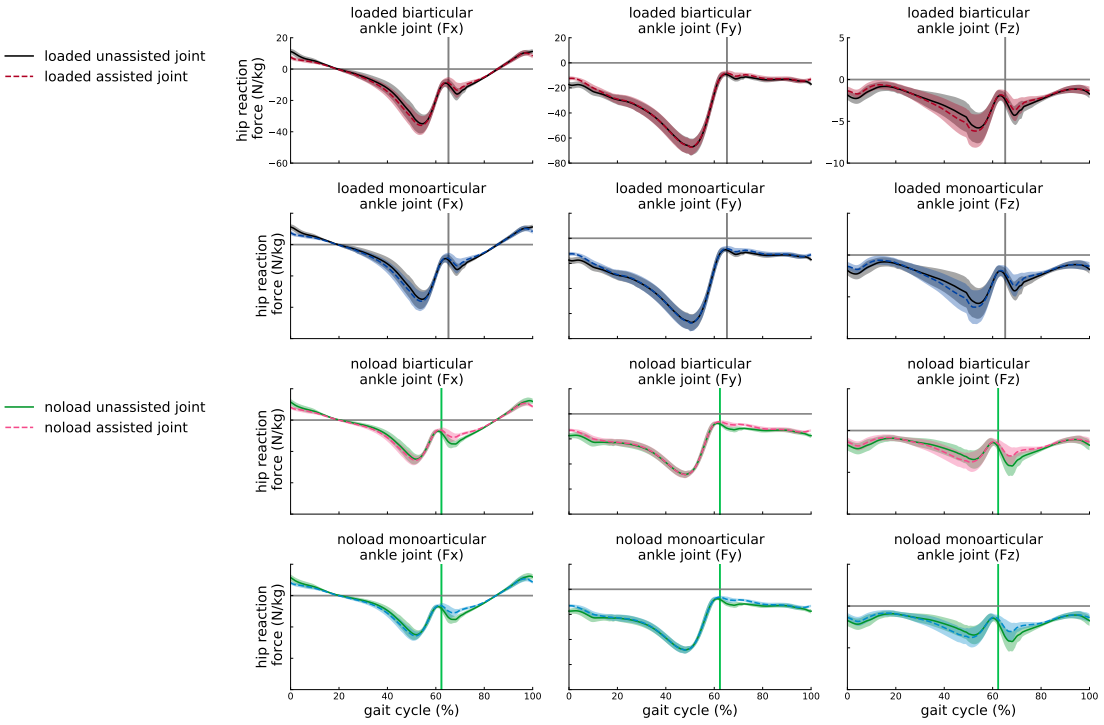

FIGURE A.1: The reaction forces of the ankle joint in anterior-Posterior (F_x), compressive (F_y), and medial-lateral (F_z) directions.

A.2 Optimal Devices Effect on Joint Reaction Forces and Moments

The color bars represent the reaction forces of subjects assisted by constrained optimal exoskeletons. The black and green profiles represent the reaction forces of unassisted subjects in *loaded* and *noload* conditions, respectively. The curves are averaged over 7 subjects with 3 trials and normalized by subject mass.

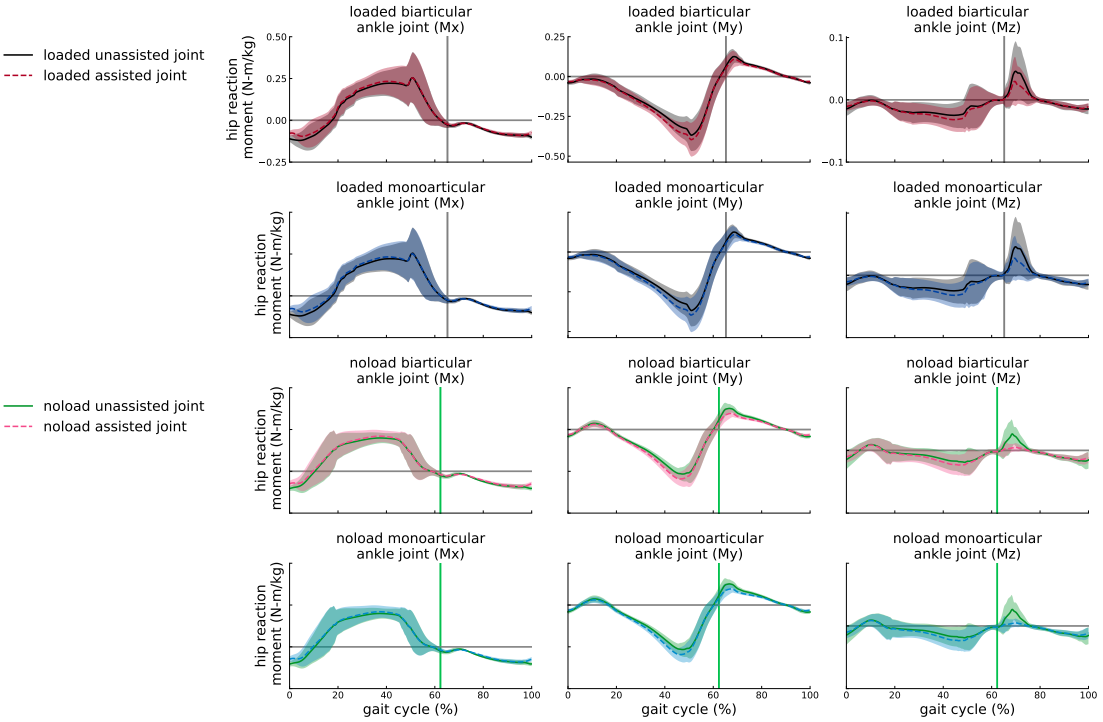

FIGURE A.2: The reaction moments of the ankle joint in adduction-abduction (M_x), internal-external rotation (M_y), and medial-lateral (M_z) directions.

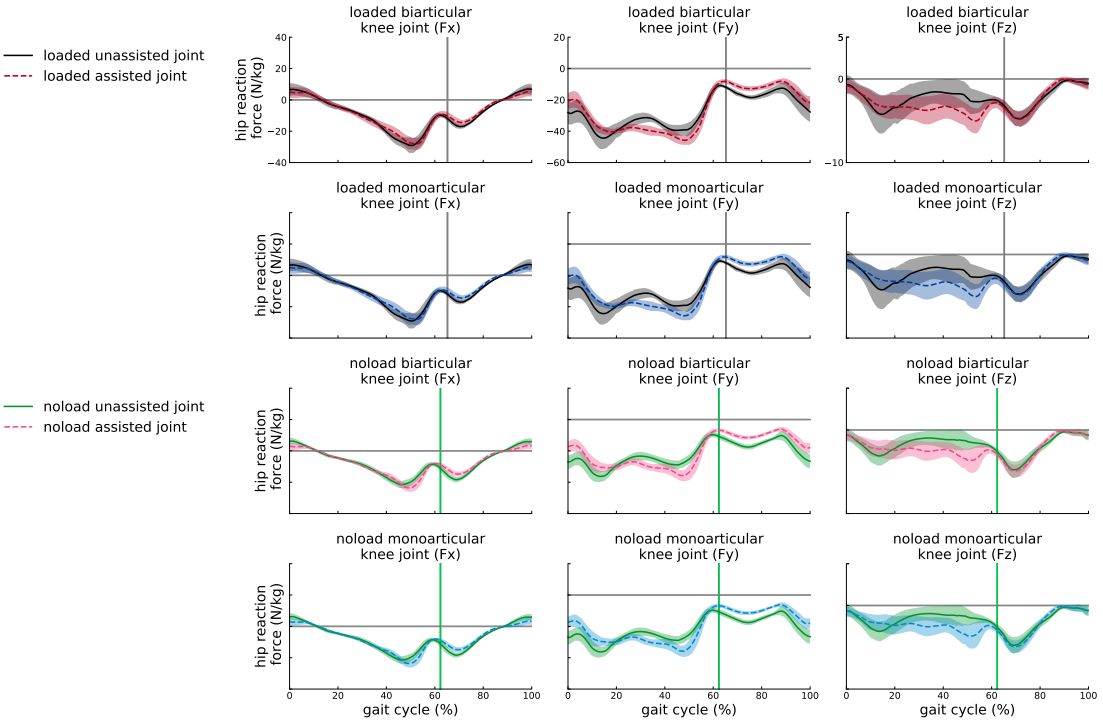

FIGURE A.3: The reaction forces of the knee joint in anterior-Posterior (F_x), compressive (F_y, i.e., tibiofemoral force), and medial-lateral (F_z) directions.

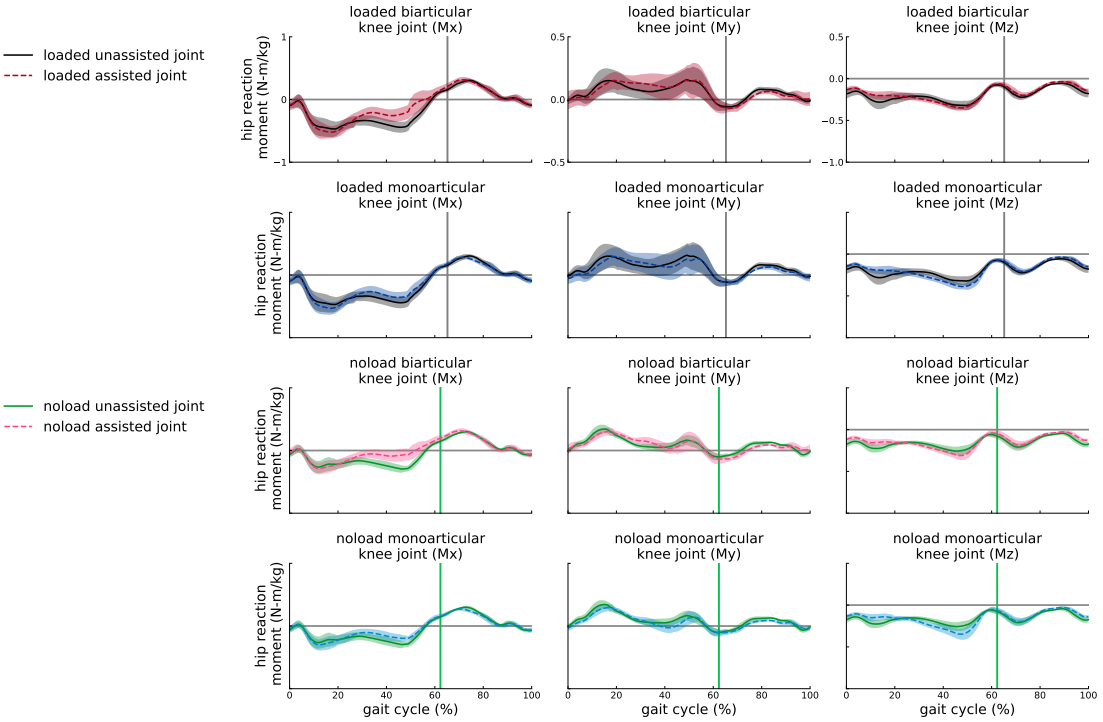

FIGURE A.4: The reaction moments of the knee joint in adduction-abduction (M_x), internal-external rotation (M_y), and medial-lateral (M_z) directions.

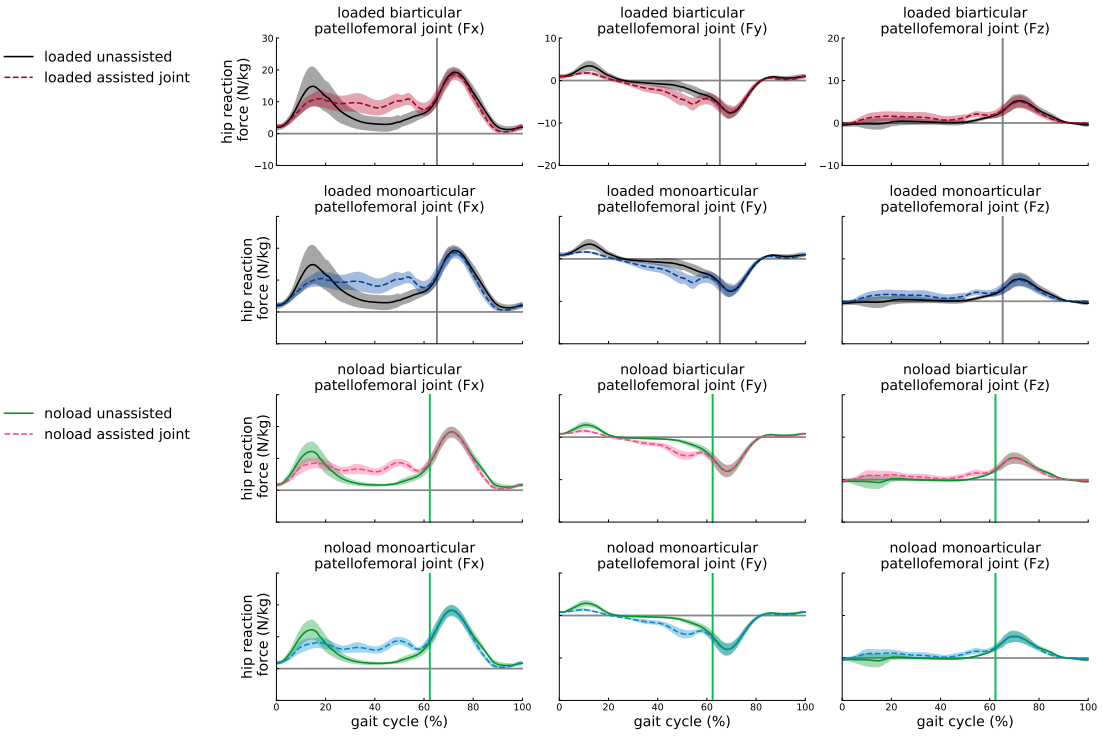

FIGURE A.5: The reaction forces of the patellofemoral joint in anterior-Posterior (F_x), compressive (F_y), and medial-lateral (F_z) directions.

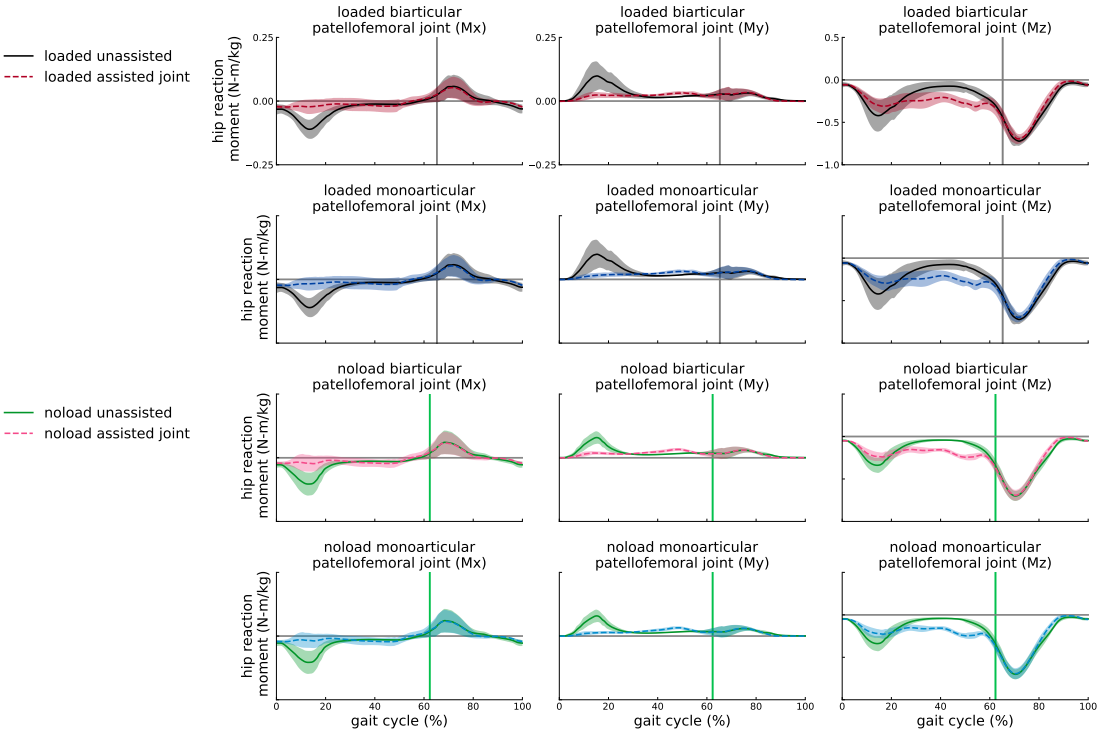

FIGURE A.6: The reaction moments of the patellofemoral joint in adduction-abduction (M_x), internal-external rotation (M_y), and medial-lateral (M_z) directions.

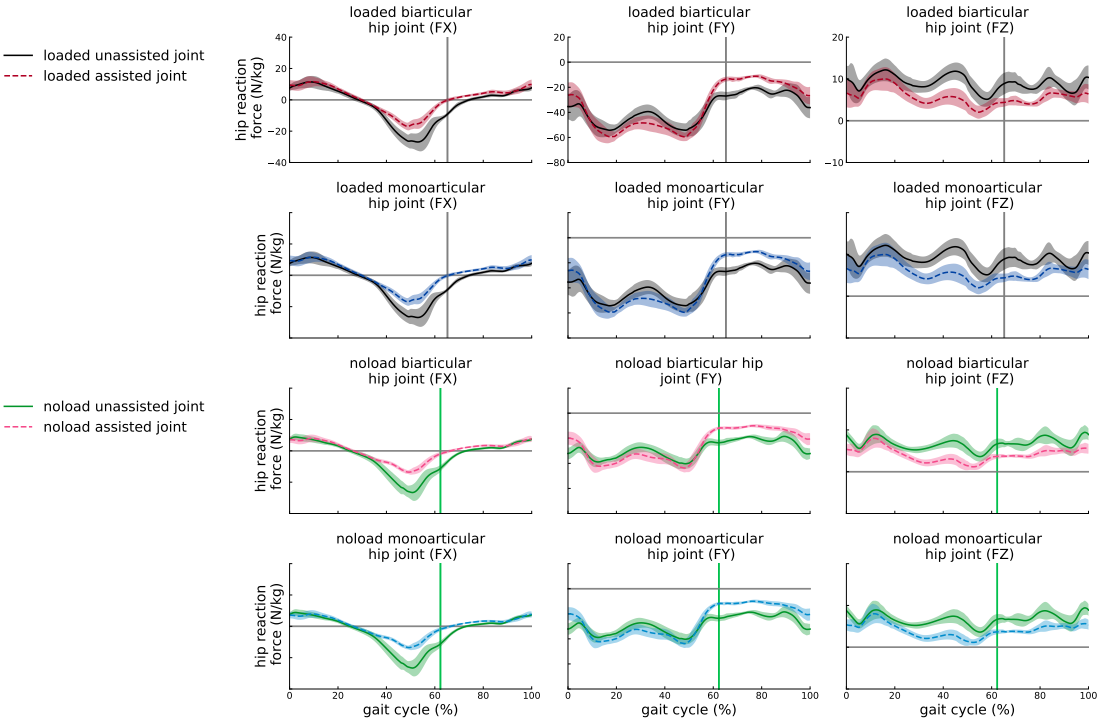

FIGURE A.7: The reaction forces of the hip joint in anterior-Posterior (F_x), compressive (F_y), and medial-lateral (F_z) directions.

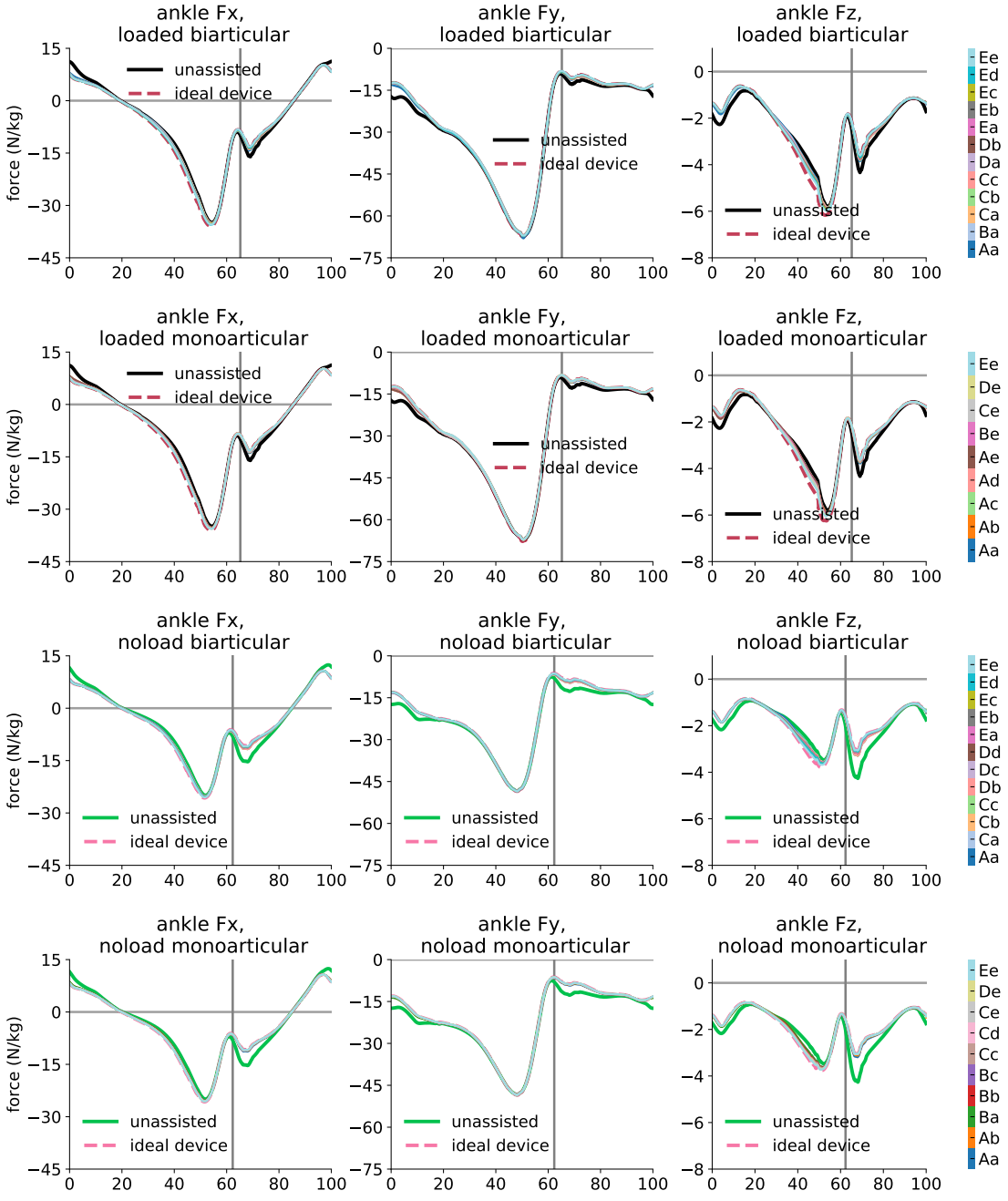

FIGURE A.8: The reaction forces of the ankle joint in anterior-Posterior (F_x), compressive (F_y), and medial-lateral (F_z) directions.

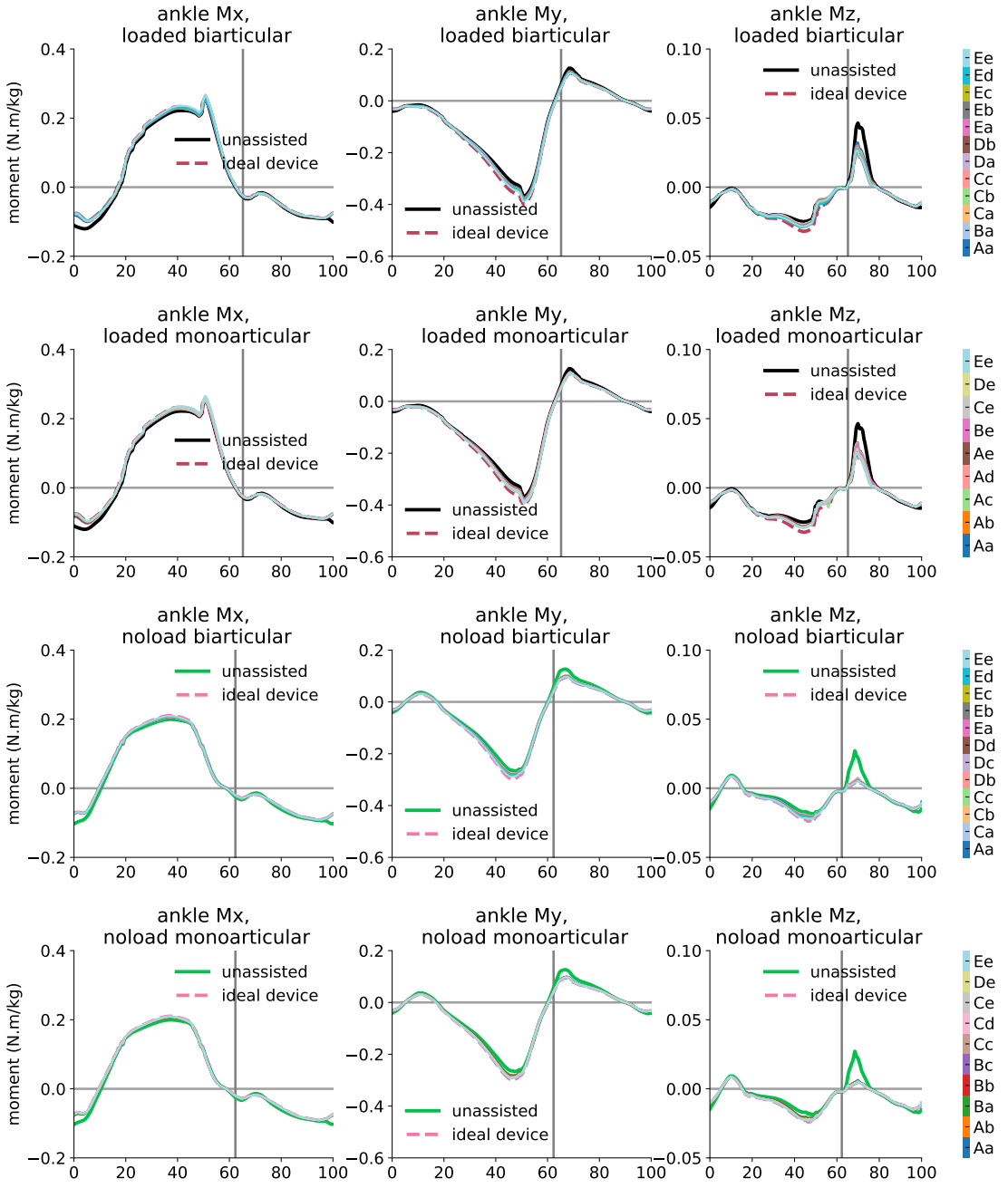

FIGURE A.9: The reaction moments of the ankle joint in adduction-abduction (M_x), internal-external rotation (M_y), and medial-lateral (M_z) directions.

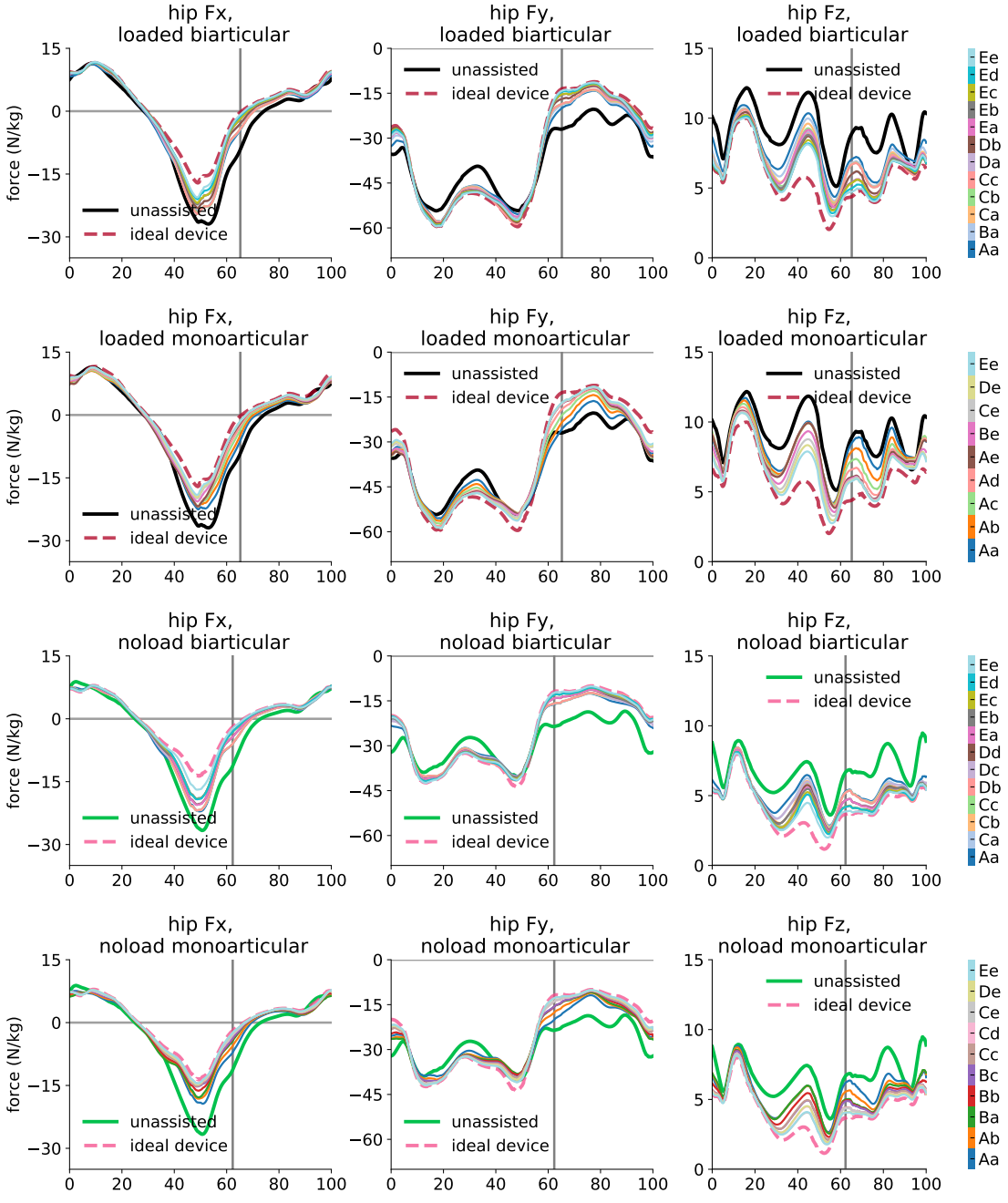

FIGURE A.10: The reaction forces of the hip joint in anterior-Posterior (F_x), compressive (F_y), and medial-lateral (F_z) directions.

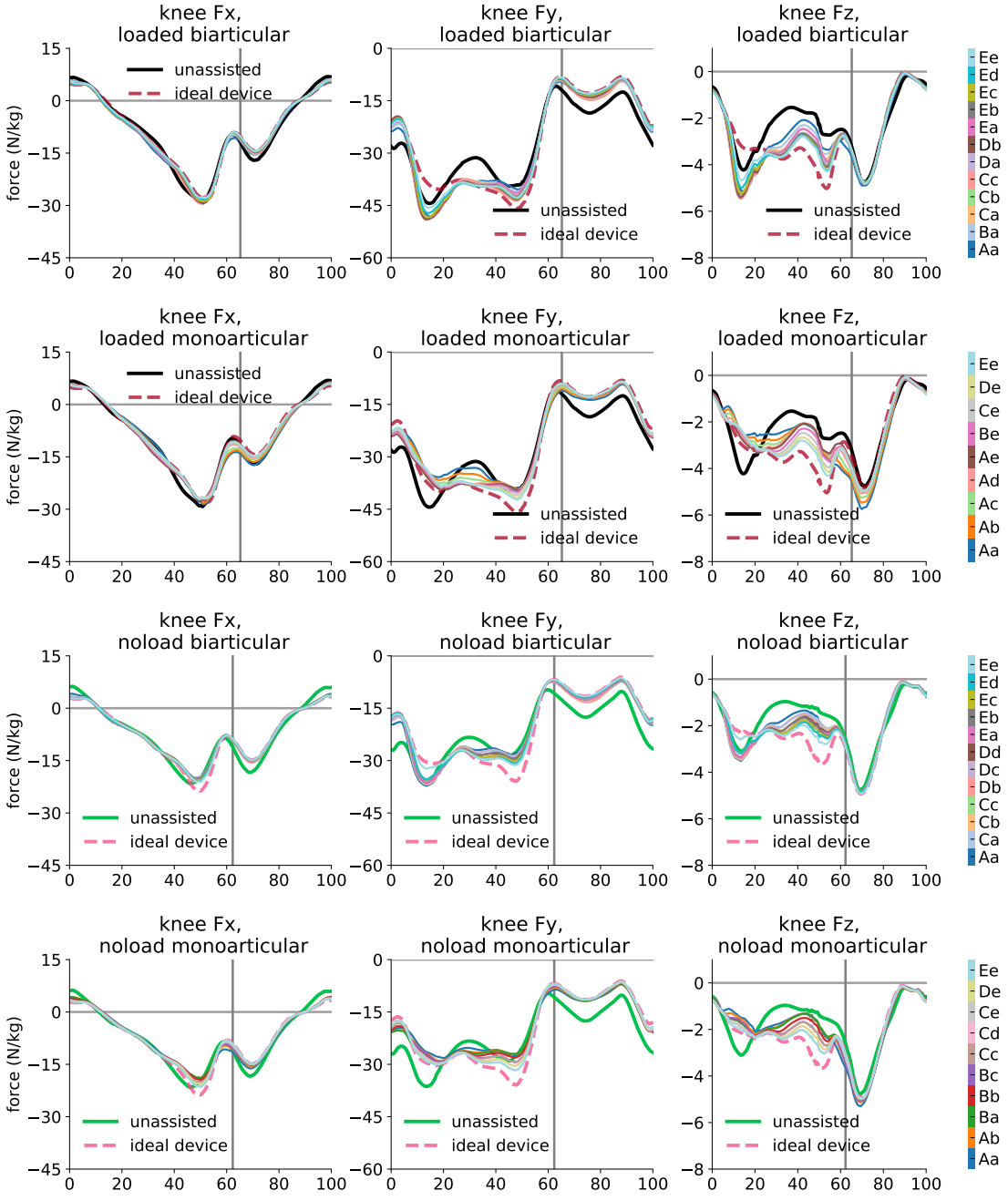

FIGURE A.11: The reaction forces of the knee joint in anterior-Posterior (F_x), compressive (F_y), and medial-lateral (F_z) directions.

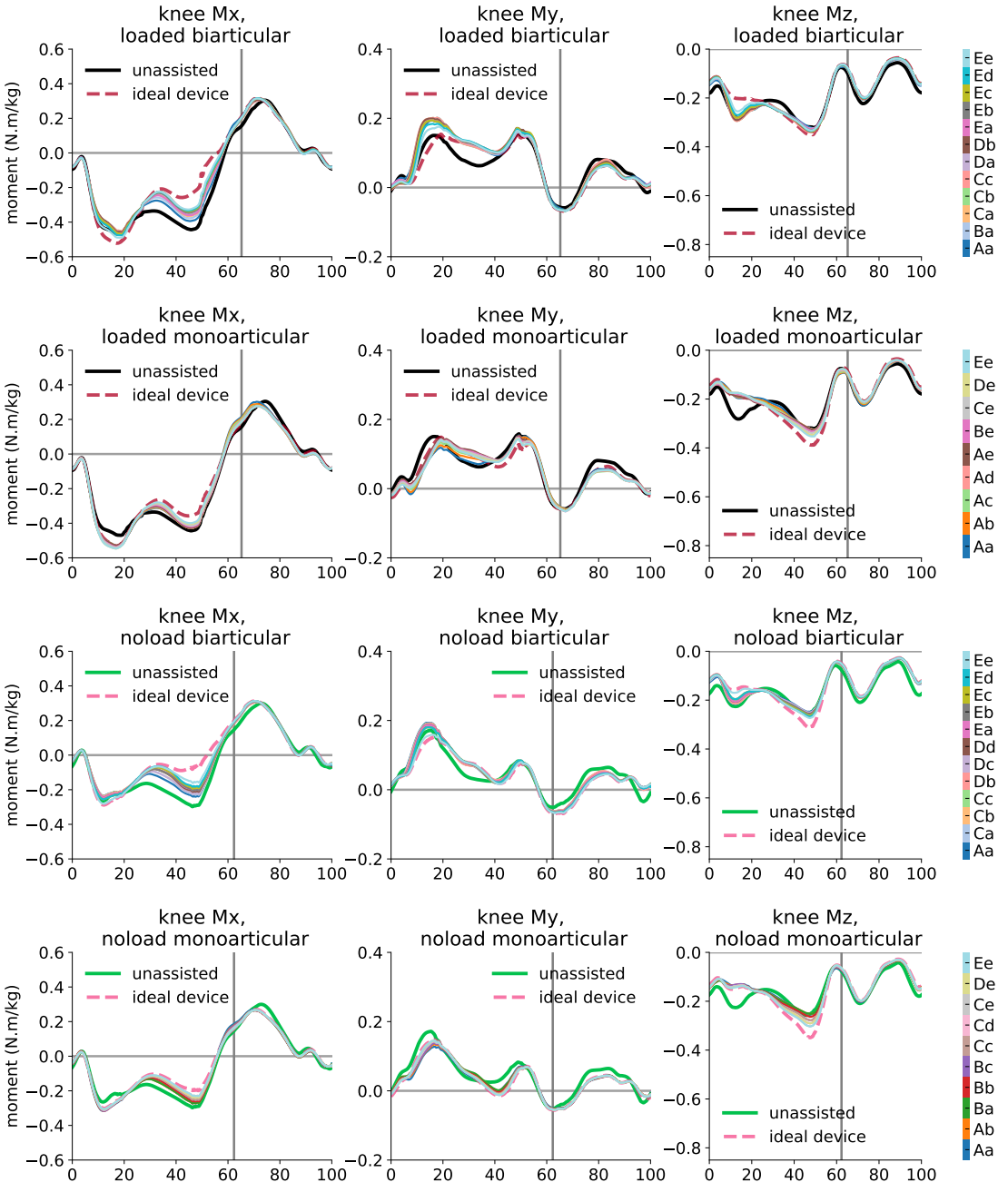

FIGURE A.12: The reaction moments of the knee joint in adduction-abduction (M_x), internal-external rotation (M_y), and medial-lateral (M_z) directions.

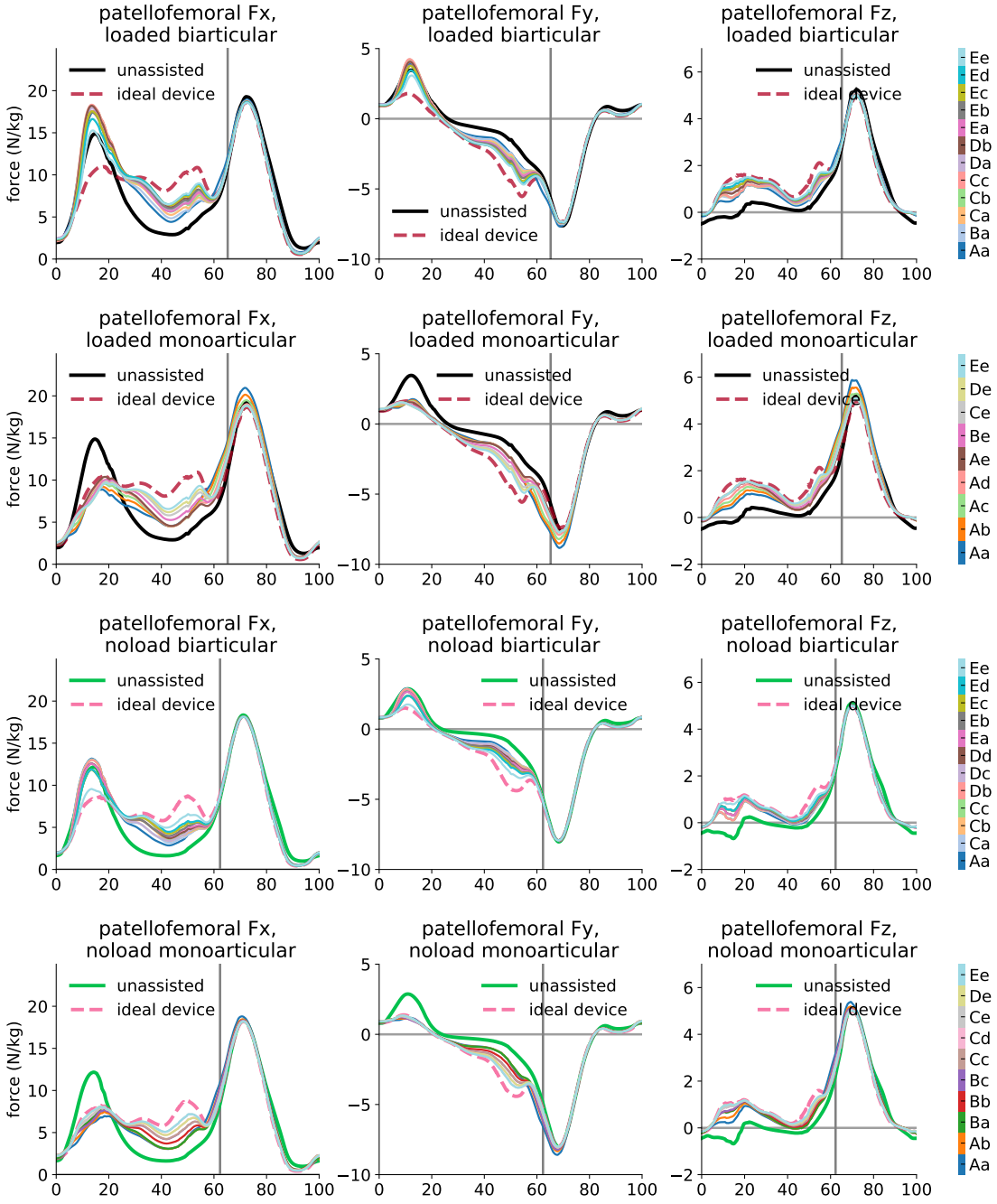

FIGURE A.13: The reaction forces of the patellofemoral joint in anterior-Posterior (F_x), compressive (F_y), and medial-lateral (F_z) directions.

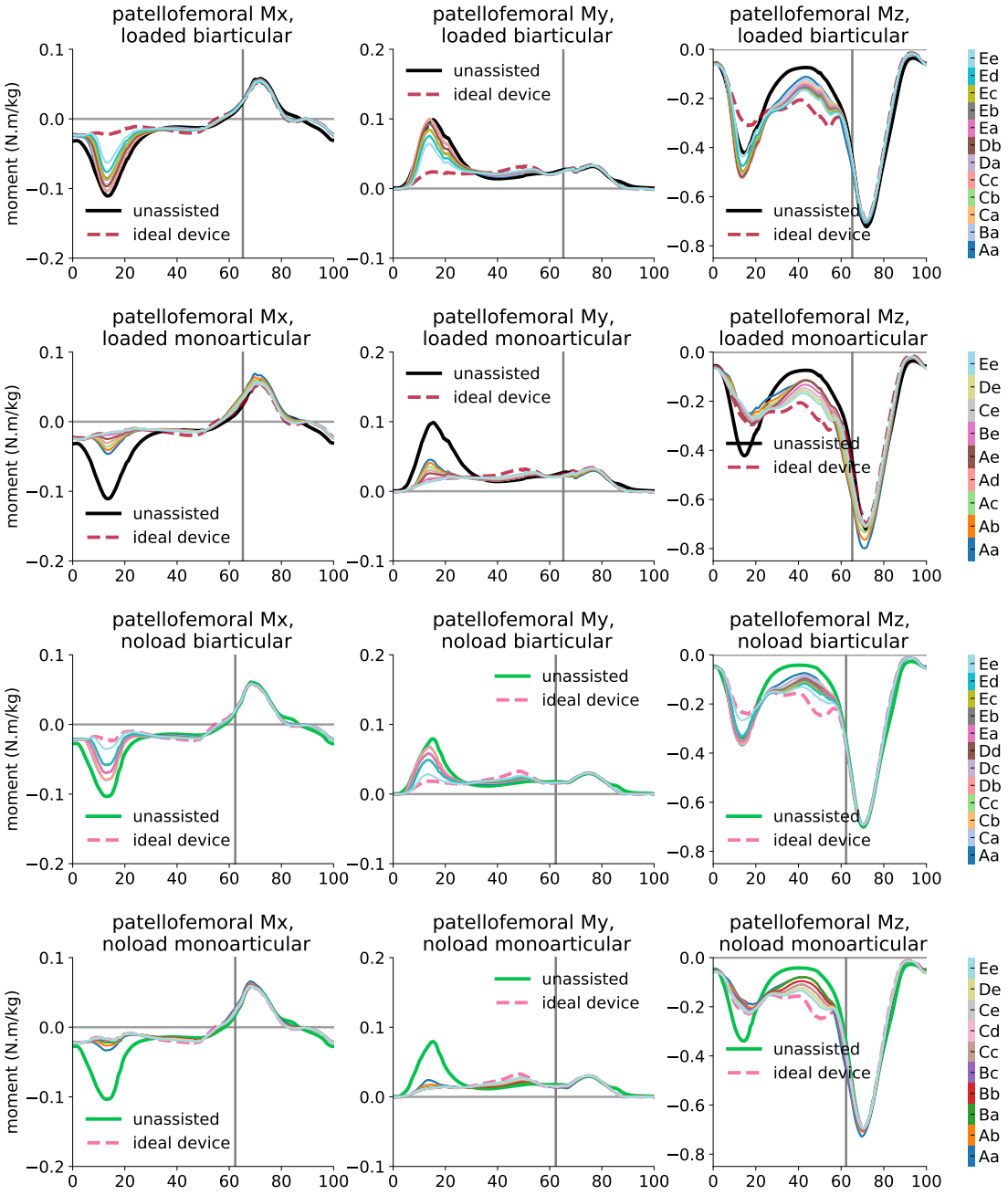

FIGURE A.14: The reaction moments of the patellofemoral joint in adduction-abduction (M_x), internal-external rotation (M_y), and medial-lateral (M_z) directions.

Appendix B

Muscle Activation and Torque Profiles of Selected Cases

The torque profiles of optimal devices selected from the Pareto front curves of mono-articular and bi-articular exoskeletons and muscle activity of subjects assisted by these optimal devices are represented in this appendix. These profiles and muscle activities are studied to gain insight into the direction change occurring during the loading response phase on optimal torque-limited bi-articular exoskeleton profiles. The torque profiles of devices with and without this direction change and their effect on muscle activity of assisted subjects were analyzed and discussed through Chapter 5.

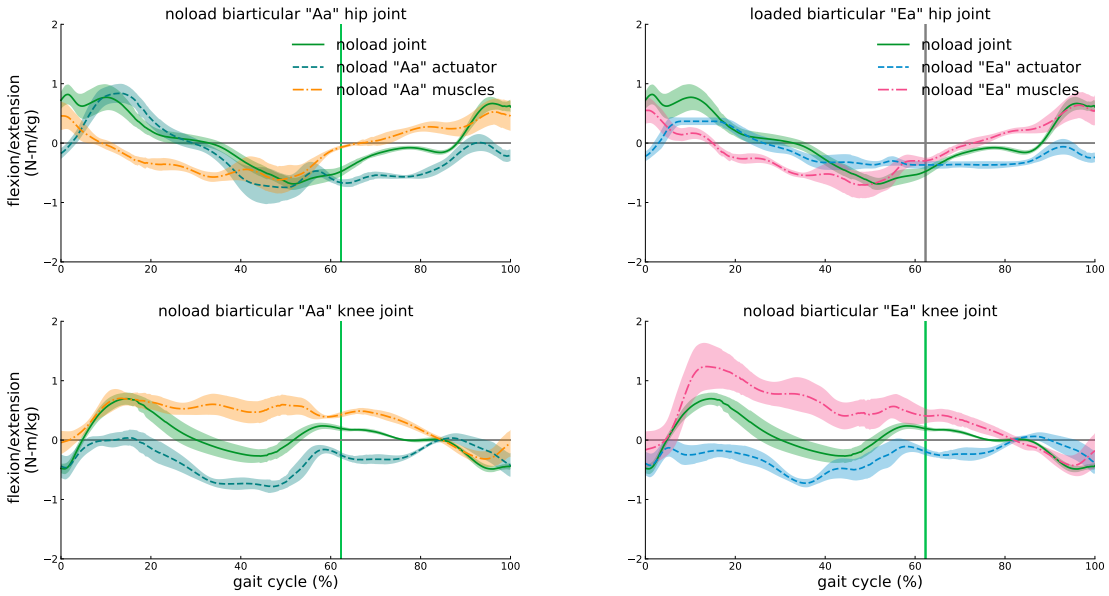

FIGURE B.1: Torque profiles of bi-articular "Aa" and "Ea" exoskeletons in *noload* condition.

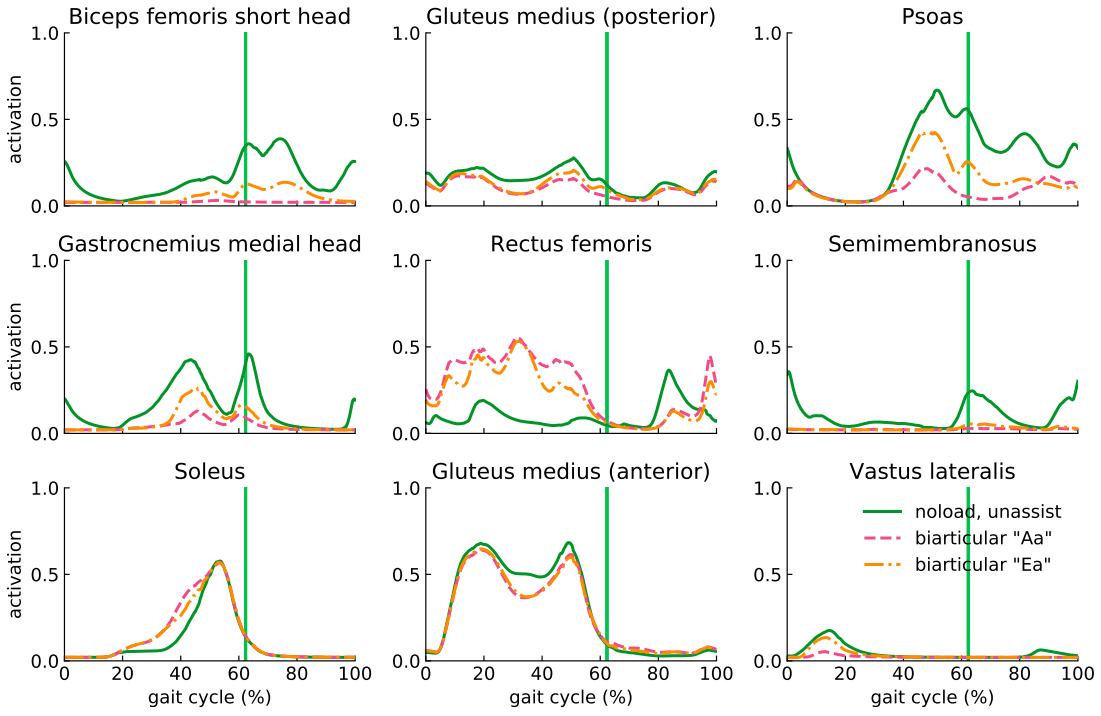

FIGURE B.2: Muscle activation of nine representative muscles of subjects assisted by bi-articular "Aa" and "Ea" exoskeletons in *loaded* condition.

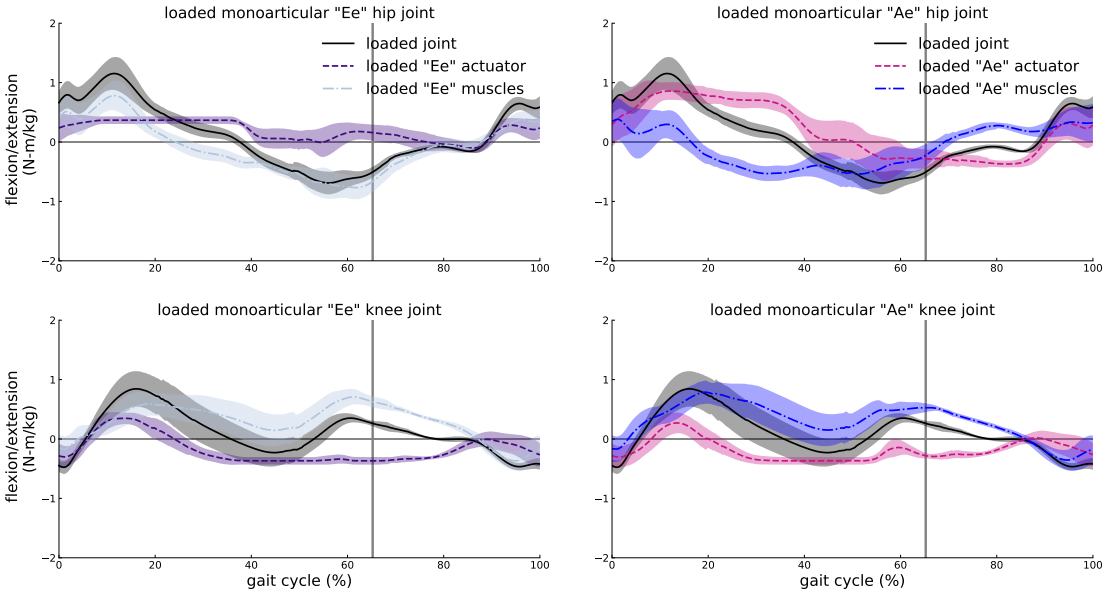

FIGURE B.3: Torque profiles of mono-articular "Ae" and "Ee" exoskeletons in *noload* condition.

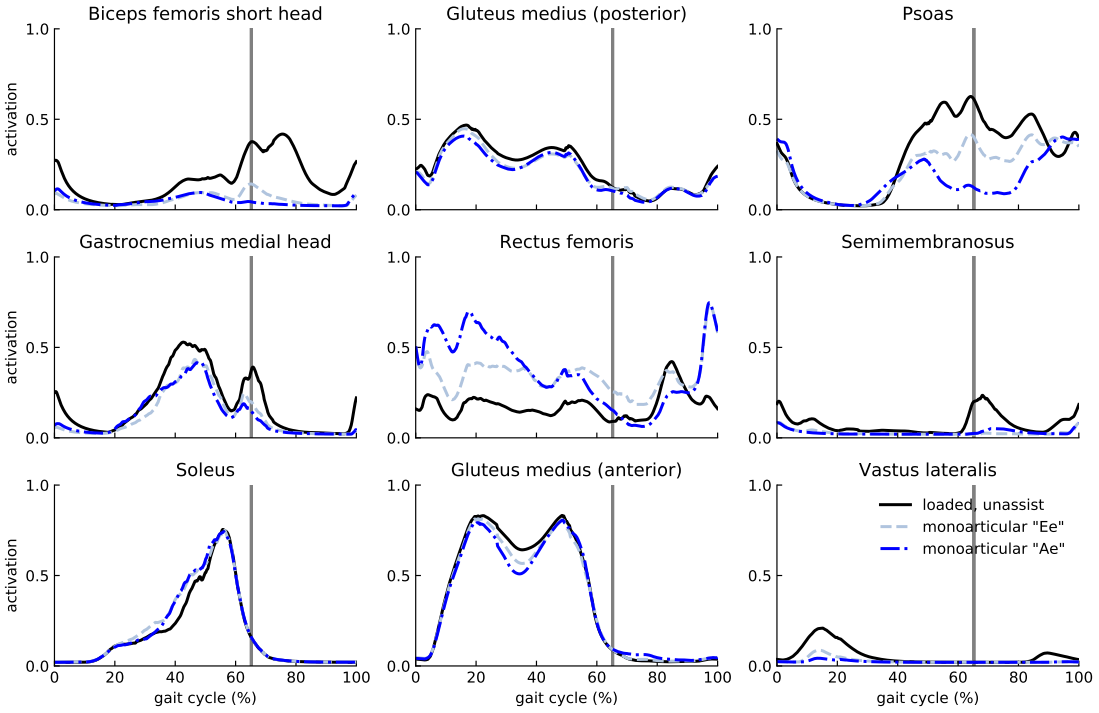

FIGURE B.4: Muscle activation of nine representative muscles of subjects assisted by mono-articular "Aa" and "Ea" exoskeletons in *loaded* condition.

Bibliography

[1] P. S. Rodman and H. M. McHenry, "Bioenergetics and the origin of hominid bipedalism," *American Journal of Physical Anthropology*, vol. 52, no. 1, pp. 103–106, 1980.

[2] T. K. Uchida, A. Seth, S. Pouya, C. L. Dembia, J. L. Hicks, and S. L. Delp, "Simulating ideal assistive devices to reduce the metabolic cost of running," *PLOS ONE*, vol. 11, pp. 1–19, 09 2016.

[3] D. R. Carrier, A. K. Kapoor, T. Kimura, M. K. Nickels, Satwanti, E. C. Scott, J. K. So, and E. Trinkaus, "The energetic paradox of human running and hominid evolution [and comments and reply]," *Current Anthropology*, vol. 25, no. 4, pp. 483–495, 1984.

[4] M. Fedak, B. Pinshow, and K. Schmidt-Nielsen, "Energy cost of bipedal running," *American Journal of Physiology-Legacy Content*, vol. 227, no. 5, pp. 1038–1044, 1974. PMID: 4440743.

[5] R. L. Schalock, "The concept of quality of life: what we know and do not know," *Journal of Intellectual Disability Research*, vol. 48, no. 3, pp. 203–216.

[6] K. Kubo, H. Kanehisa, and T. Fukunaga, "Effects of resistance and stretching training programmes on the viscoelastic properties of human tendon structures in vivo," *The Journal of Physiology*, vol. 538, no. 1, pp. 219–226.

[7] G. Lichtwark and A. Wilson, "Optimal muscle fascicle length and tendon stiffness for maximising gastrocnemius efficiency during human walking and running," *Journal of Theoretical Biology*, vol. 252, no. 4, pp. 662 – 673, 2008.

[8] P. W. Duncan, K. J. Sullivan, A. L. Behrman, S. P. Azen, S. S. Wu, S. E. Nadeau, B. H. Dobkin, D. K. Rose, J. K. Tilson, S. Cen, and S. K. Hayden, "Body-weight–supported treadmill rehabilitation after stroke," *New England Journal of Medicine*, vol. 364, no. 21, pp. 2026–2036, 2011. PMID: 21612471.

[9] B. C. Ruby, G. W. L. III, D. W. Armstrong, and S. E. Gaskill, "Wildland firefighter load carriage: effects on transit time and physiological responses during simulated escape to safety zone," *International Journal of Wildland Fire*, vol. 12, no. 1, pp. 111–116, 2003.

[10] J. J. Knapik, K. L. Reynolds, and E. Harman, "Soldier Load Carriage: Historical, Physiological, Biomechanical, and Medical Aspects," *Military Medicine*, vol. 169, pp. 45–56, 01 2004.

[11] B. J. van Vuuren, P. J. Becker, H. J. van Heerden, E. Zinzen, and R. Meeusen, "Lower back problems and occupational risk factors in a south african steel industry," *American Journal of Industrial Medicine*, vol. 47, no. 5, pp. 451–457.

[12] A. Seth, J. L. Hicks, T. K. Uchida, A. Habib, C. L. Dembia, J. J. Dunne, C. F. Ong, M. S. DeMers, A. Rajagopal, M. Millard, S. R. Hamner, E. M. Arnold, J. R. Yong, S. K. Lakshmikanth, M. A. Sherman, J. P. Ku, and S. L. Delp, "Opensim: Simulating musculoskeletal dynamics and neuromuscular control to study human and animal movement," *PLOS Computational Biology*, vol. 14, pp. 1–20, 07 2018.

[13] J. Selinger, S. O'Connor, J. Wong, and J. Donelan, "Humans can continuously optimize energetic cost during walking," *Current Biology*, vol. 25, no. 18, pp. 2452 – 2456, 2015.

[14] K. E. Gordon and D. P. Ferris, "Learning to walk with a robotic ankle exoskeleton," *Journal of Biomechanics*, vol. 40, no. 12, pp. 2636 – 2644, 2007.

[15] C. L. Dembia, A. Silder, T. K. Uchida, J. L. Hicks, and S. L. Delp, "Simulating ideal assistive devices to reduce the metabolic cost of walking with heavy loads," *PLOS ONE*, vol. 12, pp. 1–25, 07 2017.

[16] R. C. Browning, J. R. Modica, R. Kram, and A. Goswami, "The effects of adding mass to the legs on the energetics and biomechanics of walking," *Medicine & Science in Sports & Exercise*, vol. 39, no. 3, pp. 515–525, 2007.

[17] L. M. Mooney, E. J. Rouse, and H. M. Herr, "Autonomous exoskeleton reduces metabolic cost of human walking during load carriage," *Journal of NeuroEngineering and Rehabilitation*, vol. 11, p. 80, May 2014.

[18] N. Yagn, "Apparatus for facilitating walking, running, and jumping," 1890. U.S. Patents 420 179 and 438 830.

[19] A. M. Dollar and H. Herr, "Lower extremity exoskeletons and active orthoses: Challenges and state-of-the-art," *IEEE Transactions on Robotics*, vol. 24, pp. 144–158, Feb 2008.

[20] E. Garcia, J. M. Sater, and J. Main, "Exoskeletons for human performance augmentation (ehpa) : A program summary," *Journal of the Robotics Society of Japan*, vol. 20, no. 8, pp. 822–826, 2002.

[21] A. Chu, H. Kazerooni, and A. Zoss, "On the biomimetic design of the berkeley lower extremity exoskeleton (bleex)," in *Proceedings of the 2005 IEEE International Conference on Robotics and Automation*, pp. 4345–4352, April 2005.

[22] R. Riener, L. Lünenburger, I. C. Maier, G. Colombo, and V. Dietz, "Locomotor Training in Subjects with Sensori-Motor Deficits: An Overview of the Robotic Gait Orthosis Lokomat," *Journal of Healthcare Engineering*, vol. 1, no. 2, 2010.

[23] G. Zeilig, H. Weingarden, M. Zwecker, I. Dudkiewicz, A. Bloch, and A. Esquenazi, "Safety and tolerance of the rewalk™ exoskeleton suit for ambulation by people with complete spinal cord injury: A pilot study," *The Journal of Spinal Cord Medicine*, vol. 35, no. 2, pp. 96–101, 2012. PMID: 22333043.

[24] A. J. Young and D. P. Ferris, "State of the art and future directions for lower limb robotic exoskeletons," *IEEE Transactions on Neural Systems and Rehabilitation Engineering*, vol. 25, pp. 171–182, Feb 2017.

[25] S. Viteckova, P. Kutilek, and M. Jirina, "Wearable lower limb robotics: A review," *Biocybernetics and Biomedical Engineering*, vol. 33, no. 2, pp. 96 – 105, 2013.

[26] T. Yan, M. Cempini, C. M. Oddo, and N. Vitiello, "Review of assistive strategies in powered lower-limb orthoses and exoskeletons," *Robotics and Autonomous Systems*, vol. 64, pp. 120 – 136, 2015.

[27] W. Huo, S. Mohammed, J. C. Moreno, and Y. Amirat, "Lower limb wearable robots for assistance and rehabilitation: A state of the art," *IEEE Systems Journal*, vol. 10, pp. 1068–1081, Sep. 2016.

[28] P. Malcolm, W. Derave, S. Galle, and D. De Clercq, "A simple exoskeleton that assists plantarflexion can reduce the metabolic cost of human walking," *PLOS ONE*, vol. 8, pp. 1–7, 02 2013.

[29] S. H. Collins, M. B. Wiggin, and G. S. Sawicki, "Reducing the energy cost of human walking using an unpowered exoskeleton," *Nature*, vol. 522, pp. 212 EP –, Apr 2015.

[30] G. Lee, J. Kim, F. A. Panizzolo, Y. M. Zhou, L. M. Baker, I. Galiana, P. Malcolm, and C. J. Walsh, "Reducing the metabolic cost of running with a tethered soft exosuit," *Science Robotics*, vol. 2, no. 6, 2017.

[31] G. S. Sawicki, O. N. Beck, I. Kang, and A. J. Young, "The exoskeleton expansion : improving walking and running economy," vol. 9, pp. 1–9, 2020.

[32] F. A. Panizzolo, I. Galiana, A. T. Asbeck, C. Siviy, K. Schmidt, K. G. Holt, and C. J. Walsh, "A biologically-inspired multi-joint soft exosuit that can reduce the energy cost of loaded walking," *Journal of NeuroEngineering and Rehabilitation*, vol. 13, p. 43, May 2016.

[33] J. Kim, R. Heimgartner, G. Lee, N. Karavas, D. Perry, D. L. Ryan, A. Eckert-Erdheim, P. Murphy, D. K. Choe, I. Galiana, and C. J. Walsh, "Autonomous and portable soft exosuit for hip extension assistance with online walking and running detection algorithm," in *2018 IEEE International Conference on Robotics and Automation (ICRA)*, pp. 5473–5480, 2018.

[34] J. Kim, G. Lee, R. Heimgartner, D. Arumukhom Revi, N. Karavas, D. Nathanson, I. Galiana, A. Eckert-Erdheim, P. Murphy, D. Perry, N. Menard, D. K. Choe, P. Malcolm, and C. J. Walsh, "Reducing the metabolic rate of walking and running with a versatile, portable exosuit," *Science*, vol. 365, no. 6454, pp. 668–672, 2019.

[35] R. Nasiri, A. Ahmadi, and M. N. Ahmadabadi, "Reducing the energy cost of human running using an unpowered exoskeleton," *IEEE Transactions on Neural Systems and Rehabilitation Engineering*, vol. 26, pp. 2026–2032, Oct 2018.

[36] S. Lee, J. Kim, L. Baker, A. Long, N. Karavas, N. Menard, I. Galiana, and C. J. Walsh, "Autonomous multi-joint soft exosuit with augmentation-power-based control parameter tuning reduces energy cost of loaded walking," pp. 1–9, 2018.

[37] C. S. Simpson, C. G. Welker, S. D. Uhlrich, S. M. Sketch, R. W. Jackson, S. L. Delp, S. H. Collins, J. C. Selinger, and E. W. Hawkes, "Connecting the legs with a spring improves human running economy," *Journal of Experimental Biology*, vol. 222, no. 17, 2019.

[38] K. Seo, J. Lee, and Y. J. Park, "Autonomous hip exoskeleton saves metabolic cost of walking uphill," in *2017 International Conference on Rehabilitation Robotics (ICORR)*, pp. 246–251, 2017.

[39] D.-s. Kim, H.-j. Lee, S.-h. Lee, W. H. Chang, J. Jang, B.-o. Choi, G.-h. Ryu, and Y.-h. Kim, "A wearable hip-assist robot reduces the cardiopulmonary metabolic energy expenditure during stair ascent in elderly adults : a pilot cross-sectional study," pp. 1–8, 2018.

[40] K. Seo, J. Lee, Y. Lee, T. Ha, and Y. Shim, "Fully autonomous hip exoskeleton saves metabolic cost of walking," in *2016 IEEE International Conference on Robotics and Automation (ICRA)*, pp. 4628–4635, 2016.

[41] Y. Lee, S. Roh, M. Lee, B. Choi, J. Lee, J. Kim, H. Choi, Y. Shim, and Y. Kim, "A flexible exoskeleton for hip assistance," in *2017 IEEE/RSJ International Conference on Intelligent Robots and Systems (IROS)*, pp. 1058–1063, 2017.

[42] H. Lee, S. Lee, W. H. Chang, K. Seo, Y. Shim, B. Choi, G. Ryu, and Y. Kim, "A wearable hip assist robot can improve gait function and cardiopulmonary metabolic efficiency in elderly adults," *IEEE Transactions on Neural Systems and Rehabilitation Engineering*, vol. 25, no. 9, pp. 1549–1557, 2017.

[43] B. Lim, J. Lee, J. Jang, K. Kim, Y. J. Park, K. Seo, and Y. Shim, "Delayed output feedback control for gait assistance with a robotic hip exoskeleton," *IEEE Transactions on Robotics*, vol. 35, no. 4, pp. 1055–1062, 2019.

[44] L. M. Mooney, E. J. Rouse, and H. M. Herr, "Autonomous exoskeleton reduces metabolic cost of human walking Autonomous exoskeleton reduces metabolic cost of human walking," 2014.

[45] L. M. Mooney and H. M. Herr, "Biomechanical walking mechanisms underlying the metabolic reduction caused by an autonomous exoskeleton," *Journal of NeuroEngineering and Rehabilitation*, pp. 1–12, 2016.

[46] S. Galle, P. Malcolm, S. H. Collins, and D. De Clercq, "Reducing the metabolic cost of walking with an ankle exoskeleton: interaction between actuation timing and power," *Journal of NeuroEngineering and Rehabilitation*, vol. 14, no. 1, pp. 1–16, 2017.

[47] C. Khazoom, C. Véronneau, J.-p. L. Bigué, J. Grenier, A. Girard, and J.-s. Plante, "Design and Control of a Multifunctional Ankle Exoskeleton Powered by Magnetorheological Actuators to Assist Walking , Jumping , and Landing," vol. 4, no. 3, pp. 3083–3090, 2019.

[48] M. K. MacLean and D. P. Ferris, "Energetics of walking with a robotic knee exoskeleton," *Journal of Applied Biomechanics*, vol. 35, no. 5, 2019.

[49] E. Martini, S. Crea, A. Parri, L. Bastiani, U. Faraguna, Z. Mckinney, R. Molino-lova, L. Pratali, and N. Vitiello, "Gait training using a robotic hip exoskeleton improves metabolic gait efficiency in the elderly," *Scientific Reports*, pp. 1–12, 2019.

[50] L. N. Awad, J. Bae, K. O'Donnell, S. M. M. De Rossi, K. Hendron, L. H. Sloot, P. Kudzia, S. Allen, K. G. Holt, T. D. Ellis, and C. J. Walsh, "A soft robotic exosuit improves walking in patients after stroke," *Science Translational Medicine*, vol. 9, no. 400, 2017.

[51] K. Shamaei, M. Cenciarini, A. A. Adams, K. N. Gregorczyk, J. M. Schiffman, and A. M. Dollar, "Biomechanical effects of stiffness in parallel with the knee joint during walking," *IEEE Transactions on Biomedical Engineering*, vol. 62, pp. 2389–2401, Oct 2015.

[52] Y. Ding, I. Galiana, A. T. Asbeck, S. M. M. De Rossi, J. Bae, T. R. T. Santos, V. L. de Araujo, S. Lee, K. G. Holt, and C. Walsh, "Biomechanical and physiological evaluation of multi-joint assistance with soft exosuits," *IEEE Transactions on Neural Systems and Rehabilitation Engineering*, vol. 25, pp. 119–130, Feb 2017.

[53] A. Rosendo and F. Iida, "Energy efficient hopping with hill-type muscle properties on segmented legs," *Bioinspiration & Biomimetics*, vol. 11, p. 036002, apr 2016.

[54] V. D. W, *Human-exoskeleton interaction*. PhD thesis, TU Delft, 2015.

[55] T. Buschmann, A. Ewald, A. von Twickel, and A. Büschges, "Controlling legs for locomotion—insights from robotics and neurobiology," *Bioinspiration & Biomimetics*, vol. 10, p. 041001, jun 2015.

[56] G. J. V. I. Schenau, "From rotation to translation: Constraints on multi-joint movements and the unique action of bi-articular muscles," *Human Movement Science*, vol. 8, no. 4, pp. 301 – 337, 1989.

[57] K. Junius, M. Moltedo, P. Cherelle, C. Rodriguez-Guerrero, B. Vanderborght, and D. Lefeber, "Biarticular elements as a contributor to energy efficiency: biomechanical review and application in bio-inspired robotics," *Bioinspiration & Biomimetics*, vol. 12, p. 061001, nov 2017.

[58] B. I. Prilutsky and V. M. Zatsiorsky, "Optimization-Based Models of Muscle Coordination," *Exercise and Sport Sciences Reviews*, vol. 30, no. 1, pp. 32–38, 2002.

[59] J. van Leeuwen, P. Aerts, and M. G. Pandy, "Simple and complex models for studying muscle function in walking," *Philosophical Transactions of the Royal Society of London. Series B: Biological Sciences*, vol. 358, no. 1437, pp. 1501–1509, 2003.

[60] F. C. Anderson and M. G. Pandy, "Dynamic optimization of human walking," *Journal of Biomechanical Engineering*, vol. 123, pp. 381–390, May 2001.

[61] G. J. V. I. Schenau, "On the action of bi-articular muscles, a review," *Netherlands Journal of Zoology*, vol. 40, no. 3, 1989.

[62] D. Landin, M. Thompson, and M. Reid, "Actions of two bi-articular muscles of the lower extremity: A review," *Journal of Clinical Medicine Research*, vol. 8, no. 7, 2016.

[63] A. V. Voronov, "The roles of monoarticular and biarticular muscles of the lower limbs in terrestrial locomotion," *Human Physiology*, vol. 30, pp. 476–484, Jul 2004.

[64] G. J. van Ingen Schenau, M. F. Bobbert, and A. J. van Soest, *The Unique Action of Bi-Articular Muscles in Leg Extensions*, pp. 639–652. New York, NY: Springer New York, 1990.

[65] H. Elftman, "The function of muscles in locomotion," *Am. J. Physiol*, vol. 125, 1939.

[66] R. Jacobs, M. F. Bobbert, and G. J. van Ingen Schenau, "Mechanical output from individual muscles during explosive leg extensions: The role of biarticular muscles," *Journal of Biomechanics*, vol. 29, no. 4, pp. 513 – 523, 1996.

[67] H. Elftman, "The work done by muscles in running," *American Journal of Physiology-Legacy Content*, vol. 129, no. 3, pp. 672–684, 1940.

[68] B. I. Prilutsky, L. N. Petrova, and L. M. Raitsin, "Comparison of mechanical energy expenditure of joint moments and muscle forces during human locomotion," *Journal of Biomechanics*, vol. 29, no. 4, pp. 405 – 415, 1996.

[69] R. Wells, "Mechanical energy costs of human movement: An approach to evaluating the transfer possibilities of two-joint muscles," *Journal of Biomechanics*, vol. 21, no. 11, pp. 955 – 964, 1988.

[70] J. Cleland, "On the actions of muscles passing over more than one joint," *Journal of anatomy and physiology*, vol. 1, no. 1, pp. 85–93, 1867. 17230710[pmid].

[71] W. O. Fenn, "The mechanics of muscular contraction in man," *Journal of Applied Physics*, vol. 9, no. 3, pp. 165–177, 1938.

[72] C. English, *Stiffness behaviour in two degree of freedom mechanisms*. PhD thesis, Carleton University,Ottawa, Ontario, 1999.

[73] N. Hogan, "The mechanics of multi-joint posture and movement control," *Biological Cybernetics*, vol. 52, pp. 315–331, Sep 1985.

[74] N. Hogan, "Adaptive control of mechanical impedance by coactivation of antagonist muscles," *IEEE Transactions on Automatic Control*, vol. 29, pp. 681–690, August 1984.

[75] N. Hogan, *Mechanical Impedance of Single- and Multi-Articular Systems*, pp. 149–164. New York, NY: Springer New York, 1990.

[76] J. McIntyre, F. A. Mussa-Ivaldi, and E. Bizzi, "The control of stable postures in the multijoint arm," *Experimental Brain Research*, vol. 110, pp. 248–264, Jul 1996.

[77] F. Iida, J. Rummel, and A. Seyfarth, "Bipedal walking and running with spring-like biarticular muscles," *Journal of Biomechanics*, vol. 41, no. 3, pp. 656 – 667, 2008.

[78] M. A. Sharbafi, C. Rode, S. Kurowski, D. Scholz, R. Möckel, K. Radkhah, G. Zhao, A. M. Rashty, O. von Stryk, and A. Seyfarth, "A new biarticular actuator design facilitates control of leg function in BioBiped3," *Bioinspiration & Biomimetics*, vol. 11, p. 046003, jul 2016.

[79] W. Roozing, Z. Ren, and N. G. Tsagarakis, "Design of a novel 3-dof leg with series and parallel compliant actuation for energy efficient articulated robots," in *2018 IEEE International Conference on Robotics and Automation (ICRA)*, pp. 1–8, May 2018.

[80] H. Höppner, W. Wiedmeyer, and P. van der Smagt, "A new biarticular joint mechanism to extend stiffness ranges," in *2014 IEEE International Conference on Robotics and Automation (ICRA)*, pp. 3403–3410, May 2014.

[81] J. Dean and A. Kuo, "Elastic coupling of limb joints enables faster bipedal walking," *Journal of The Royal Society Interface*, vol. 6, no. 35, pp. 561–573, 2009.

[82] M. F. Eilenberg, J.-Y. Kuan, and H. Herr, "Development and Evaluation of a Powered Artificial Gastrocnemius for Transtibial Amputee Gait," *Journal of Robotics*, vol. 2018, p. 15, 2018.

[83] K. Endo, E. Swart, and H. Herr, "An artificial gastrocnemius for a transtibial prosthesis," in *2009 Annual International Conference of the IEEE Engineering in Medicine and Biology Society*, pp. 5034–5037, Sep. 2009.

[84] M. F. Eilenberg, K. Endo, and H. Herr, "Biomechanic and Energetic Effects of a Quasi-Passive Artificial Gastrocnemius on Transtibial Amputee Gait," *Journal of Robotics*, vol. 2018, p. 12, 2018.

[85] L. Flynn, J. Geeroms, R. Jimenez-Fabian, B. Vanderborght, N. Vitiello, and D. Lefeber, "Ankle–knee prosthesis with active ankle and energy transfer: Development of the cyberlegs alpha-prosthesis," *Robotics and Autonomous Systems*, vol. 73, pp. 4 – 15, 2015. Wearable Robotics.

[86] M. Eslamy, M. Grimmer, and A. Seyfarth, "Adding passive biarticular spring to active mono-articular foot prosthesis: Effects on power and energy requirement," in *2014 IEEE-RAS International Conference on Humanoid Robots*, pp. 677–684, Nov 2014.

[87] B. T. Quinlivan, S. Lee, P. Malcolm, D. M. Rossi, M. Grimmer, C. Siviy, N. Karavas, D. Wagner, A. Asbeck, I. Galiana, and C. J. Walsh, "Assistance magnitude versus metabolic cost reductions for a tethered multiarticular soft exosuit," *Science Robotics*, vol. 2, no. 2, 2017.

[88] M. B. Wiggin, G. S. Sawicki, and S. H. Collins, "An exoskeleton using controlled energy storage and release to aid ankle propulsion," in *2011 IEEE International Conference on Rehabilitation Robotics*, pp. 1–5, June 2011.

[89] C. Xiong, T. Zhou, L. Zhou, T. Wei, and W. Chen, "Multi-articular passive exoskeleton for reducing the metabolic cost during human walking," in *2019 Wearable Robotics Association Conference (WearRAcon)*, pp. 63–67, March 2019.

[90] E. P. Grabke, K. Masani, and J. Andrysek, "Lower Limb Assistive Device Design Optimization Using Musculoskeletal Modeling: A Review," *Journal of Medical Devices*, vol. 13, 10 2019. 040801.

[91] H. Aftabi, R. Nasiri, and M. N. Ahmadabadi, "A kinematic index for estimation of metabolic rate reduction in running with i-run," *bioRxiv*, 2020.

[92] R. W. Jackson, C. L. Dembia, S. L. Delp, and S. H. Collins, "Muscle – tendon mechanics explain unexpected effects of exoskeleton assistance on metabolic rate during walking," pp. 2082–2095, 2017.

[93] D. J. Farris, J. L. Hicks, S. L. Delp, and G. S. Sawicki, "Musculoskeletal modelling deconstructs the paradoxical effects of elastic ankle exoskeletons on plantar-flexor mechanics and energetics during hopping," pp. 4018–4028, 2014.

[94] G. S. Sawicki and N. S. Khan, "A Simple Model to Estimate Plantarflexor Muscle – Tendon Mechanics and Energetics During Walking With Elastic Ankle Exoskeletons," vol. 63, no. 5, pp. 914–923, 2016.

[95] B. Lim, S. Hyung, K. Kim, J. Lee, J. Jang, and Y. Shim, "Simulating Gait Assistance of a Hip Exoskeleton : Feasibility Studies for Ankle Muscle Weaknesses," pp. 5664–5669, 2016.

[96] B. Lim, S. Hyoung, J. Lee, K. Seo, J. Jang, and Y. Shim, "Simulating Gait Assistance of a Hip Exoskeleton : Case Studies for Ankle Pathologies," vol. 1, no. 1, pp. 1022–1027, 2017.

[97] S. L. Delp, F. C. Anderson, A. S. Arnold, P. Loan, A. Habib, C. T. John, E. Guendelman, and D. G. Thelen, "Opensim: Open-source software to create and analyze dynamic simulations of movement," *IEEE Transactions on Biomedical Engineering*, vol. 54, pp. 1940–1950, Nov 2007.

[98] J. L. Hicks, T. K. Uchida, A. Seth, A. Rajagopal, and S. L. Delp, "Is my model good enough?: Best practices for verification and validation of musculoskeletal models and simulations of movement," *Journal of Biomechanical Engineering*, vol. 137, pp. 020905–020905–24, Feb 2015.

[99] D. F. N. Gordon, G. Henderson, and S. Vijayakumar, "Effectively quantifying the performance of lower-limb exoskeletons over a range of walking conditions," *Frontiers in Robotics and AI*, vol. 5, p. 61, 2018.

[100] C. F. Ong, J. L. Hicks, and S. L. Delp, "Simulation-based design for wearable robotic systems: An optimization framework for enhancing a standing long jump," *IEEE Transactions on Biomedical Engineering*, vol. 63, pp. 894–903, May 2016.

[101] T. W. Dorn, J. M. Wang, J. L. Hicks, and S. L. Delp, "Predictive simulation generates human adaptations during loaded and inclined walking," *PLOS ONE*, vol. 10, pp. 1–16, 04 2015.

[102] C. L. Dembia, N. A. Bianco, A. Falisse, J. L. Hicks, and S. L. Delp, "Opensim moco: Musculoskeletal optimal control," *bioRxiv*, 2019.

[103] T. Geijtenbeek, "Scone: Open source software for predictive simulation of biological motion," *Journal of Open Source Software*, vol. 4, p. 1421, 6 2019.

[104] V. Q. Nguyen, B. R. Umberger, and F. C. Sup, "Predictive simulation of human walking augmented by a powered ankle exoskeleton," in *2019 IEEE 16th International Conference on Rehabilitation Robotics (ICORR)*, pp. 53–58, June 2019.

[105] A. K. LaPrè, B. R. Umberger, and F. Sup, "Simulation of a powered ankle prosthesis with dynamic joint alignment," in *2014 36th Annual International Conference of the IEEE Engineering in Medicine and Biology Society*, pp. 1618–1621, Aug 2014.

[106] J. Zhao, K. Berns, R. de Souza Baptista, and A. P. L. Bó, "Design of variable-damping control for prosthetic knee based on a simulated biped," in *2013 IEEE 13th International Conference on Rehabilitation Robotics (ICORR)*, pp. 1–6, June 2013.

[107] M. L. Handford and M. Srinivasan, "Robotic lower limb prosthesis design through simultaneous computer optimizations of human and prosthesis costs," *Scientific Reports*, vol. 6, pp. 19983 EP –, Feb 2016. Article.

[108] M. L. Handford and M. Srinivasan, "Energy-optimal human walking with feedback-controlled robotic prostheses: A computational study," *IEEE Transactions on Neural Systems and Rehabilitation Engineering*, vol. 26, pp. 1773–1782, Sep. 2018.

[109] M. Sreenivasa, M. Millard, M. Felis, K. Mombaur, and S. I. Wolf, "Optimal control based stiffness identification of an ankle-foot orthosis using a predictive walking model," *Frontiers in Computational Neuroscience*, vol. 11, p. 23, 2017.

[110] N. P. Fey, G. K. Klute, and R. R. Neptune, "Optimization of Prosthetic Foot Stiffness to Reduce Metabolic Cost and Intact Knee Loading During Below-Knee Amputee Walking: A Theoretical Study," *Journal of Biomechanical Engineering*, vol. 134, 10 2012. 111005.

[111] R. Jacobs, M. F. Bobbert, and G. J. van Ingen Schenau, "Mechanical output from individual muscles during explosive leg extensions: The role of biarticular muscles," *Journal of Biomechanics*, vol. 29, no. 4, pp. 513 – 523, 1996.

[112] B. I. Prilutsky and V. M. Zatsiorsky, "Tendon action of two-joint muscles: Transfer of mechanical energy between joints during jumping, landing, and running," *Journal of Biomechanics*, vol. 27, no. 1, pp. 25 – 34, 1994.

[113] G. Kenneally, A. De, and D. E. Koditschek, "Design principles for a family of direct-drive legged robots," *IEEE Robotics and Automation Letters*, vol. 1, pp. 900–907, July 2016.

[114] S. Seok, A. Wang, D. Otten, and S. Kim, "Actuator design for high force proprioceptive control in fast legged locomotion," in *2012 IEEE/RSJ International Conference on Intelligent Robots and Systems*, pp. 1970–1975, Oct 2012.

[115] P. M. Wensing, A. Wang, S. Seok, D. Otten, J. Lang, and S. Kim, "Proprioceptive actuator design in the mit cheetah: Impact mitigation and high-bandwidth physical interaction for dynamic legged robots," *IEEE Transactions on Robotics*, vol. 33, pp. 509–522, June 2017.

[116] B. Siciliano, L. Sciavicco, L. Villani, and G. Oriolo, *Robotics: modelling, planning and control*. Springer, 2010.

[117] M. Grimmer, *Neuro-Robotics*, vol. 2 of *Trends in Augmentation of Human Performance*. Dordrecht: Springer Netherlands, 2014.

[118] A. Rajagopal, C. L. Dembia, M. S. DeMers, D. D. Delp, J. L. Hicks, and S. L. Delp, "Full-body musculoskeletal model for muscle-driven simulation of human gait," *IEEE Transactions on Biomedical Engineering*, vol. 63, no. 10, pp. 2068–2079, 2016.

[119] D. G. Thelen, F. C. Anderson, and S. L. Delp, "Generating dynamic simulations of movement using computed muscle control," *Journal of Biomechanics*, vol. 36, no. 3, pp. 321 – 328, 2003.

[120] B. R. UMBERGER, K. G. GERRITSEN, and P. E. MARTIN, "A model of human muscle energy expenditure," *Computer Methods in Biomechanics and Biomedical Engineering*, vol. 6, no. 2, pp. 99–111, 2003. PMID: 12745424.

[121] T. K. Uchida, J. L. Hicks, C. L. Dembia, and S. L. Delp, "Stretching your energetic budget: How tendon compliance affects the metabolic cost of running," *PLOS ONE*, vol. 11, pp. 1–19, 03 2016.

[122] K. M. Steele, M. S. DeMers, M. H. Schwartz, and S. L. Delp, "Compressive tibiofemoral force during crouch gait," *Gait & Posture*, vol. 35, no. 4, pp. 556 – 560, 2012.

[123] T.-w. P. Huang and A. D. Kuo, "Mechanics and energetics of load carriage during human walking," *Journal of Experimental Biology*, vol. 217, no. 4, pp. 605–613, 2014.

[124] A. Silder, S. L. Delp, and T. Besier, "Men and women adopt similar walking mechanics and muscle activation patterns during load carriage," *Journal of Biomechanics*, vol. 46, no. 14, pp. 2522–2528, 2013.

[125] J. Merlet, *Parallel Robots*, vol. 128. Springer Science & Business Media, 2006.

[126] IBM Corp., "Ibm spss statistics for windows."

[127] M. S. DeMers, S. Pal, and S. L. Delp, "Changes in tibiofemoral forces due to variations in muscle activity during walking," *Journal of Orthopaedic Research*, vol. 32, no. 6, pp. 769–776, 2014.

[128] B. van Veen, E. Montefiori, L. Modenese, C. Mazzà, and M. Viceconti, "Muscle recruitment strategies can reduce joint loading during level walking," *Journal of Biomechanics*, vol. 97, p. 109368, 2019.

[129] K. Sasaki and R. R. Neptune, "Individual muscle contributions to the axial knee joint contact force during normal walking," *Journal of Biomechanics*, vol. 43, pp. 2780–2784, oct 2010.

[130] K. B. Shelburne, M. R. Torry, and M. G. Pandy, "Contributions of muscles, ligaments, and the ground-reaction force to tibiofemoral joint loading during normal gait," *Journal of Orthopaedic Research*, vol. 24, pp. 1983–1990, oct 2006.

[131] D. R. Carter and M. Wong, "The role of mechanical loading histories in the development of diarthrodial joints," *Journal of Orthopaedic Research*, vol. 6, pp. 804–816, nov 1988.

[132] C. Waller, D. Hayes, J. E. Block, and N. J. London, "Unload it: the key to the treatment of knee osteoarthritis," *Knee Surgery, Sports Traumatology, Arthroscopy*, vol. 19, pp. 1823–1829, nov 2011.

[133] A. Baliunas, D. Hurwitz, A. Ryals, A. Karrar, J. Case, J. Block, and T. Andriacchi, "Increased knee joint loads during walking are present in subjects

with knee osteoarthritis," *Osteoarthritis and Cartilage*, vol. 10, pp. 573–579, jul 2002.

[134] L. Sharma, D. E. Hurwitz, E. J. Thonar, J. A. Sum, M. E. Lenz, D. D. Dunlop, T. J. Schnitzer, G. Kirwan-Mellis, and T. P. Andriacchi, "Knee adduction moment, serum hyaluronan level, and disease severity in medial tibiofemoral osteoarthritis," *Arthritis and Rheumatism*, vol. 41, no. 7, pp. 1233–1240, 1998.

[135] T. J. Schnitzer, J. M. Popovich, G. B. J. Andersson, and T. P. Andriacchi, "Effect of piroxicam on gait in patients with osteoarthritis of the knee," *Arthritis & Rheumatism*, vol. 36, pp. 1207–1213, sep 1993.

[136] P. Y. Papalambros and D. J. Wilde, *Principles of Optimal Design: Modeling and Computation*. Cambridge University Press, 2 ed., 2000.

[137] R. Marler and J. Arora, "The weighted sum method for multi-objective optimization: New insights," *Structural and Multidisciplinary Optimization*, vol. 41, pp. 853–862, 06 2010.

[138] R. Unal, G. Kiziltas, and V. Patoglu, "A multi-criteria design optimization framework for haptic interfaces," in *2008 Symposium on Haptic Interfaces for Virtual Environment and Teleoperator Systems*, pp. 231–238, 2008.

[139] R. Unal, G. Kiziltas, and V. Patoglu, "Multi-criteria design optimization of parallel robots," in *2008 IEEE Conference on Robotics, Automation and Mechatronics*, pp. 112–118, Sep. 2008.

[140] A. Kamadan, G. Kiziltas, and V. Patoglu, "Co-design strategies for optimal variable stiffness actuation," *IEEE/ASME Transactions on Mechatronics*, vol. 22, no. 6, pp. 2768–2779, 2017.

[141] Y. Aydin, O. Tokatli, V. Patoglu, and C. Basdogan, "A computational multi-criteria optimization approach to controller design for physical human-robot interaction," *IEEE Transactions on Robotics*, vol. 36, no. 6, pp. 1791–1804, 2020.

[142] R. Marler and J. S. Arora, "Survey of multi-objective optimization methods for engineering," *Structural and Multidisciplinary Optimization*, vol. 26, pp. 369–395, 2004.

[143] K. Miettinen, F. Ruiz, and A. P. Wierzbicki, *Introduction to Multiobjective Optimization: Interactive Approaches*, pp. 27–57. Berlin, Heidelberg: Springer Berlin Heidelberg, 2008.

[144] W. Jakob and C. Blume, "Pareto optimization or cascaded weighted sum: A comparison of concepts," *Algorithms*, vol. 7, no. 1, pp. 166–185, 2014.

[145] D. A. W. Yacov Y. Haimes, Leon S. Lasdon, "On a bicriterion formulation of the problems of integrated system identification and system optimization," *IEEE Transactions on Systems, Man, and Cybernetics*, vol. SMC-1, no. 3, pp. 296–297, 1971.

[146] M. Laumanns, L. Thiele, and E. Zitzler, "An efficient, adaptive parameter variation scheme for metaheuristics based on the epsilon-constraint method," *European Journal of Operational Research*, vol. 169, no. 3, pp. 932–942, 2006.

[147] K. Chircop and D. Zammit-Mangion, "On epsilon-constraint based methods for the generation of pareto frontiers," *Journal of Mechanics Engineering and Automation*, vol. 3, pp. 279–289, 05 2013.

[148] P. [de Leva], "Adjustments to zatsiorsky-seluyanov's segment inertia parameters," *Journal of Biomechanics*, vol. 29, no. 9, pp. 1223 – 1230, 1996.

[149] G. S. Sawicki and D. P. Ferris, "Mechanics and energetics of level walking with powered ankle exoskeletons," *Journal of Experimental Biology*, vol. 211, no. 9, pp. 1402–1413, 2008.

[150] B. Laschowski, J. McPhee, and J. Andrysek, "Lower-Limb Prostheses and Exoskeletons With Energy Regeneration: Mechatronic Design and Optimization Review," *Journal of Mechanisms and Robotics*, vol. 11, 05 2019. 040801.

[151] S. Seok, A. Wang, M. Y. Chuah, D. J. Hyun, J. Lee, D. M. Otten, J. H. Lang, and S. Kim, "Design principles for energy-efficient legged locomotion and implementation on the mit cheetah robot," *IEEE/ASME Transactions on Mechatronics*, vol. 20, no. 3, pp. 1117–1129, 2015.

[152] J. M. Donelan, Q. Li, V. Naing, J. A. Hoffer, D. J. Weber, and A. D. Kuo, "Biomechanical energy harvesting: Generating electricity during walking with minimal user effort," *Science*, vol. 319, no. 5864, pp. 807–810, 2008.

[153] D. Torricelli, J. Gonzalez, M. Weckx, R. Jiménez-Fabián, B. Vanderborght, M. Sartori, S. Dosen, D. Farina, D. Lefeber, and J. L. Pons, "Human-like compliant locomotion: State of the art of robotic implementations," *Bioinspiration and Biomimetics*, vol. 11, no. 5, 2016.

[154] J. Perry, J. R. Davids, *et al.*, "Gait analysis: normal and pathological function," *Journal of Pediatric Orthopaedics*, vol. 12, no. 6, p. 815, 1992.

[155] E. Schertzer and R. Riemer, "Harvesting biomechanical energy or carrying batteries? An evaluation method based on a comparison of metabolic power," *Journal of NeuroEngineering and Rehabilitation*, vol. 12, no. 1, pp. 1–12, 2015.

[156] R. Riemer and A. Shapiro, "Biomechanical energy harvesting from human motion: Theory, state of the art, design guidelines, and future directions," *Journal of NeuroEngineering and Rehabilitation*, vol. 8, no. 1, pp. 1–13, 2011.

[157] T. D. Royer and P. E. Martin, "Manipulations of leg mass and moment of inertia: effects on energy cost of walking," *Medicine & Science in Sports & Exercise*, vol. 37, no. 4, pp. 649–656, 2005.

[158] R. G. Soule and R. F. Goldman, "Energy cost of loads carried on the head, hands, or feet.," *Journal of Applied Physiology*, vol. 27, no. 5, pp. 687–690, 1969. PMID: 5360445.

[159] G. Aguirre-Ollinger, J. E. Colgate, M. A. Peshkin, and A. Goswami, "Design of an active one-degree-of-freedom lower-limb exoskeleton with inertia compensation," *International Journal of Robotics Research*, vol. 30, no. 4, pp. 486–499, 2011.

[160] E. Colgate, *The Interaction of Robots with Passive Environments: Application to Force Feedback Control*. Springer-Verlag, 1989.

[161] J. E. COLGATE and N. HOGAN, "Robust control of dynamically interacting systems," *International Journal of Control*, vol. 48, no. 1, pp. 65–88, 1988.

[162] R. W. Jackson and S. H. Collins, "An experimental comparison of the relative benefits of work and torque assistance in ankle exoskeletons," *Journal of Applied Physiology*, vol. 119, no. 5, pp. 541–557, 2015. PMID: 26159764.

[163] C. L. Lewis and D. P. Ferris, "Invariant hip moment pattern while walking with a robotic hip exoskeleton," *Journal of Biomechanics*, vol. 44, no. 5, pp. 789 – 793, 2011.

[164] P.-C. Kao, C. L. Lewis, and D. P. Ferris, "Invariant ankle moment patterns when walking with and without a robotic ankle exoskeleton," *Journal of Biomechanics*, vol. 43, no. 2, pp. 203 – 209, 2010.

[165] S. Galle, P. Malcolm, W. Derave, and D. D. Clercq, "Adaptation to walking with an exoskeleton that assists ankle extension," *Gait & Posture*, vol. 38, no. 3, pp. 495 – 499, 2013.

[166] J. R. Koller, D. A. Jacobs, D. P. Ferris, and C. D. Remy, "Learning to walk with an adaptive gain proportional myoelectric controller for a robotic ankle exoskeleton," *Journal of NeuroEngineering and Rehabilitation*, vol. 12, no. 1, p. 97, 2015.

[167] T. Lenzi, M. C. Carrozza, and S. K. Agrawal, "Powered hip exoskeletons can reduce the user's hip and ankle muscle activations during walking," *IEEE*

Transactions on Neural Systems and Rehabilitation Engineering, vol. 21, pp. 938–948, Nov 2013.

[168] M. T. Vanderpool, S. H. Collins, and A. D. Kuo, "Ankle fixation need not increase the energetic cost of human walking," *Gait & Posture*, vol. 28, no. 3, pp. 427 – 433, 2008.

[169] M. Cenciarini and A. M. Dollar, "Biomechanical considerations in the design of lower limb exoskeletons," in *2011 IEEE International Conference on Rehabilitation Robotics*, pp. 1–6, June 2011.

[170] M. Johnson, J. Polgar, D. Weightman, and D. Appleton, "Data on the distribution of fibre types in thirty-six human muscles: An autopsy study," *Journal of the Neurological Sciences*, vol. 18, no. 1, pp. 111 – 129, 1973.

[171] D. J. Newham, K. R. Mills, B. M. Quigley, and R. H. T. Edwards, "Pain and fatigue after concentric and eccentric muscle contractions," *Clinical Science*, vol. 64, no. 1, pp. 55–62, 1983.

[172] I. Das and J. Dennis, "Normal-boundary intersection: A new method for generating the pareto surface in nonlinear multicriteria optimization problems," *SIAM Journal on Optimization*, vol. 8, no. 3, pp. 631–657, 1998.

[173] J. Zhang, P. Fiers, K. A. Witte, R. W. Jackson, K. L. Poggensee, C. G. Atkeson, and S. H. Collins, "Human-in-the-loop optimization of exoskeleton assistance during walking," *Science*, vol. 356, no. 6344, pp. 1280–1284, 2017.